CHEMICAL REVIEWS

Review

pubs.acs.org/CR

Light-Driven and Phonon-Assisted Dynamics in Organic and Semiconductor Nanostructures

Svetlana Kilina,[†] Dmitri Kilin,[‡] and Sergei Tretiak*[,§]

[†]Chemistry and Biochemistry Department, North Dakota State University, Fargo, North Dakota 5810, United States

[‡]Department of Chemistry, University of South Dakota, Vermillion, South Dakota 57069, United States

[§]Theoretical Division, Center for Nonlinear Studies (CNLS) and Center for Integrated Nanotechnologies (CINT), Los Alamos National Laboratory, Los Alamos, New Mexico 87545, United States

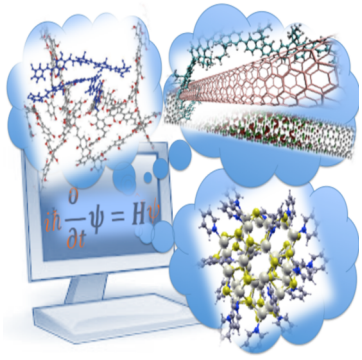

CONTENTS

Special Issue: Calculations on Large Systems

Received: January 10, 2015
Published: May 20, 2015

DOI: 10.1021/acs.chemrev.5b00012
Chem. Rev. 2015, 115, 5929–5978

1. INTRODUCTION

Rapid advances in chemical synthesis and fabrication techniques have led to a boost in manufacturing and design of novel nanostructured materials that exhibit unique and often unforeseen properties.[1,2] One of the greatest advantages of these nanosystems is the ability to control their electronic and optical properties through the sample's size, shape, and topology utilizing a broad variety of organic and inorganic materials. This tunability together with a very small size and a relatively low fabrication cost open new ways to exploit nanostructures as the main building blocks in next generation technologies ranging from electronics and photovoltaics to biology and medicine. Semiconductor colloidal quantum dots (QDs),[3] single-walled carbon nanotubes (SWNTs),[4] and conjugated polymers (CPs), also called organic semiconductors,[5] are the most common examples of low-dimensional nanostructured materials. In recent decades, they have been the targets of many experimental, theoretical, and technological investigations. Photophysical properties and their sensitivity to the structural disorder and surface effects of these three types of nanomaterials are overviewed in this Review with the main focus on their theoretical description at the atomistic level.

1.1. Confinement Effects in Carbon-Based and Inorganic Nanomaterials

Dimensionality and dielectric permittivity are general descriptors critically affecting electronic properties of these materials. The QD, or a nanocrystal, is made from an inorganic semiconductor crystal a few nanometers in size. While QDs typically have a roughly spherical shape, cylindrical (nanorods), oblate and prolate elliptical, and rectangular shapes have been also broadly explored.[6] In their inner (core) part, the QD remains structurally identical to the bulk crystal.[7] Therefore, the electronic structure of QDs holds partially the features of the electronic structure of the parent bulk material. The nanometer scale of a QD leads to its zero-dimensionality (0-D). SWNTs and isolated chains of CPs represent quasi one-dimensional (1-D) nanostructures with low dielectric constant ($\varepsilon \leq 10$), as compared, for example, to that of conventional semiconductors ($10 < \varepsilon \leq 100$). SWNTs can be thought of as a one-atom-thick layer of graphite rolled into long rigid cylinders a few nanometers in diameter. The honeycomb-like structure of connected C_6 rings with the sp^2-bond character provides a scaffold for the π-conjugation of SWNTs and highly delocalized nature of electrons. Likewise, delocalized π-electrons is a main feature of CPs, where the carbon−carbon bonds have varying π-electronic density as reflected in their triple-, double-, and single-like bond character. A common key feature of any nanosystem is a quantum confinement defined by its dimensionality, a major factor determining the underlining electronic structure and photophysics. For example, in 0-D semiconductor QDs, the electronic excitation confinement is determined by the QD's size. This results in a band gap and an optical gap to be strongly dependent on the QD diameter D ($\sim 1/D^2$ as hinted by a simple particle in a spherical box picture). Thus, the energy gap increases as the QD size decreases.[3,7] Similarly, due to the quantum confinement,[8] the optical gap of isolated chains of CPs is blue-shifted with decrease of their conjugated length given by the oligomer's length or a characteristic segment length of the polymer. Because of circumferential confinement, the energy gap of a semiconductor SWNT is roughly inversely proportional to its diameter.[9] However, the direction of the tube's rolling, a chiral vector (n,m), defines whether a nanotube has a metal or a semiconductor-like electronic structure and a specific value of its band gap.[4] Moreover, many other complex factors such as surface chemistry, structural disorder, and interfacial interactions also affect electronic properties of individual QDs, SWNTs, and CPs. These factors usually define electronic functionalities of nanostructures in device setting (e.g., light harvesting and carrier transport in the form of excitons, charges, and spins), providing a plethora of synthetic means to achieve desired properties.

1.2. Sensitivity of Photophysics of Quantum Dots to Surface Chemistry

It is established that photophysics of QDs is extremely sensitive to their surface chemistry and chemical environment, resulting in bleaching (luminescence intensity degrades over time) and blinking (fluorescence intermittency); all of these create technical problems for practical applications of QDs in solid-state lighting, optical amplifiers, and fluorescent biolabels[10] and sensors.[11] The QD consists of the core preserving structure of its parent bulk crystal, surface atoms in the outer shell with morphology distinct from the bulk,[12,13] and organic ligand surface layer naturally passivating unsaturated chemical bonds forming during QD synthesis in a solution comprised of special surfactants.[14] While the core is responsible for the main physical properties of the QD determined by its bulk crystal structure and the confinement effect, the surface layer perturbs these properties. Passivating ligands are fundamental for enhancing the solubility and reducing chemical reactivity of the QDs, while strongly affecting the electronic and spectroscopic properties of the materials. The high surface-to-volume ratio of QDs and imperfect surface passivation, mainly determined by various types of ligands and partial surface coverage, lead to impurities and defects. The latter adds the manifold of additional surface states and trap states to the electronic structure of the QD, as illustrated in Figure 1, and thus affects radiative and nonradiative decay, carrier trapping, and energy dissipation processes. Recent spectroscopic experiments have demonstrated that radiative quantum yield,[15] exciton lifetime,[16] and relaxation rates (rates of electronic energy conversion to heat)[15b,17] are strongly affected by the type of ligands passivating the QD surface. While much is known about the size-dependence of the QD properties due to quantum confinement,[3,7,18] considerably less is understood about the effects the surface morphology and passivation layer have on the photoexcited dynamics of QDs. Thus, the QD surface plays a critical role in defining the charge and energy transfer processes that govern light harvesting and conversion of light energy to electric current.[19] However, control of the surface chemistry of QDs in various technological applications is still limited.

1.3. Chemical Functionalization and Electronic Properties of Carbon Nanotubes

In contrast to QDs, SWNTs have an extremely chemically stable surface that is relatively weakly sensitive to the environment, due to the fully saturated sp^2-conjugated lattice of the graphene sheet, but many various topological perturbations and defects are still possible. For example, vacancy defects associated with the formation of a few five- and seven-membered rings appear in SWNTs upon high-energy electronic beam irradiation, which lead to significant changes in their electronic structure.[20] Advances in synthetic techniques were able to address early problems in the preparation of

DOI: 10.1021/acs.chemrev.5b00012
Chem. Rev. 2015, 115, 5929−5978

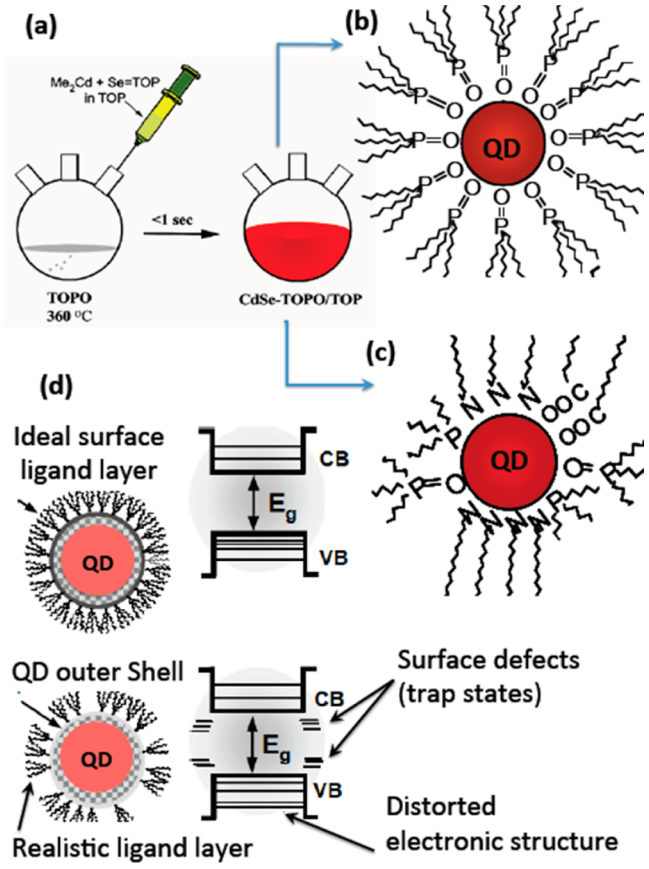

Figure 1. Schematic representation of the synthetic procedure (a) and chemical structure of colloidal quantum dots (QDs) with identical ligands (b) and different ligands (c) passivating the surface. (d) The electronic structure of ligated QDs illustrating the appearance of trap states due to imperfect surface passivation.

SWNT materials, such as chemical defects, tube bundling due to strong van der Waals interactions and uncontrolled inhomogeneous mix of different chiralities, orientations, and lengths of the tubes in a single sample. Highly purified single-chirality SWNT materials with well-defined surface coverage (such as DNA[21] or polymer wrapped[22] or covered by an organic surfactant shell[23]) were recently obtained[24] and experimentally studied.[25] This progress suggests many potential electronic SWNTs applications such as field-effect transistors[26] and biosensors,[27] light-emitting diodes (LED),[28] and solar cells.[29] Enabling any of these technologies would require full control over optical (e.g., light absorption and emission) and electronic (e.g., exciton and charge dynamics) properties. For example, the existence of optically forbidden "dark" states that lie below the lowest optically allowed bright state[30,31] and nonradiative recombination of freely diffusing 1D excitons at defect sites[32] are deterministic factors limiting fluorescence quantum yield of SWNTs to less than 10% (~1% in typical samples). To address the above issues, chemical doping by reactive small molecules,[33] such as diazonium salts,[34] atomic gold,[35] hydrogen,[36] and oxygen,[37] has been established. Such chemical functionalization potentially locally breaks conjugation by introducing sp^3-bonds, and thus changes potential energy landscape, resulting in the appearance of new emission bands and enhanced fluorescence efficiency due to a deep trap state below the tube excitonic bands.[38] This already implies the potential of chemical doping yet to be fully uncovered in future SWNTs studies.

1.4. Self-Assembly and Disorder in Conjugated Polymer Materials

Despite decades of work on the synthesis, characterization, and simulations of CP-materials, their intrinsic optoelectronic properties continue to generate considerable controversy and challenges due to highly disordered morphology of these materials and strong sensitivity of their photophysics to structural disorders.[39] Organic semiconductors have attractive electronic properties and low production costs that give them the potential to revolutionize electronic,[40] photovoltaic,[41] display,[42] sensing,[43] and lighting technologies.[44] Over the past decade, the first phase of organic electronics commercialization took place. For example, more than 2 million organic LED displays are now produced each month, with new organic-based lighting panels, thin film transistor circuits, solar cells, and chemical sensors becoming commercially available every year. Despite the development of sophisticated synthetic protocols, control of the materials packing and morphology remains challenging. This includes the complex interplay of crystalline, self-assembled ordered, and fully amorphous phases, and a variety of buried interfaces (e.g., interfaces in bulk heterojunction devices[45]). Unlike inorganic semiconductors, disorder in conjugated polymers is not typically associated with broken chemical bonds forming defects. Disorder in CP has two origins: Intramolecular conformations lead to variations in bond lengths, torsion angles, and the appearance of on-chain defects, whereas intermolecular interactions arise from morphology, chain alignment, and packing.[46] In films, CP-materials are typically self-organized into several distinct supramolecular structures, where crystalline domains are separated by less ordered or completely amorphous regions.[47] In the same CP-material, therefore, different concentrations of ordered and disordered domains are present.[48] While it is well-known that the energy and charge carrier mobilities are limited and subject to losses in CP materials due to disorder and "trap" states, it is extremely challenging to experimentally define the exact chemical and structural origins of the defects because of the microscopically heterogeneous morphology of CP films.[49] Additional challenges originate from oxidation on CP-film surfaces and chemical impurities.[50] All of these factors lead to vast differences in their photophysical and transport properties, which are challenging to control and improve in such highly disordered "soft" materials.[51]

1.5. Role of Computational Modeling toward Establishing Structure–Property Relationships in Nanostructured Materials

The examples above illustrate some of the efforts made to improve our understanding of the role of surface chemistry, structural disorder, and interfacial interactions in nanomaterials, which will allow for better exploration and utilization of the unique properties of QDs, SWNTs, and CPs in various technologies. Yet, gaining fundamental knowledge on functionalized nanomaterials, such as the effects of organic–inorganic interactions on morphology, electronic structure, and photodynamics in these systems, is still far from completion, impending applications of full their potential in efficiently working devices. Even the most thorough experimental characterization is unable to provide important information on many electronic and structural properties such as atomistic interfacial structure and energetic location of optically

DOI: 10.1021/acs.chemrev.5b00012
Chem. Rev. 2015, 115, 5929–5978

forbidden (dark) states. Theory, modeling, and simulation have all potentials to complement experimental advances providing interpretation of the data and extracting relevant information on photoexcitation, emission, transport, and decay mechanisms, which is vital for designing new functional nanomaterials and devices. Specifically, over the years, electronic structure calculations, such as density functional theory (DFT), had a transformational impact on materials science being able to describe the electronic structure and complex dynamics in molecules with hundreds of atoms.[52] Subsequently, this led to many modeling and simulation efforts aiming to predict physical phenomena and deliver a comprehensive theoretical framework on conformational structure, electronic properties, and light-driven processes in nanosystems, most of which we briefly review in the next sections.

However, there are multiple challenges awaiting the modeler in the realm of large nanostructured materials. The first difficulty arises from the computationally unmanageable number of atoms in the nanosystems of interest forcing compromises such as use of less accurate methods, simpler Hamiltonians, and smaller basis sets.[53] Notably, even defining an experimentally relevant system is frequently arduous because exact elemental composition, binding pattern, and conformational structure may be unknown. The necessity of sampling huge parameter space (e.g., exploration of a multidimentional potential energy surface (PES) for a given electronic state) constitutes another serious problem. Finally, the complexity and multiscale nature of electronic phenomena such as excitonic effects,[63] requiring accounting for electronic correlations (e.g., see recent review[54]), and complex photoinduced dynamics,[55] necessitating departure from Born−Oppenheimer approximation and treatment of electron−vibrational couplings (e.g., see review[56]), possess formidable challenges in modern first-principle computational techniques.

In this Review, we exemplify how electronic structure methodology based on DFT and semiempirical Hamiltonian models can be applied to QDs, SWNTs, and CPs materials and provide specific experimentally relevant predictions on the electronic structure, optical properties, and excited-state dynamics. We discuss in detail merits and limitations of each method and the validity of approximations used for describing specific properties and/or physical processes in these three distinct classes of systems, with a central focus on practical value of simulations. The topics of this Review span from obtaining ground-state geometries, to analysis of electronic structure calculations, to modeling spectroscopic data, to accounting effects of electron−vibrational coupling, and to simulating nonadiabatic excited-state dynamics and nonradiative relaxation processes. All model chemistry approaches considered here are exemplified on specific cases complementing synthetic fabrication and experimental characterization efforts allowing one to build structure−property profiles for a variety of nanomaterials, and aiming to determine their suitability for electronic, lighting, sensing, photovoltaic, fluorescent labeling, and optical amplifying applications.

This Review is organized as follows: Section 2 introduces basic theoretical methodologies and their performance for description of ground-state properties and structures. Section 3 outlines methods for calculating electronic excitations, optical spectra, and exemplifies their applications to several systems. Section 4 illustrates complex cases when electronic properties of nanosystems are affected by specific chemical functionalizations or conformational changes. Section 5 describes electron−vibrational phenomena and associated effects on the electronic wave functions such as excitation self-trapping. Section 6 delineates modeling of excited-state dynamics and nonradiative relaxation beyond Born−Oppenheimer approximation. Finally, section 7 presents our perspectives on the role of electronic structure modeling in nanomaterials and concludes. Out of the scope of this Review are a detailed description of theoretical methodologies (e.g., advancements in development of exchange-correlation functionals in DFT, methodologies for nonadiabatic dynamics simulations) and applications of ab initio wave function approaches targeting smaller systems.

2. GEOMETRY OPTIMIZATION AND GROUND-STATE ELECTRONIC STRUCTURE

The first step of any electronic structure calculations is obtaining reasonable and experimentally relevant geometries of molecular systems in the ground state. Although geometry optimization is a relatively cheap numerical procedure that usually does not require a high level of theory, obtaining geometries of extended systems with complex morphology and interfaces is a daunting task. The challenge frequently originates from the lack of periodicity/symmetry and large number of atoms (N) in the system, as well as uncertainty of the elemental compositions of surfaces and interface morphologies due to complicated organic−organic (e.g., CPs and SWNTs materials) and organic−inorganic (e.g., ligated QDs) interactions. This leads to very complicated ground-state PESs being a function of $3N$ nuclei coordinates. The PESs are the most challenging in soft materials like amorphous CPs: there are many distinct local potential minima where the system can be trapped depending on its initial configuration during the optimization procedure. Overall, depending on the type and size of the nanosystems, different methods may be chosen to get reasonable geometries and the electronic structure of the system.

2.1. Applicability of Force Field, Semiempirical, and DFT Methods

Among the oldest numerical methods for exploration of PESs and finding energy minima are Monte Carlo and classical dynamics techniques relying on force field (FF) calculations. Here, the quality of PES description relies on FF functions and parameter sets derived from experimental data and/or high-level quantum chemical calculations. Such parametrizations are well established for organic conjugated molecules (e.g., MM3 FF[57]) and biosystems (e.g., AMBER[58] or CHARMM FFs[59]), but are difficult to derive for complex systems and electronically excited states, making an accuracy of FF problematic for nanocomposites. Usually, the FF approaches are easily applicable to larger systems of 1000 and more atoms providing structural and dynamical information only (electronic properties are generally not calculated).

Electronic structure simulations typically rely on the Born−Oppenheimer approximation, where electrons adjust instantaneously to the slower motion of the nuclei. Consequently, the classical nuclear positions enter as parameters to the electronic Hamiltonian. The starting point of ground-state simulations, particularly attractive for large systems, is the Hartree−Fock (HF) approximation, where each electron moves in a mean field crated by the other electrons. Subsequently, electrons occupy single-particle states (molecular orbitals, MOs), and the results can be easily interpreted and analyzed. The ground state energy and the forces (i.e., the PES gradients) can be easily calculated in the variational Self-Consistent-Field (SCF)

DOI: 10.1021/acs.chemrev.5b00012
Chem. Rev. 2015, 115, 5929−5978

approach. In terms of molecular Hamiltonian, semiempirical all-valence approaches, such as Austin Model 1 (AM1[60]) or intermediate neglect of differential overlap (INDO[61]) models, are well-established methodologies for molecular systems consistent of more than 1000 of atoms. Notably, the use of semiempirical or tight-binding methods is strictly limited to the systems and quantities for which they were parametrized. For example, among newer well-parametrized semiempirical methods[62] with conjugated molecules in their training sets is PM7, showing universality and accuracy for geometries and formation energies (~10 kcal/mol). Notably, an accuracy of semiempirical methods is quite limited for atoms with d valence electrons effectively putting the majority of inorganic materials (e.g., QDs considered in this Review) beyond the reach of these simple approaches.

Another step up in computational complexity is DFT, currently the primary model chemistry approach for nanosystems we consider. The numerical cost of DFT calculations is moderately high, effectively limiting the range of treatable systems by $\sim 10^3$ atoms.[63] Overall, DFT retains the simplicity of the SCF framework and promises to attain an accurate result with refined exchange-correlation functionals. With years, more and more accurate DFT models were developed well beyond the Adiabatic Local Density Approximation (ALDA) and the Generalized Gradient Approximation (GGA) (e.g., BLYP and PBE models). Hybrid functionals[64] (e.g., B3LYP, PBE0, etc.) mix a fraction of orbital (HF) exchange and allow for spanning all intermediates between ALDA and HF limits. Recently developed long-range-separated density functionals including variable fractions of orbital exchange,[65] such as CAM-B3LYP, LC-wPBE, and wB97X, eliminate the spurious long-range self-repulsion intrinsic to ALDA and GGA. Finally, we mention the ionization potential (IP)-tuning procedure, allowing one to optimally fit the range-separation for a given molecular system[66,67] and the availability of empirical corrections for most DFT models to account for dispersive and noncovalent interactions.[68] We further direct the reader to several recent DFT overviews[52] providing comprehensive accounts on the progress in this field. We strongly emphasize that, for all practical applications, every DFT model serves as an effective approximate method being able to correctly describe only a specific realm of physical phenomena. Intent to only reproduce experimentally measured quantities frequently leads to incorrect interpretations (i.e., getting the right number for the wrong reason). Subsequently, some deep deliberations and literature study should be given on which DFT model is appropriate for a particular system/quantities to be modeled, before attempting any actual numerical simulations. In this Review, we will provide multiple examples why specific DFT models work and others fail for various molecular systems.

Finally, accounting for a molecular environment allows for more realistic and experimentally relevant simulations. The simplest way to study the effects of dielectric environment in static simulations is to use a Polarizable Continuum Model (PCM[69] or simpler conductor-like screening method (COSMO[70]) alternatively called the conductor-like PCM (CPCM[71,72])) with an appropriate dielectric constant. In dynamical simulations (see sections 5 and 6), an empirical thermostat model[73] (e.g., Langevin thermostat[74]) is useful to model thermal bath effects. Finally, rapidly developing Quantum Mechanics/Molecular Mechanics (QM/MM) methodologies[75] potentially can address both issues on a more accurate level by interfacing quantum mechanical representation of the solute and FF description of solvent on the atomistic level.

In terms of computational codes, commonly available packages generally use either localized Gaussian (or the Slater type) basis sets or a plain wave basis. The former is typically applied to finite molecules and, to a lesser extent, to periodic systems, whereas the opposite is true for the latter. Among software particularly suitable for calculations of large molecular systems, available options include but are not limited to Gaussian,[76] Q-Chem,[77] Turbomole,[78] ADF,[79] GAMESS[80] (all are based on localized basis set), as well as VASP[81] and NWChem[82] (botn are using plain wave basis set) ab initio suites, and the semiempirical MOPAC[83] package. The compatibility and accuracy of most of these program packages in applications to small organic molecules has been discussed in ref 84.

2.2. An Interplay of σ- and π-Bonding in Carbon-Based Systems

2.2.1. Conjugated Polymers and Oligomers. We start our discussion with a brief description of modeling of ground-state geometries of conjugated oligomers, which has been perfected for decades using various theoretical approaches.[85] The conjugated backbone is a scaffold of σ-bonded atoms holding polarizable π-electronic system. By elongating the oligomer length, it is possible to asymptotically approach the infinite chain polymer limit.[8,86] For practical purposes to reduce numerical expense, it is frequently common to replace nonconjugated side groups (e.g., alkyl chains) with hydrogens or methyl groups.[87] The degree of electronic delocalization of π-electronic system is a defining factor for optoelectonic properties of the material. It can be characterized using one geometric descriptor, the bond length alternation (BLA) defined as the alternation of carbon−carbon bond length along the backbone of the polymer.[88] Likewise, a torsional angle between repeat units is another useful descriptor quantifying the extent of π-conjugation and predicting the degree of localization of distortion in conjugated molecular chains.[89] Both BLA defining π-electronic dimerization along the chain and torsional potential enter as empirical parameters in the simplest π-electron Pariser−Parr−Pople (PPP) Hamiltonian.[90] All valence electron semiempirical models (such as AM1) are able to describe these two geometric parameters relatively well without additional fitting. In fact, calculations of π-conjugated oligomers[85,91] provide a standard example of successful applications of semiempirical methods.

Being a good compromise between computational cost and accuracy, DFT is currently broadly used for CP-materials. In particular, IP-tuned modeling is quickly gaining popularity as a quantitative method.[92] It is instructive to follow how the BLA and torsional angle change for equilibrium geometry when varying the DFT model:[93] the smallest (largest) BLA and torsion angle are obtained at ALDA/GGA (HF) limit.[94] Thus, an increase of orbital exchange in the functional leads to a continuing transition from delocalized to localized π-electrons. Sections 3 and 5 provide more detailed discussion on the importance of orbital exchange in the DFT model for various electronic excitations. While DFT and semiemirical calculations of individual oligomers became a standard, application of these methods to bulk CP-materials (such as amorphous aggregates and crystals) remains very challenging due to the inability of simple methods to account for dispersive interactions (London

DOI: 10.1021/acs.chemrev.5b00012
Chem. Rev. 2015, 115, 5929−5978

forces) and the uncertainty of materials packing spanning very large conformational space (see our discussion in section 4).

2.2.2. Single-Wall Carbon Nanotubes. Because of multiple similarities in electronic structure and bonding, most of the electronic structure techniques used for CP oligomers are formally transferrable to SWNTs, which are much larger systems: SWNTs used in experiments typically have lengths of hundreds of micrometers, while their diameter is a few nanometers. This large length-to-diameter ratio allows for applying periodic boundary conditions (PBC) to treat SWNTs as infinitely long quasi 1-D objects[95] and, thus, reduce computational cost. However, DFT applications in this case are still numerically expensive, limiting calculations to narrow-diameter SWNTs with small unit cells containing only 10−100 atoms.[53,107] Zigzag tubes with a zero chiral angle have the smallest unit cells. Therefore, many DFT calculations reported in the literature are focused on this type of SWNTs,[96] although zigzag tubes are not the main focus of experimental studies. In calculations with the periodic boundary conditions, it is convenient to use the plane wave basis[95a,b,97] set, although Gaussian orbital bases were used as well.[95c,98] Among different functionals, numerically efficient GGA models have been used the most.[95a,b,97] To offset numerical cost, many investigations of SWNTs have invoked empirical tight-binding approximations.[99] However, it was shown that hybridization of the σ- and π-states of the graphene network is important for band-folding effects in small radius SWNTs and has to be included into the tight-binding model; otherwise, tubes predicted to be semiconducting can be metallic, instead.[100]

In contrast to solid-state like approaches being standard in the field, SWNTs can be also considered as a large molecule. With this approach,[38,101] one models finite size SWNTs with the length (e.g., ∼10 nm) to be significantly larger than the tube diameter and a typical spatial extent of the excitonic or polaronic wave functions experimentally detected to be in the range of 2−3 nm.[102] Therefore, such "molecular-type" calculations are expected to reproduce the basic properties of longer SWNTs and to be, at least, qualitatively consistent with the infinite-size limit. For example, the π-election PPP Hamiltonian has been utilized for geometry and the electronic structure calculations of various chiral tubes of finite lengths.[103] To account for valence electrons, one needs to cap unsaturated chemical bonds at the open tube ends with hydrogens, as described in detail in ref 101a. Such capping allows for eliminating the midgap states caused by dangling bonds. One advantage of the finite length SWNTs use is a convenient modeling framework for many extrinsic factors such as inhomogeneity of the local dielectric environment,[104] structural conformations,[101c,d] and defects[38,101f] and functionalization.[105] Overall, due to rigid geometry, the electronic structure of SWNTs is expected to be weakly dependent on the method used for geometry optimization.[104,106] In particular, AM1 reproduces the curvature-mediated σ- and π-interactions and the relevant vibrational effects at reduced computational cost enabling geometry optimizations of the SWNTs with up to 1000 atoms in size.[63c,101a−c,h,106]

The obtained geometries can be further used at the level of DFT and TD-DFT for calculations of electronic and optical properties of SWNTs at single point. Such a finite-tube approach has already successfully resulted in a number of studies addressing electronic properties of SWNTs from a very different perspective as compared to approaches using periodic boundaries. This includes quantification of exciton−phonon couplings and Huang−Rhys factors,[101a,b] predictions of the Peierls distortion and exciton self-trapping,[101c] characterization of delocalization of excitonic transitions,[101h] study of transverse polarized absorption in nanotubes,[101g] energetics of dark states,[104] and a violation of Franck−Condon approximation in SWNTs.[101d]

2.3. Quantum Dots: Shapes, Bonds, and Ligand Binding

Even after decades of research, precise atomistic structure and chemical functionalization of QD surface by ligands is still generally unknown, necessitating approximations for theoretical methods. Early approaches modeled the QD surface as an infinite potential barrier around the dot. Adopting this approximation of the QD's surface, the electronic structure is easily obtained by describing the electronic wave function of the QD as a product of Bloch functions, capturing bulk properties, and an envelope function representing solution for an electron with an effective mass in a spherical well, so-called effective mass approach.[18,107] More sophisticated models of QDs have represented the QD core through the bulk atoms using semiempirical tight-binding[108] and pseudopotential[109] approaches, while the passivating molecules have been modeled through either single oxygen atoms[108a] or simplified model potentials.[110] Any realistic model, however, has to explicitly describe bonding between the QD and the ligands, which is lacking or not complete in the semiempirical pseudopotential-based approaches. Several attempts have been done to model ligated CdSe QDs using force field,[111] Monte Carlo,[112] and coarse grained[113] methods. These methods, however, are based on a model description of the molecular framework and interactions. Such parameters are unavailable from measurements, putting the justification of these approaches under scrutiny. To overcome this problem, the model parameters are typically derived from DFT calculations or higher level theories for smaller clusters.[58]

2.3.1. Models of Magic Size Nanocrystals. First-principle quantum-chemical methods, such as DFT, are able to describe bonding, QD−ligand interactions, and the electronic structure with a reasonable level of accuracy. Unfortunately, DFT is numerically expensive, limited to maximum QD sizes of 2 nm, as compared to 2−10 nm systems typically in the focus of experimental studies, as reviewed in ref 114. The situation is rapidly changing with recent introduction of stable synthetic routes for realization of very small (1−2 nm size-range) CdSe, CdS and PbSe, PbS nanocrystals,[115,116] allowing for direct comparison between DFT results and experimental data. Therefore, in this Review, we mostly focus only on these types of QDs. For example, "magic-size" structures of Cd_nSe_n with n = 19, 33, 34 have been resolved recently by means of mass spectroscopy with the majority of $Cd_{34}Se_{34}$ observed in samples.[115] Small, magic-size PbSe and PbS QDs have been also observed experimentally.[117] All magic-size nanocrystals demonstrate good photostability and high quantum yield. Therefore, most of the DFT calculations are focused on models of small (1−1.5 nm) magic-size bare CdSe,[112,118a] Si,[118b] and PbSe[119] QDs, which initially hold their bulk symmetry. Size-wise, clusters with the stoichiometric structure A_nB_n (A = Cd, Zn, Pb..., B = Se, Te, S, ..., and n = 4, 6, 11, 13, 19, 33, 34) have been computationally explored most intensively.[120] For example, recent exhaustive DFT computations of conformational structures of CdSe and ZnS clusters with sizes up to 1.5 nm have addressed shapes of small QDs:[112,121] Small molecules are predicted to have

DOI: 10.1021/acs.chemrev.5b00012
Chem. Rev. 2015, 115, 5929−5978

spheroids and tubular shapes (n = 6, 8−12, 15−19), whereas the larger systems adopt wurtzite (n = 23−27, 36, 37) and cage-core (n = 13, 29−35) structures. To reduce the computational cost of DFT calculations, the core atoms of QDs can be simulated using bulk structures, while dangling bonds on the surface may be artificially terminated with covalently bonded hydrogen ions.[122] For example, this DFT-based approach within PBE functional and the plane wave basis set have shown excellent agreement with the results of cyclic voltammetry measurements of the size quantization effect on the HOMO−LUMO gap of CdTe QDs.[123] Overall, this approach allows for accurate modeling of the confinement effect in QDs. However, the description of a surface chemistry of QDs is beyond this method.

2.3.2. Simulations of Surface Capping. Direct incorporations of ligands to the DFT calculations have been done for various CdSe,[119c,124] CdTe,[125] and ZnS[126] nanostructures with the diameter smaller than[120b,125b] or equal to[112,124b] 1.5 nm and with one[127] or more[124a,b,125a] capping ligands adsorbed on the surface. Structural models used in these calculations are illustrated in Figure 2. However, computational results might

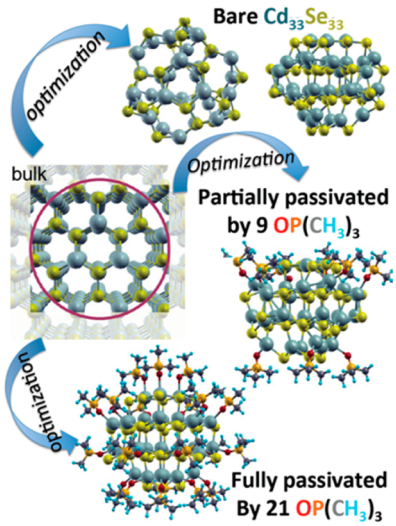

Figure 2. Structures of the simulated $Cd_{33}Se_{33}$ QDs constructed from the ideal CdSe bulk crystal after optimization in the absence (top) and in the presence of surface ligands, $OP(CH_3)_3$, with a full passivation of each surface Cd ions (bottom) and a partial passivation of only 2-coordinated cadmiums (middle). Optimized structures were obtained from DFT calculations using PBE functional and plane wave basis set within ultrasoft pseudopotentials, as implemented in VASP software, used in refs 124a and 124b.

be sensitive to the methodology, including DFT model and the basis set used for calculations. Systematic studies of dependence of the QD-ligand binding energy, bond length, electronic structure, and the lowest excitation energy on the choice of basis sets and functionals have been reported for small CdSe clusters of a few atoms in size[120d,128] and larger CdSe QDs of 1.5 nm in diameter[129,130] interacting with a single ligand molecule. Dielectric media effects have been also discussed within the PCM framework.[112,124b] It was found that inclusion of a polar solvent has a dramatic effect on the QD−ligand binding, decreasing the interaction more than twice as compared to vacuum calculations.[129] This is rationalized by the polar character of both QD and ligand structures, whose dipole moments are getting screened by the solvent environment. Consequently, incorporation of the solvent into the calculations is absolutely necessary to obtain realistic QD−ligand interactions.

2.3.3. Benchmarking DFT Methods for Quantum Dot Systems. Overall, the main conclusion of all reported studies on benchmarking DFT methodology in application to QD systems is that, depending on the specific physical properties that are modeled, a specific functional/basis set combination has to be chosen for proper simulations of the ligated QDs. For example, both geometries and QD−ligand binding energies computed for the ligated CdSe cluster are strongly dependent on basis set size: the binding energy generally decreases with increasing basis size.[129] According to ref 129, inclusion of polarization functions at least to the part of the basis set associated with ligand atoms is crucial for obtaining these properties with a reasonable accuracy. This statement was further extended in ref 128, where it was evaluated that among the localized Gaussian-type basis sets with effective core potentials (ECPs) allowing for calculations of heavy elements of the periodic table, the def2-TZVP provides the best accuracy for the ground- and excited-state properties, as well as for structural characteristics, as was tested for A_6B_6 clusters (A = Cd or Zn and B = S, Se, or Te). To reduce computational effort, the SBKJC or even def2-SV(P) are the next basis set options providing a reasonable description of the QD/ligand systems.[128]

As for DFT functionals, ALDA models overestimate the QD−ligand interactions and underestimate the length of Cd−Se and Cd−O bonds in ligated QDs.[129] However, semilocal GGA functionals, in particular PBE,[128] have been found to provide satisfactory results for geometrical structures[124a,129] and vibrational frequencies,[131] but perform rather poorly for excitation energies.[128] Long-range asymptotically corrected functionals, such as CAM-B3LYP and LC-wPBE, provide Cd−Se and Cd−O bond lengths in $Cd_{33}Se_{33}$ QDs capped by phosphine oxide ligands similar to those results of higher-accuracy CCSD theory applied to smaller clusters of a few atoms in size,[120d] but they strongly blue-shift optical transitions as compared to reference energies.[124a,129] The hybrid PBE0 (or PBE1) is the best performing model both for the geometry and for the electronic structure properties.[128,129] Other well-behaved functionals usually include a small portion of HF exchange (not more than 30%) and, in some cases, also the kinetic energy density, like M05 and TPSSh.[74]

In principle, computational packages implementing periodic boundaries and plan wave basis can be efficiently used for DFT modeling of finite size QDs. For example, in many studies,[118a,119a,b,123,124,132] the structures of QDs were initially constructed from the bulk lattice and then relaxed to its lowest energy configuration using GGA functionals in VASP software. To prevent spurious interactions between periodic images of the QD, the calculation cell is constructed to have 8−10 Å of vacuum between the QD replicas. On the basis of the optimized structures, to explore electronic structure, a single-point DFT/time-dependent DFT simulation can be carried out using more accurate hybrid functionals[124a,b] to minimize computational cost. In fact, many investigations observed that the ground and excited states are well reproduced even when the electronic starting structure calculation comes from a functional different from the one used to optimize the QD's geometry.[128,129,133]

DOI: 10.1021/acs.chemrev.5b00012
Chem. Rev. 2015, 115, 5929−5978

3. CALCULATIONS AND ANALYSIS OF ELECTRONIC EXCITATIONS

An electronic excitation is a transition of a system to another electronic state higher in energy than the ground state and, in the context of this Review, is frequently referred to as an excitonic transition. An exciton is a bound state of an electron and a hole created, for instance, by photoexcitation or by electrical charge injection. Perhaps, the simplest illustration of this concept would be the HOMO−LUMO transition; however, such description completely misses an electron−hole interaction or many-body correlation effects beyond the mean-field approximation. The majority of molecular examples here have a singlet ground state. Subsequently, all excitons considered are either singlet or triplet spin states (multiple exciton excitations, which may adapt higher spin states, are beyond the scope of this Review). Besides excitons, other examples of significant electronic excitations are charged states, anion (or negative polaron) and cation (or positive polaron) being doublet spin states. Again, multiply charged systems with higher spin states are not considered here. These excitonic and polaronic states are the main energy and charge (spin) carriers, respectively, in all materials/devices composed of QDs, SWNTs, and CPs. Needless to say that an accurate description of these electronic excitations is a primary goal in the majority of quantum-chemical investigations of these systems.

3.1. ΔSCF and Time-Dependent SCF Methods for Simulations of Electronic Excitations

The simplest and frequently sufficiently accurate way to calculate electronic excitations is to use the so-called ΔSCF approach, where the desired state (e.g., triplet or polaron) is computed using the SCF variational framework subject to an appropriate constrain such as spin and/or charge.[134,135] Subsequently, its properties such as excitation energy and charge density are obtained as a difference between the reference (e.g., ground state) and the target state. Such simulations are similar to the ground-state calculations providing a numerically inexpensive path toward equilibrium geometries and other quantities of interest for electronic excitations. Similar ΔSCF ideas have recently led to the development of the constrained DFT (CDFT) method,[136] providing a robust and numerically efficient way to compute the lowest charge-transfer states of the complex (here constrain is a specific spatial charge separation between components of the system). Notably, the ΔSCF approach becomes numerically impractical when several electronic excitations of the same type need to be calculated (e.g., manifold of singlet or triplet states). Such manifolds are easily calculated and interpreted as transitions between single-particle hole- to electron-states (molecular or Kohn−Sham (KS) orbitals) provided by the ground-state SCF calculations. However, orbital relaxation effects and many-body electron−hole interactions are absent in the latter description. Nevertheless, this approach is still at least qualitatively adequate for systems with small excitonic effects (e.g., see our discussion in section 3.1 on QDs). Correlated excited-state calculations are more involved as compared to the ground-state calculations as exemplified by an enormous body of work done in the realm of ab initio wave function theories.[137,138]

Among simple and practical techniques able to account for excitonic effects are the Configuration Interaction Singles (CIS) and the time-dependent HF (TD-HF) theory,[63a,b] which have been widely applied to molecular modeling. For example, coupled with simplified semiempirical Hamiltonian models (e.g., PPP or Zerner's INDO, ZINDO), these methods have been routinely used to calculate electronic excitations of large molecular systems at a significantly reduced computational cost for many years.[85a,91] More than a decade ago, the TD-HF technique was extended to the more general hybrid HF/DFT models, and the time-dependent SCF (TD-SCF) method, which spans the range between adiabatic time-dependent DFT (TD-DFT) and TD-HF limits, has emerged.[139] This approach deals only with the one-electron density matrix, and has become a workhorse for the computation of excited-state properties in nanosized materials and solids.[140] Advances in the development of new density functionals have, so far, continuously improved accuracy in the computation of electronic excitations in molecular materials. Solution of the TD-SCF equations in the frequency-domain leads to the Random-Phase Approximation (RPA) eigenvalue problem.[141] Effective Krylov subspace algorithms and iterative techniques are able to efficiently calculate the portion of the eigenspectrum of the RPA matrix necessary for modeling electronic excitations and optical response. Such diagonalizers[139b,142] became common in nearly all modern quantum-chemical codes, generally reaching $O(N^2)-O(N^4)$ size scaling for excited-state calculations. Moreover, numerically efficient analytical gradients are available in TD-SCF techniques, allowing one to exploit the excited-state PESs and to optimize their geometries. Both singlet and triplet excitonic states can be obtained using the TD-SCF approach based on the reference singlet ground SCF state.[140b,142a] Excited states of polarons can potentially be obtained as well by starting from the respective reference charged ground state; however, currently the TD-SCF methodology for an open-shell reference state is not yet well established and is a subject of intense development.[143,144] Additionally, using periodic boundary conditions for TD-SCF methodology remains problematic particularly in the cases when the Hamiltonian/functional includes long-range orbital exchange.

Notably, there are multiple pitfalls when using the TD-SCF methods to calculate large systems. The results are strongly dependent on the underlining electronic Hamiltonian or DFT model. Among possible issues we mention a few: Being a single-reference method, generally the TD-SCF approach is unable to calculate highly correlated electronic states (e.g., so-called double excitations).[145] TD-SCF calculations based on DFT functionals with a large fraction of orbital exchange can severely underestimate energies of triplet states (the so-called triplet instability).[146] TD-SCF calculations based on the ALDA/GGA models and even functionals with a small amount of orbital exchange (e.g., B3LYP, PBE0) frequently lead to unphysical low-lying charge-transfer states.[147] While discussion of wave function methods remains beyond the scope of this Review, we emphasize importance of the comparisons of results obtained using "simpler" methods (such as ΔSCF or TD-SCF) with high accuracy ab initio approaches (for example, the GW approximation and Bethe−Salpeter Equation (BSE),[53,148] coupled cluster,[137b] or configuration interaction (CI)[149] and multiconfigurational self-consistent field (MCSCF)[120a,150] methods) for small reference molecules. Having said that, we further notice that a good performance achieved for small molecules is not always transferrable to the world of large systems, potentially featuring a different set of physical phenomena. Along with benchmarks against available experimental data, such comparisons provide confidence in the use of

DOI: 10.1021/acs.chemrev.5b00012
Chem. Rev. 2015, 115, 5929−5978

a specific approach and facilitate further methodology development (e.g., better density functionals).

For instance, comparison of absorption and emission spectra likely provides the easiest link between computational results and experimental data. Typically TD-SCF (or any other approach for excited-state calculations) produces a set of transition energies between the ground and electronically excited states ω_n with corresponding oscillator strengths f_n (e.g., in a single-particle approximation to the excited states, transition energies are transitions between molecular or Kohn−Sham orbitals). In the case of large molecular systems, calculation of vibrational effects (see section 5) can be numerically intractable, and excited-state manifold is typically very dense. Subsequently, Gaussian

$$A_G(\omega) = \sum_n f_n \exp \frac{-(\omega_n - \omega)^2}{\sigma^2} \quad (1)$$

or Lorentzian

$$A_L(\omega) = \sum_n \mathrm{Re}\left[\frac{f_n}{\omega_n^2 - (\omega_n + i\sigma)^2}\right] \quad (2)$$

line shape[151] with an empirical line-broadening parameter σ (which is typically in the range of 30−100 meV, depending on experimental conditions) can be used for a crude evaluation of theoretical absorption profiles.

Likewise, ionization potential (IP) and electron affinity (EA) provide important electronic characteristics relevant to molecular response to charging and functionality of the system in the device environment. These quantities can be evaluated as a difference between total energies of neutral (0) and charged (+ or −) states using the ΔSCF results:[94]

$$\mathrm{IP} = E(+) - E(0) \quad \text{and} \quad \mathrm{EA} = E(0) - E(-) \quad (3)$$

Notably, IP and EA can be also crudely evaluated from the HOMO and LUMO orbital energies (Koopmans theorem),[149] subject to multiple approximations, particularly in the DFT case.[152]

Finally, we note that both ΔSCF or TD-SCF are operating with single-electron density matrices defined as

$$\rho_{\alpha\beta}^{mn} = \langle \psi_m | c_\alpha^+ c_\beta | \psi_n \rangle \quad (4)$$

where ψ_m and ψ_n represent global electronic states (n, m = 0,1,2...), α and β denote the basis functions, and $c_\alpha^+(c_\alpha)$ are the Fermi annihilation (creation) operators for the αth basis set orbital. These quantities are generally sufficient for calculating experimental observables and convenient for analyzing the underlining electronic properties. For example, ground $\rho_{\alpha\beta}^{gg}$ and excited $\rho_{\alpha\beta}^{nn}$ state density matrices contain information on charge density distribution and chemical bonding, whereas ground-to-excited-state transition density matrices $\rho_{\alpha\beta}^{gn}$ define the respective dipole moments (and oscillator strengths f_n) and reflect changes in the density matrix upon transition to another electronic state.[31,153] Decomposition of $\rho_{\alpha\beta}^{mn}$ into natural orbitals is a handy orbital analysis tool, for example: natural bond orbitals (NBO) for chemical bonding,[154] natural orbitals (NO) for unpaired electrons in charge and triplet states, and natural transition orbitals (NTO) for electron and hole orbitals in excitonic states.[155]

3.2. Single-Electron versus Many-Electron Approaches to Excitations in Quantum Dots

We start our discussion with QDs because excitonic effects are expected to be weak in bulk inorganic materials: large dielectric permittivity and large exciton Bohr radius result in strong screening of the Coulomb interaction between an electron and a hole. For example, the binding energies of bulk exciton in CdSe and CdS are 12 and 28 meV, whereas the respective Bohr radii are 55 and 25 A.[3,156] Indeed, the excitonic effect is stronger in QDs (~0.8 eV in 1.5 nm CdSe QDs[109b]) than in bulk semiconductors due to strong confinement of an electron−hole wave function.[157] However, it still can be considered as a small perturbation to the energy gap of QDs, because the confinement energy (~$1/D^2$) is much larger than the electron−hole Coulomb energy (~$1/D$) in 1−5 nm (D < 10 nm) QDs.reports that have appeared relatively recently[109] Such dependence for CdSe QDs and comparison between computational and experimental values has been presented and discussed in ref 109b and is illustrated in Figure 3A. Deviations between computational results (black squares and purple circles in Figure 3A) and experiment-based values (diamonds, triangles, stars, and plus symbols in Figure 3A) for small size QDs are associated with high surface to volume ratios in small QD resulting in dominating effects of surface defects on their optical properties, which are not included in the computational models.[109] Comparison of these data with a simple perturbative approach demonstrates that in the strong confinement regime the electron−hole Coulomb energy is well reproduced by a perturbative approach.[109c]

Subsequently, representation of the excited state as an excitation of an electron from an occupied to a virtual single-particle KS orbital is a valid zero-order approximation for simulations of optical spectra of ligated QDs with and without surface defects, being computationally much cheaper than the CI or TD-DFT simulations. The latter quickly become numerically expensive for QD systems containing more than 100 atoms. As compared to the TD-DFT treatment of organic molecules, where simulations of systems with several hundred atoms are feasible, in QDs computational cost rises due to two factors: the presence of transition metals and heavy elements (such as Cd, Pb, Te) requiring extended basis sets[129] and the necessity of computing many excited states (>100) to describe multiple absorption peaks in the UV−vis region of experimental relevance.

In refs 124a,b, the effect of many-body correlations on the optical response of the bare and ligated CdSe QDs has been evaluated by comparing absorption spectra obtained by a single-particle KS orbital approach and a TD-DFT methodology. While correlated methods such as TD-DFT produce better agreement with the experimental data, a single-particle KS approach to the excited state in QDs describes the main features of absorption spectra of QDs qualitatively well. Figure 3B exemplifies this conclusion for absorption spectra of $Cd_{33}Se_{33}$ cluster, bare (unpassivated) and passivated with amines. All calculated low-energy optical transitions (2.5−4 eV) are dominated by the QD character and are reasonably well described by the single-particle approach: a uniform blue-shift of transition energies by about 0.3 eV is observed, while the shapes and profiles of the spectra coincide with those obtained by TD-DFT calculations.[124a,b] Notable is that the 0.3 eV shift does not necessarily measure the exciton binding energy; this shift results from an interplay of many factors, including orbital relaxation, exchange, Coulomb interactions, etc. We also

DOI: 10.1021/acs.chemrev.5b00012
Chem. Rev. 2015, 115, 5929−5978

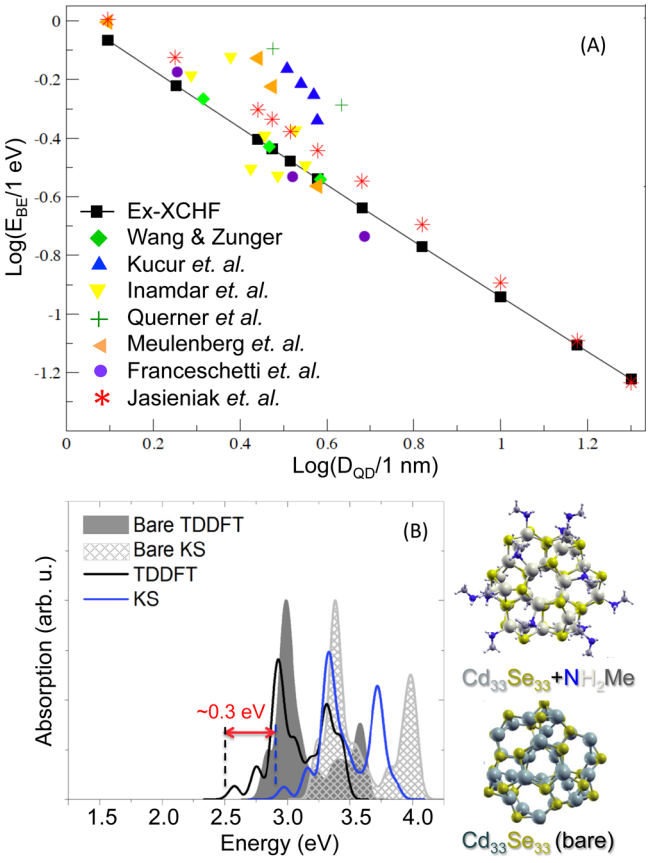

Figure 3. Excitonic effect in QDs. (A) Dependence of log of the binding energy on the log of the diameter of CdSe QDs computed with the electron–hole explicitly correlated Hartree–Fock (eh-XCHF) method. Computational values (squares and circles) are compared to experimental data. Reprinted with permission from ref 109b. Copyright 2013 American Chemical Society. (B) Optical spectra of $Cd_{33}Se_{33}$ QD fully passivated by amines (lines) and nonpassivated, bare (shaded area) $Cd_{33}Se_{33}$ calculated using TD-DFT (black line and filled gray) and single-particle KS approaches (blue line and pattern gray). Aside from a systematic blue-shift, the single-particle KS results are in good agreement with the TD-DFT method, reproducing the main spectral features, including near-gap small peaks. In both approaches, B3LYP functional and LANL2DZ basis set are used within Gaussian 09. Reprinted with permission from ref 124b. Copyright 2012 Royal Chemical Society.

emphasize ligand effects on the spectra causing modifications of similar magnitude[124b] (see Figure 3B). An accuracy of the single-particle approximation is expected to further improve for optical spectra of larger dots featuring less electron–hole correlations, as can be seen in the log–log plot of the exciton binding energy versus the QD diameter shown in Figure 3A. Nevertheless, one should always carefully scrutinize the applicability of such simple approach,[122b] particularly when considering excited states of nature different from QD–QD (such as surface states and QD–ligand transitions).

Thus, the majority DFT studies of QD excited states and optical spectra have been performed using a single-particle approximation[118a,119a,b,132,158] along with fewer TD-DFT reports that have appeared relatively recently.[120,125] Usually, hybrid functionals (with 20–30% of orbital exchange) and local basis sets with effective pseudo potentials for core electrons have been used for such calculations.[120,125] These methods typically adequately account for many-body dynamical correlation effects in the ground-state description. Long-range corrected functionals known for their overcorrecting nature of the exciton interactions typically result in optical transition energies of QDs systematically blue-shifted as compared to the reference data.[128,129] It is well understood that the portion of the orbital exchange used in the DFT changes the optical gap: the larger is the HF exchange portion, the larger is the gap. Such tunability generally allows for matching the calculated and experimental energy gaps. Nevertheless, the spectral shapes across many hybrid functionals remain roughly the same. For example, despite a blue shift in the energy due to a high portion of the HF exchange, the CAM-B3LYP functional has been shown[119c,159] to provide qualitatively similar results to hybrid functionals such as PBE0 and B3LYP. The latter models are usually able to accurately reproduce optical spectra of individual CdSe[112] and PbSe[117] QDs.

3.3. Excitonic Effects in Conjugated Polymers and Carbon Nanotubes

The situation is different for SWNTs and CPs, where due to 1-D confinement and small dielectric constants, a photoexcited electron–hole pair is strongly interacting forming an exciton with large binding energy (~0.5 eV) compared to the energy gap (1.3–2.5 eV). This makes a profound impact on all optical and electronic properties of the system. Therefore, excitonic effects can neither be neglected nor treated as a small perturbation in these materials, in contrast to the semiconductor QDs (see ref 55a for more detailed discussion). More than 2 decades ago numerous experimental and theoretical studies[160] have established a fundamental excitonic character of excited states in CPs. Early theoretical approaches based on the semiempirical methods (e.g., PPP or ZINDO Hamiltonians) and CIS approximation were able to reproduce excitonic phenomena reasonably well.[160a,161] Modern TD-DFT simulations have a luxury of choice among hundreds of functionals exhaustively spanning parameter space between the ALDA and HF limits to improve agreement with experiments. In this Review, out of the broad variety of CP materials, poly(*p*-phenylenevinylene) (PPV) and its derivatives have been primarily chosen for computational examples, as these prototypical polymer backbone structures have undergone the most complete study, while remaining a promising choice for various optoelectronic applications (see the recent review in ref 47a). Many experimental[162] and theoretical studies[163] have highlighted the dependence of electronic properties of PPVs on the interchain interactions[164] and intrachain conformational disorder, including distributions in torsional angles and defects.[165] It is instructive to illustrate a dramatic effect of the HF exchange in the functional on the excitonic properties following ref 166. The electron–hole interaction can be interpreted as a competition between a long-range Coulomb attraction induced by HF exchange and local strong repulsion brought by the ALDA component, as illustrated in Figure 4. The size of the exciton and, therefore, an effective Coulomb attraction between an electron and a hole depend on the amount of the HF exchange in the functional. Figure 4 (top) emphasizes this attraction–repulsion interplay by showing variations of the TD-DFT optical gap and the HOMO–LUMO gap for small and large PPV chains as a function of the Hamiltonian model.[166a] The band gap energy is smaller than the HOMO–LUMO gap for both molecules in the HF method because an effective electron–hole attraction stabilizes the HOMO–LUMO gap, which corresponds to noninteracting

DOI: 10.1021/acs.chemrev.5b00012
Chem. Rev. 2015, 115, 5929–5978

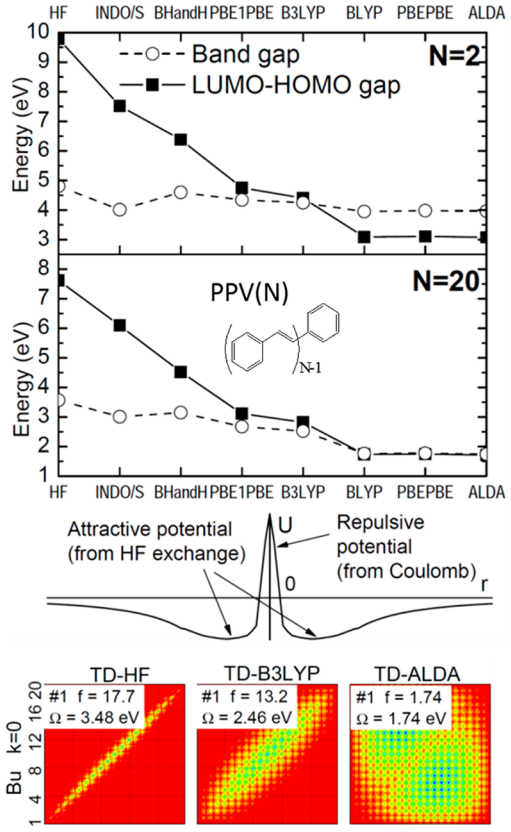

Figure 4. Top: Variation of HOMO−LUMO gap and band gap energies as a function of density functional in short, PPV(2), and long, PPV(20), oligomers, which mimic confined and infinite chain limits, respectively. The inset shows the structure of poly(*p*-phenylenevinylene) (PPV). The middle panel schematically shows an effective potential between an electron and a hole in the hybrid TD-DFT case. Bottom: Contour plots of transition density matrices from the ground state to low-energy excited states in PPV(20). The insets give corresponding state number, oscillator strength, and transition frequency. The axis labels represent individual repeat units along the oligomer chain. The color code is given at the bottom. Each plot depicts probabilities of an electron moving from one molecular position horizontal axis to another vertical axis upon electronic excitation. The amplitudes scale from red (0) to violet (1) through the natural rainbow color sequence. Reprinted and modified with permission from refs 166a and 166b. Copyright 2007 American Institute of Physics and 2005 American Physical Society.

particles. In contrast, the situation is opposite in ALDA and GGA models in the small (N = 2) molecule due to electron−hole repulsion. In the large (N = 20) chain, when an electron and a hole can be well separated and their localized repulsion is no longer relevant, the band gap asymptotically coincides with the HOMO−LUMO gap (a typical property of TD-DFT in solids).

The excitonic properties can be conveniently followed by examining the structure of transition density matrices for respective electronic states in the real space, Figure 4 (bottom).[165b,166a] Here, the axes of the plots can be interpreted as coordinates of an electron and a hole. Consequently, the diagonal of the plot reflects the position of the exciton's center of mass, whereas the off-diagonal extent defines the distance between these two particles.[85a] Figure 4 (bottom) shows such plots for the lowest $1B_u$ singlet state in PPV(20). It is clear that pure TD-ALDA and TD-HF methods roughly represent two extreme cases of unbound Wannier−Mott and tightly bound Frenkel excitons, respectively, whereas the B3LYP model recovers an intermediate case. Previous theoretical and experimental studies have unambiguously shown that conjugated polymers belong to an intermediate class, which can be described by hybrid functionals spanning ranges between HF and ALDA extremes. For example, the exciton size in PPV is about 6−7 (B3LYP), 5−6 (PBE0), 4−5 (BHandH or CAM-B3LYP), 3−4 (LC-wPBE), 1−2 (HF), 4−5 (ZINDO), 4−5 (GW approximation)[85a,c,165b,166a] repeat units, given the uncertainty of conformational disorder and interchain interactions as discussed in section 4. Binding energy of the lowest $1B_u$ singlet exciton was evaluated to be about 0.4−1 eV depending on the system and theoretical or experimental method.[160b,167] Other excitons such as triplet and high-energy states have been broadly explored in spectroscopic and theoretical studies of CP over the past decades. Recently developed IP-tuning procedure provides a possible guideline toward nonempirical choice of the DFT model for excited-state calculation.[92a]

An exciton is an example of a quasiparticle, the motion of which is confined within a conjugated chain network. Such quasiparticle representation has been used to effectively compute electronic states (the excitation energies) and optical spectra of conjugated macromolecules by solving effective scattering equations for the excitonic wave functions (equivalent to a generalized "particle in a box" problem). The resulting exciton scattering (ES) model[168] is a numerically efficient multiscale approach for calculation of excited states extending the commonly used quantum-chemical methods to the realm of very large systems with thousands of atoms.[169] Other electronic states and their dynamics in CPs have been associated with quasiparticles as well as biexcitons, polarons, bipolarons, solitons, breathers, etc.[8,55b,170] Finally, we mention a fundamental relationship between correlated description and the single-particle states near the energy gap. In fact, for a given system, NTOs representing an electron and hole in the exciton, NO of cation and anion, and LUMO and HOMO have very similar spatial distribution of the orbital density for negative and positive carriers, respectively.[171] This justifies highly intuitive qualitative interpretation of frontier orbitals and applicability of single-particle description for polaronic states in various carrier transport models.

As compared to CPs, excitonic effects in SWNTs have been discovered much later, and a common description of electronic excitations relied on dynamics of weakly interacting charges.[95,97] However, first principle calculations,[96a,98,172] transient spectroscopy, and nonlinear absorption experiments[96b,106,173,174] have unambiguously proved that the low energy optical excitations of SWNTs are dominated by excitonic states with large binding energies of 0.2−0.5 eV, depending on the tube diameter and chirality.[99] The electronic structure of SWNTs, predicted by tight-binding Hamiltonian models, provides equally spaced sub-bands of valence (VB) and conduction bands (CB) with diverging density of states at the edges, known as van Hove singularities (VHS). Thus, in terms of free electron−hole pairs, optically excited states, E_{ii}, SWNTs correspond to the transitions between ith VHS at the VB and ith VHS at the CB[4] (e.g., E_{11} and E_{22} transitions shown schematically in Figure 5), which are doubly degenerate because of the cylindrical symmetry of the tube. For free electron−hole pairs, this leads to four distinct but degenerate interband transitions with different angular momen-

DOI: 10.1021/acs.chemrev.5b00012
Chem. Rev. 2015, 115, 5929−5978

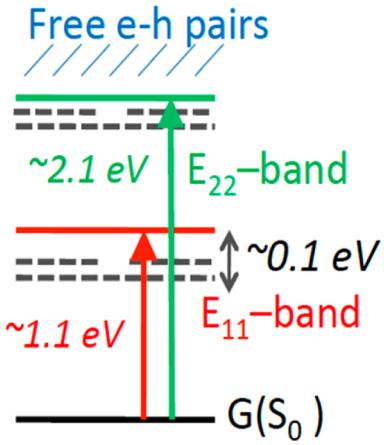

Figure 5. Schematics of the excitonic structure of SWNTs.

ta.[96a,99c,175,176] However, a strong interaction between a photoexcited electron and a hole lifts the degeneracy and introduces a complex structure of overlapping excitons, where only one is optically "bright" and the others are "dark" (optically forbidden) because of the difference in their parity.[30a,177] Interactions with the environment, edge effects, defects, and impurities in the tube lattice split and mix energies of excitonic bands even further.[99d,101g]

The energy alignment and the nature of the dark and the bright excitons strongly affect the photophysical properties of SWNTs. The existence of the lowest-energy dark excitons has been explicitly verified via time-resolved spectroscopy,[178] two-photon spectroscopy,[179] and PL spectroscopy in the presence of high magnetic fields altering the optical selection rules ("magnetic brightening" experiments)[30b,c,180] as well as many theoretical calculations.[99,101g,104] Although both experimental and theoretical results conclude that the lowest energy singlet state in SWNTs is optically forbidden, the precise ordering and energy splitting between bright and other dark excitons are highly method sensitive. For example, calculations based on the many body theory combined with tight-binding model[30a] predict the two degenerate dark states from the 4-fold first band being slightly above the bright exciton, with the lowest fourth dark exciton. The ab initio calculations[177,181] predict splitting between the lowest dark and bright E_{11} excitons to be about 10 meV. Magnetic brightening experiments have resulted in similar values.[180] However, for long but finite-size tubes, calculations based on the PPP Hamiltonian[176] provide two degenerate dark states and one weakly allowed state between the bright exciton and the lowest dark one. Here, the splitting between dark and bright states is predicted to be significantly larger (~100 meV) and agrees with the results from time-resolved spectroscopy.[178] Other calculations of the finite-size SWNTs using the ZINDO approach give the bright exciton as the second state after the dark one and the two remaining states as semidark excitons lying above the bright state.[101g,104]

TD-DFT calculations of singlet states in finite-size SWNTs predict three nominally dark exciton bands below the bright exciton,[104,178] but the energy and the character of each exciton strongly depend on the density functional. Figure 6a compares the energies of the lowest dark I and bright IV excitons as the function of the tube diameter calculated by different methods.[104] Hybrid functionals show qualitative agreement with experimental data,[9] with some overestimation of the exciton energies. The calculated nanotubes have short 10–12 nm lengths, so that confinement effects from the edges lead to a blue-shift of the excitations.[104] In addition, use of small basis sets such as STO-3G also increases the excitation energies. It was shown in ref 63c that extension of the basis set to 6-31G decreases the transition energies by about 0.15 eV, while not changing the qualitative trends. TD-DFT predicts bright–dark exciton splitting to be about 50–100 meV.[101g,104] This value is weakly dependent on the tube chirality and is almost independent of the HF exchange portion in the functional. In contrast, similar to the CP case, delocalization properties of excitons are very sensitive to the hybrid component in the functional. Figure 6b displays plots of transition density matrices corresponding to four fundamental excitons in (9,1) SWNT calculated using representative functionals.[104] The GGA functionals such as PBE predict all excitons to be completely delocalized (unbound case representing non-interacting electron and hole). In contrast, all hybrid functionals recover bound excitonic states with a significant degree of spatial localization. Similar to our observations in CPs shown in Figure 4, the exciton localization (and the electron–hole binding energy) increases with an increase of HF portion in the functional. References 63c, 104, and 178 conclude that the TD-DFT approach based on functionals with small hybrid component (e.g., B3LYP or PBE0 model) is sufficiently accurate to represent excited-state properties in the finite-size SWNTs by incorporating excitonic effects, providing diameter/chirality scaling trends and the energy splitting between bright and dark states. Finally, we mention a few joined experimental and theoretical studies exploring other excitonic states in SWNTs such as higher lying excitations (E_{22} and E_{33} bands),[101h] two-photon, and triplet[63c] states.

4. IMPACT OF CONFORMATIONAL DISORDERS AND SURFACE CHEMISTRY ON ELECTRONIC PROPERTIES

To this point, we have overviewed methodologies for ground- and excited-state calculations able to capture an essential physics in CPs, SWNTs, and QDs. Next, we consider more complicated cases when there is a significant uncertainty in elemental composition and/or conformational structure of the system. A common but very difficult question is "To what extent are the model systems studied by quantum-chemical techniques representatives of the realistic materials under experimental investigation?" Taking clues from structural materials characterization (such as TEM and STM images or spatially resolved spectroscopic probes) frequently helps to construct such model nanostructures.[105a] Computations of electronic properties of the latter allow for subsequent comparisons with spectroscopic or electrical experimental data.[140,142,145,146] Notably, an exact reconstruction of the chemical structure based on spectra, images, or device characteristics is rarely attainable in theoretical modeling of large systems.[182] Nevertheless, computations can predict well trends in electronic structure upon varying composition, bonding, or conformations. Examples of such studies include theoretical predictions of changes in electronic spectra upon deviation from the stoichiometric structure A_nB_n in QDs toward excess of one element;[183] detection of spectroscopic signatures of surface agents in QDs[124c] and polymer wrapper or chemical dopant in functionalized SWNTs;[101e,f,105b] and modifications of carrier transport efficiency due to trap states as a function of structural disorder in CPs.[87,163c]

DOI: 10.1021/acs.chemrev.5b00012
Chem. Rev. 2015, 115, 5929–5978

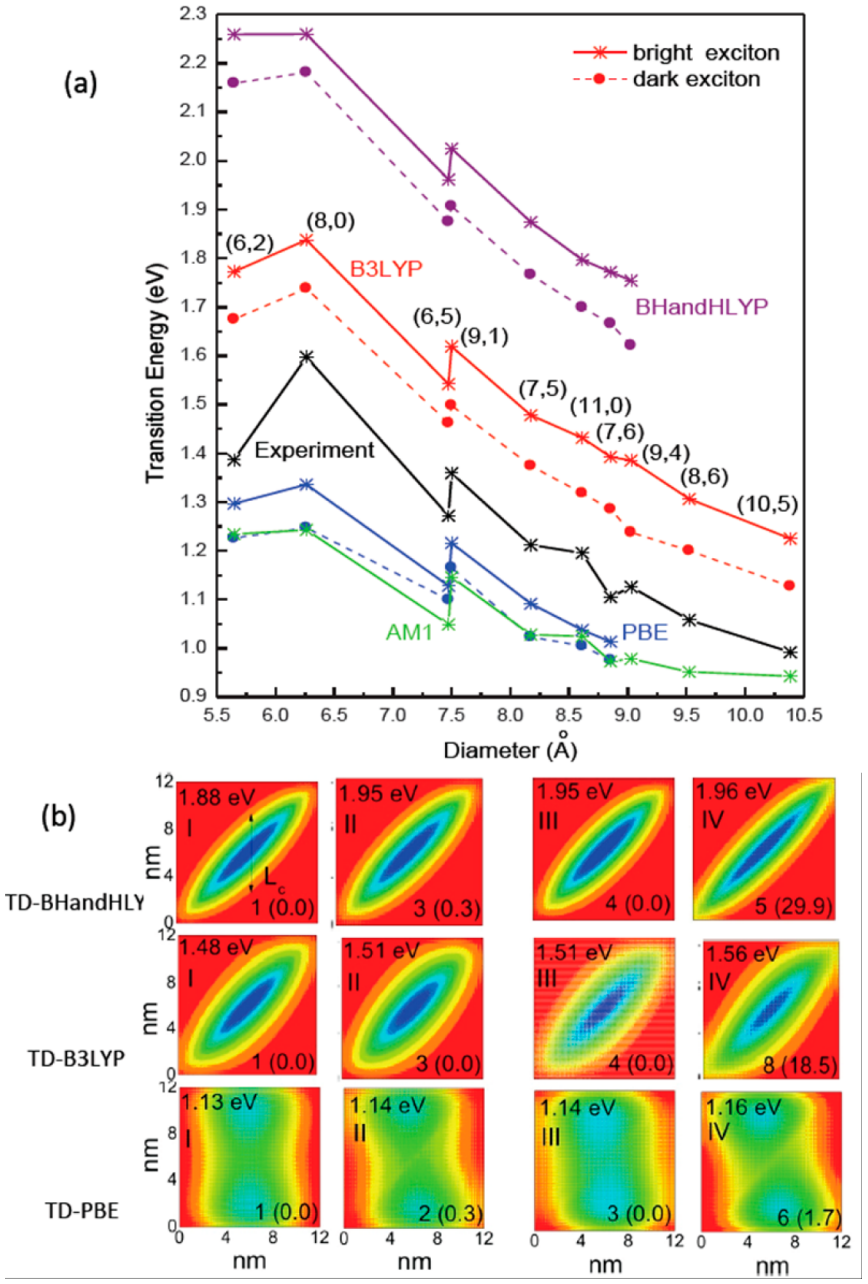

Figure 6. Bright and dark excitons in the TD-DFT methodology. (a) The energies of the lowest dark (circles and dashed lines) and bright (stars and solid lines) excitons as a function of the tube diameter calculated using TD-BHandHLYP, TD-B3LYP, TD-PBE, and TD-HF-AM1 methods with STO-3G basis set, as implemented in Gaussian 09 software. The black line represents the respective experimental data from ref 9. (b) Excitonic transition density matrices of a 12 nm (9,1) tube calculated using TD-DFT with different functionals. The four main excitons from the first band are presented by two-dimensional contour plots as a function of the electron (vertical axis, nanometers) and hole (horizontal axis, nanometers) coordinates along the tube axis. The oscillator strength of each exciton is shown in parentheses. Reprinted and modified with permission from refs 9 and 104. Copyright 2003 American Chemical Society and 2009 Royal Chemical Society.

Sampling of conformational space is frequently done using the classical molecular dynamics (MD) approach using open or periodic boundary conditions in the presence of the thermostat. For example, in the constant temperature Langevin dynamics, nuclei evolve along the PES according to

$$M_i\ddot{\mathbf{R}}_i(t) = -\nabla E(\mathbf{R}(t)) - \gamma M_i\dot{\mathbf{R}}_i(t) + \mathbf{A}(t) \quad (5)$$

M_i, $\ddot{\mathbf{R}}_i$, and $\dot{\mathbf{R}}_i$ denote the mass, acceleration, and velocity, respectively, of the ith nucleus. The stochastic force, $\mathbf{A}$, depends on the bath temperature and the friction coefficient, γ (ps^{-1}). Nuclear motion is governed by PES energy gradients $\nabla E(\mathbf{R}(t))$. The latter can be calculated by the electronic structure means in the ab initio MD approaches. For example, using this approach, one could explore motion of ligands on the QD surface.[158c] Such simulations, however, are numerically expensive and become unfeasible for large systems (hundreds of atoms) or long trajectories (hundreds of picoseconds). The availability of reliable FFs can greatly reduce computational costs. Subsequently, only a limited number of conformational snapshots from classical MD can be examined using quantum-chemical techniques for their electronic features as illustrated for the CP case in section 4.3.

DOI: 10.1021/acs.chemrev.5b00012
Chem. Rev. 2015, 115, 5929−5978

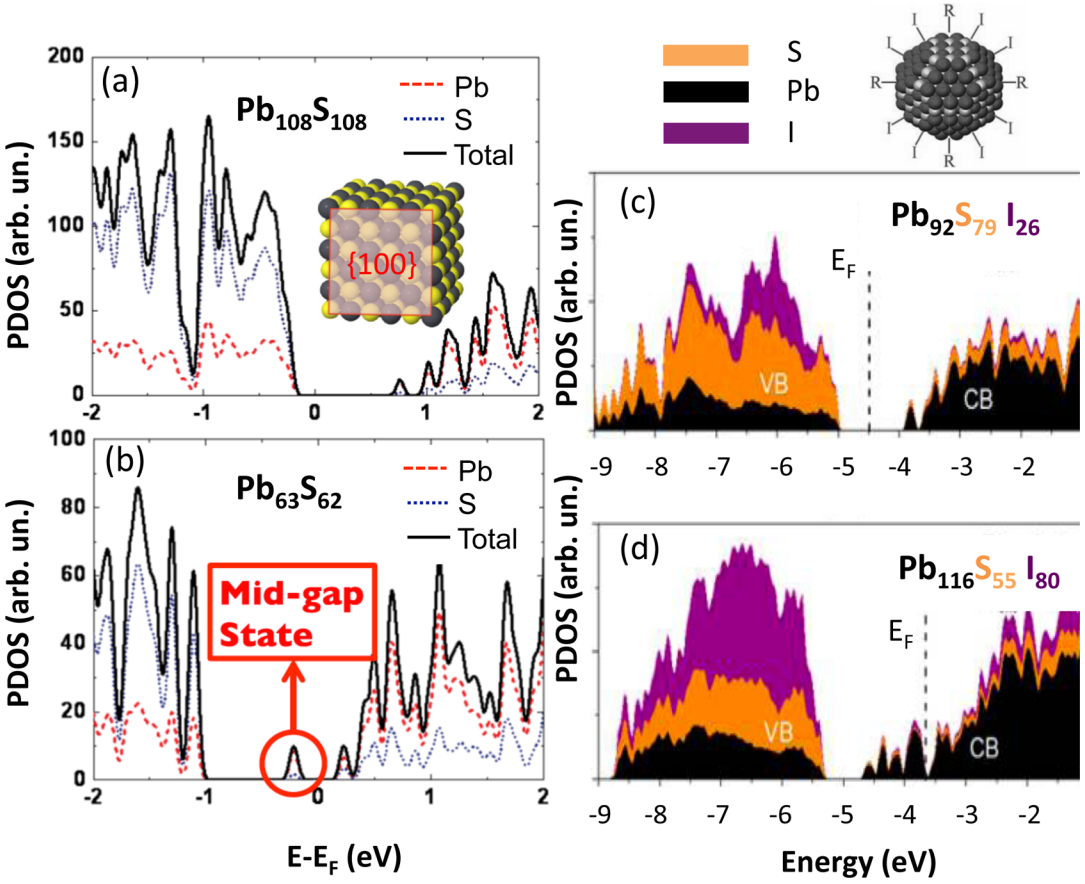

Figure 7. Projected density of states (PDOS) of stoichiometric and off-stoichiometric bare and ligated PbS QDs, computed by DFT with PBE GGA functionals using VASP (a,b) and SIESTA (c,d) software. Reprinted and modified with permission from refs 186 and 187. Copyright 2013 American Physical Society (a) and 2012 American Chemical Society (b).

4.1. Stoichiometry and Surface Ligands in Quantum Dots

While the majority of theoretical studies of QDs assumed the stoichiometric structure A_nB_n,[119,124−126] the stoichiometry of QDs is found to be critical in determining charge carrier trapping and, thus, radiative and nonradiative pathways. It was experimentally detected that the Cd:Se ratio increases as the size of the QD decreases.[184] It was also shown that hole trap states resulting in quenching of band edge emission originate from an excess of nonmetal terminated sites in CdX (X = S, Se, and Te) QDs, while it fully recovered when QDs are cadmium terminated.[183,185] Recent DFT calculations[186] have demonstrated that off-stoichiometric PbSe and PbS QD structures with disproportionate numbers of metal and nonmetal ions lead to the trap midgap states that partially or completely close the band gap of the QD, while the stoichiometric magic-sized QD structures demonstrate a well-opened band gap, as illustrated in Figure 7a,b. Attachment of an optimal amount of ligands such as halide ions to off-stoichiometric QDs eliminates such midgap states,[187] Figure 7c,d. Similarly, for zinc blende CdSe QDs, it was computationally predicted that infilling of surface vacancies with foreign cations or anions can deactivate deep and shallow traps.[188] Quality of surface passivation (ligand coverage) is also critical in maintaining emissive properties of QDs.[15a,b] For example, DFT simulations demonstrate that for magic size $Cd_{33}Se_{33}$ constructed from wurtzite lattice, surface ligands, such as prime amines (reduced to NH_2CH_3), phosphine (reduced to $P(CH_3)_3$), and phosphine oxides (TOPO reduced to $OP(CH_3)_3$), do not contribute trap states to the band gap or near the band edges of the QD, if the ligands passivate all 2- or/and 3-coordinated Cd ions on the surface,[124a,133] as illustrated in Figure 8a. The HOMO−LUMO transitions are optically active for both bare and fully ligated QDs. However, when one ligand is removed from the most reactive (2-coordinated) Cd ions at the surface creating a surface defect, the trap state near the conduction band appears, Figure 8b. This trap state might have optically dark or semidark character, depending on the position of the removed ligand. Strong confinement results in some delocalization of orbitals over the QD, rather than their complete localization at a surface defect. This "leakage" of the wave function is responsible for weak oscillator strengths of the lowest energy transitions associated with the surface defects. A polar solvent delocalizes the orbitals even more and may eliminate the surface/trap states from the gap.[124b]

In addition to controlling the midgap states, surface ligands make profound changes to the higher energy excitations. While states near the band gap have predominantly the QD character, the states deeper in the VB and CB bands have highly delocalized nature with orbitals spreading over the QD and the ligands, that is, the hybridized orbitals,[124a,b] as illustrated in Figure 9. The surface reconstruction and strong QD−ligand interactions lead to substantial change redistribution and charge polarization on the surface in the fully ligated clusters, resulting in the appearance of several manifolds of QD−ligand hybridized states. In the experimental spectra, optical absorption of ligand and hybridized states typically becomes noticeable in the spectra for excitation energies larger than two

DOI: 10.1021/acs.chemrev.5b00012
Chem. Rev. 2015, 115, 5929−5978

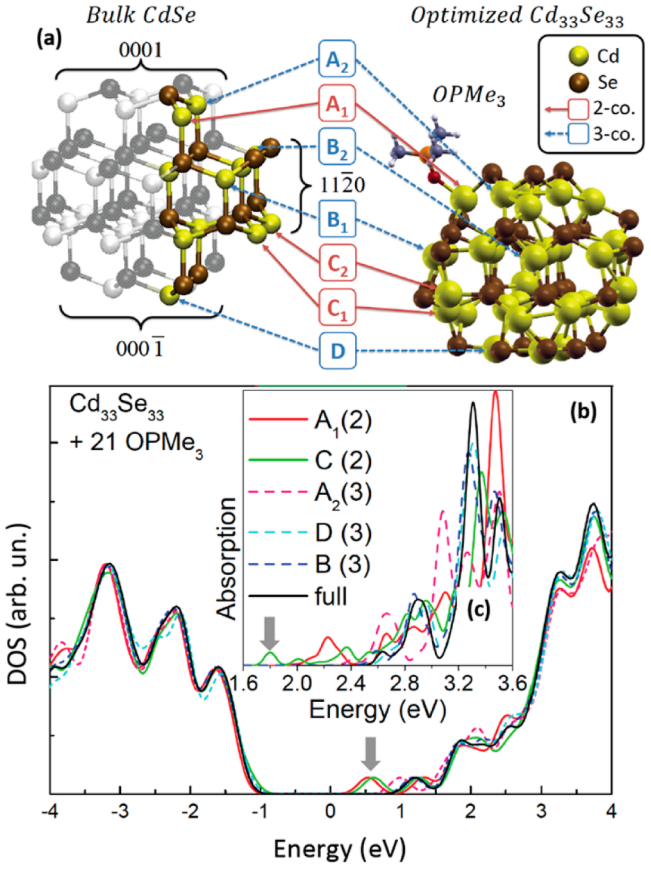

Figure 8. Calculated electronic and optical spectra of the $Cd_{33}Se_{33}$ fully passivated by $OPMe_3$ ligands and with one ligand lost from the sites A–D. (a) Compares the bulk and optimized structures of the $Cd_{33}Se_{33}$ with identified 2-coordinated (red) and 3-coordinated (blue) surface cadmiums. Solid black lines stay fully ligated by 21 (b) ligands. Insets show the absorption spectra calculated by TD-B3LYP with LANL2DZ basis set. The vertical arrows indicate the trap states associated with the surface defects due to a lost ligand. Reprinted and modified with permission from ref 124a. Copyright 2009 American Chemical Society.

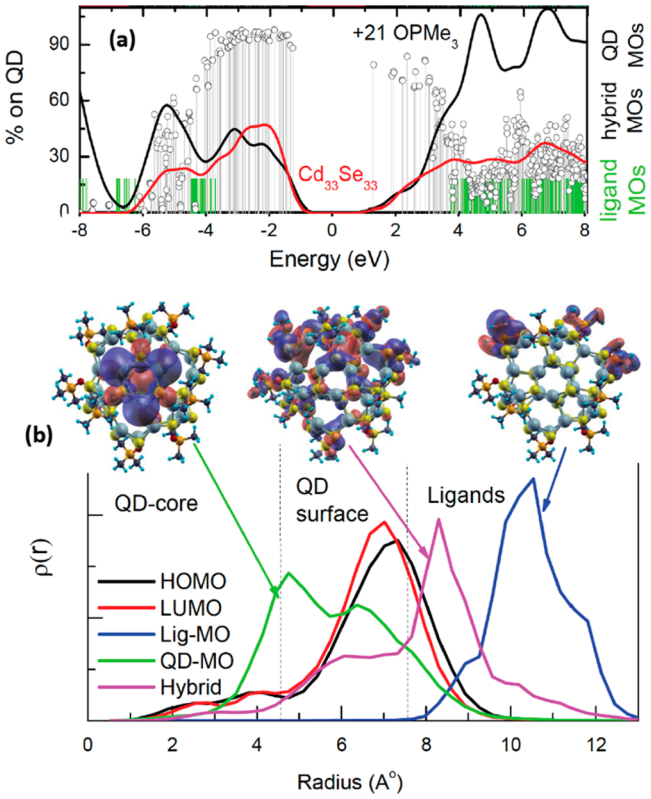

Figure 9. Density of states (DOS) and percent of the orbital localization on the QD or ligand atoms for the $Cd_{33}Se_{33}$ fully passivated by phosphine oxide ligands, $OPMe_3$ (a). The DOS of the bare $Cd_{33}Se_{33}$ (red line) is shown as a reference. Green lines show the pure ligand orbitals, when the ligands are removed from the QD structures with the same geometry as they had on the QD surface. (b) KS orbitals representing typical states localized on the QD, on ligands, and delocalized over the QD and ligands (hybridized), and their corresponding angle-averaged electronic density distributions calculated as functions of the QD radius. Calculations are performed by B3LYP functional and LANL2DZ (Cd, Se)/6-31G* mixed basis set, as implemented in Gaussian 09 software. Reprinted and modified with permission from ref 124a. Copyright 2009 American Chemical Society.

energy gaps. Most of the hybridized states that are relatively close to the edges of the CB and the VB are optically dark and are not seen in the absorption spectra. The densities and the positions of the hybridized states with respect to the Fermi level of the system depend on the capping ligands.[124a] Indeed, these trends in ligand's state energetic alignment and hybridization with QD's states are sensitive to the type of the molecule and, in particular, the linkage group attaching the molecule to the QD surface, as was detected experimentally and computationally.[120e,189] For example, ref 189a reports on joined experimental electrochemical and DFT studies of CdSe QDs to assess the combined effects of quantum confinement and ligand-induced shifts on the QD's valence band position. It was found that QDs capped by phenlyphosphonic acid exhibited change in energies as a function of the QD size very similar to that found for TOPO-capped CdSe, due to similar phosphonate group linking the molecules to the QD surface and dominating QD character of states near the band gap in both systems. In contrast, the molecules linked via thiol and thiolate groups have the HOMO and LUMO localized primarily on the ligand orbitals, and for these ligands the charge displacement per ligand does not change significantly with coverage and the QD size. Overall, thiol ligands are also known for introducing hole/electron trap states to the QD band gap.

Besides ligands, optically or electrically functional groups can also be attached to the QD surface. For example, use of different metal–organic dyes such as functional groups of the QDs has great promise to serve as an important element for both solar-to-electrical and solar-to-chemical energy conversion.[190] In both types of applications, conditions and mechanisms of the charge transfer from the photoexcited QD to the dye or backward play a crucial role in the device performance. On the other hand, these processes are extremely sensitive to a complicated surface chemistry of QDs and the QD–dye interactions, the fundamental understanding of which is still far from completion. Recent DFT simulations of different derivatives of Ru(II)-polypyridines attached to the CdSe QDs via carboxylate group have shown that the unoccupied dye-localized orbitals are introduced to the band gap of the QD, but close to the edge of the CB,[119c,159] thus controlling the energy transfer from the photoexcited QD to the dye. Negatively charged ligands, such as thiocyanate ligands in the black dye, significantly destabilize the dye's occupied orbitals by lifting them toward the very edge of the VB, thus providing favorable

DOI: 10.1021/acs.chemrev.5b00012
Chem. Rev. 2015, 115, 5929–5978

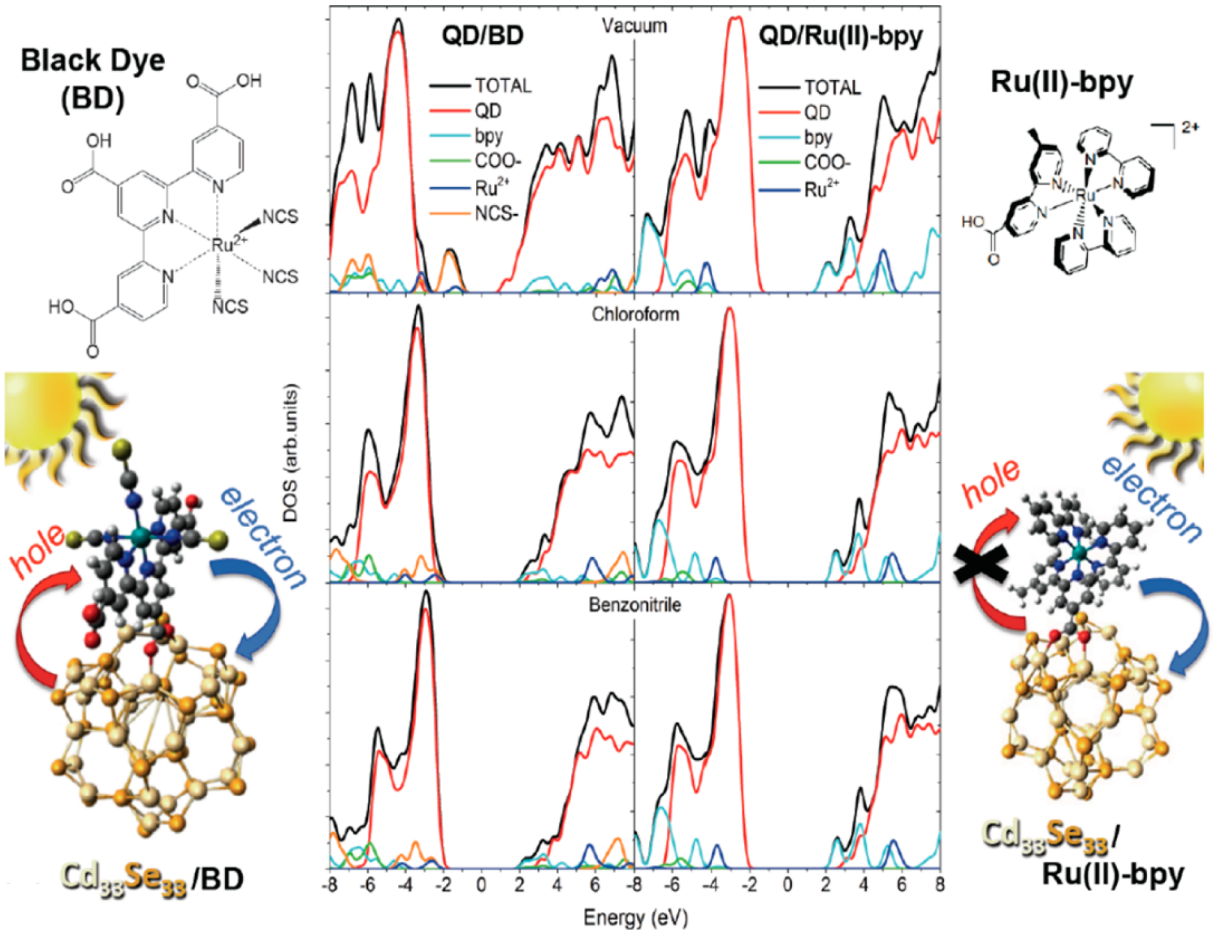

Figure 10. Calculated projected density of states of the $Cd_{33}Se_{33}$ QD functionalized by the black dye (left) and the Ru(II)-bypiridine (right) dyes. NCS-groups are responsible for alignment of dye's orbitals at the edge of the valence band of the QD providing favorable thermodynamic conditions for the hole transfer from the photoexcited QD to the dye, especially in nonpolar solvents. Calculations are performed by CAM-B3LYP functional and LANL2DZ (Cd,Se,Ru)/6-31G* mixed basis set using CPCM solvent model, as implemented in Gaussian 09 software. Reprinted and modified with permission from ref 159. Copyright 2014 American Chemical Society.

conditions for the hole transfer,[159] as illustrated in Figure 10. The localized character of dye's orbitals originates from strong electrostatic dipole−dipole couplings between the QD and the dye, which decrease the dipole moment of the dye's part in the QD/dye composite, as compared to the isolated dye. This decrease in the dipole moment shifts the electronic charge density toward the Ru(II) center, rather than to the linking carboxylate group, leading to a more localized character of the dye and QD associated orbitals in composites, despite relatively strong dye−QD interactions and confinement effects, which typically result in hybridization of QD and molecule orbitals. DFT and TDDFT calculations presented in ref 159 demonstrate the dominating role of the QD−dye interactions on the mutual alignment of their electronic levels, resulting in stabilization of the dye orbitals with respect to the QD's VB edge. Subsequently, the energy offsets in the composites do not represent a simple difference of the isolated metal complexes and the QDs, which should be accounted for in the experimental studies.

4.2. Inter- and Intramolecular Disorder in Conjugated Polymers

CP materials exemplify a great variety of solid-state packing spanning the range from molecular crystals to self-assembled layers to amorphous structures. At the moment, we cannot even predict computationally if molecular crystal or self-assembled structure would be a preferential way for materials packing (e.g., due to complex polymorphism, soft torsional potentials, etc.). Notably, accurate modeling of torsional potentials of individual molecules does provide insights if the dihedral angles are "locked" in a planar conformation with a negligible population of alternative rotamers, thus hinting if the material can form stable crystals.[171b,191] When the crystal structure of CP is known, fully atomistic modeling of charge and energy transport is possible using DFT or semiempirical framework.[171a,192,193] However, the situation is more challenging in the case of amorphous CP composites able to adapt multiple conformational structures as evidenced by the enormous amount of experimental work on fabrication and characterization of these materials.[49,194] The great computational challenge is an unmanageable number of atoms in the realistic amorphous polymer samples and our inability to exhaustively explore the conformational space. As such, atomistic information on the amorphous morphology is generally not affordable by quantum chemistry calculations, such as DFT and semiempirical methods, in contrast to a complete characterization of optical and electronic properties of individual molecules, as we discussed in section 3.

4.2.1. Combined Force-Field/DFT Methods for Amorphous Structures. A promising approach to more realistic CP

DOI: 10.1021/acs.chemrev.5b00012
Chem. Rev. 2015, 115, 5929−5978

materials is the consideration of small amorphous aggregates, where samples of molecular conformations are obtained by molecular dynamics using FF methods (eq 5), while the electronic structure is calculated by DFT using the FF geometries.[87,163c,d,195,196] If electronic transport properties are desired, hopping probabilities between electronic states can be also obtained, and the electrical transport properties can be extracted from a master equation or the kinetic Monte Carlo approach.[87,197] Therefore, these approaches, in principle, are able to establish the relationships between the structure of the material and its electrical properties and can be potentially used to design materials with better electrical transport characteristics. Figure 11 illustrates this approach used for simulations of

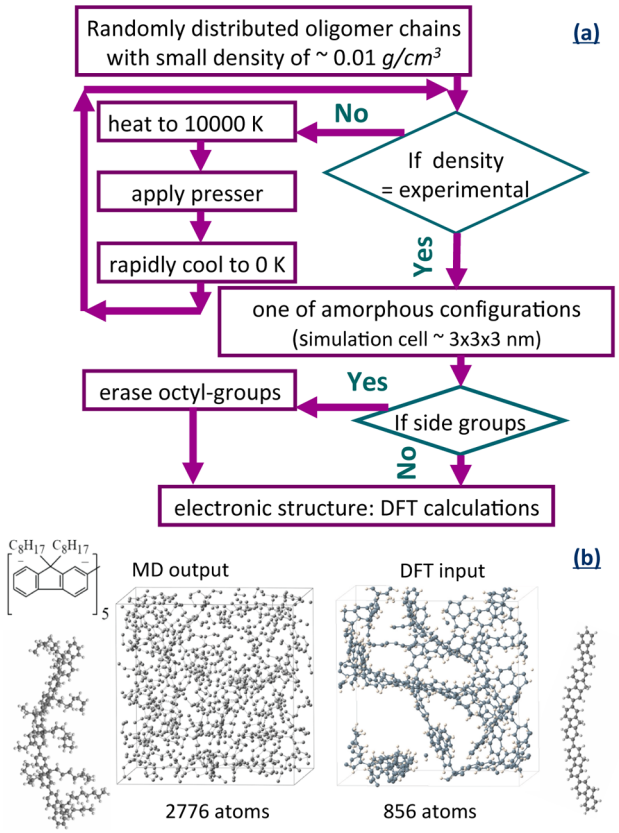

Figure 11. Classical MD approach to generating amorphous samples of CPs for subsequent DFT calculations. (a) The block scheme illustrating the MD computational procedure. (b) Representative snapshots of the MD-simulated structures of eight PFO pentamers in the simulation cell used for DFT calculations. Reprinted and modified with permission from refs 87 and 163c. Copyright 2008 American Chemical Society and 2013 American Chemical Society.

conformational disorder and the electronic structure of small amorphous aggregates of widely explored CP materials for lighting and energy applications, such as PPV (poly(*p*-phenylenevinylene)),[163d] its derivative MEH-PPV[163c] (poly(2-methoxy-5-(2-ethyl-hexyloxy)PPV), and PFO (poly(9,9′-dioctylfluorene)).[87] The main benefit of such approach is getting insights into the role of intermolecular interactions and conformational disorder on the formation of carrier's trap states in CPs of different chemical compositions and structures. FF used for these calculations is usually reparameterized based on DFT calculations of isolated CP chains. For example, for PPV, PFO, and MEH-PPV amorphous samples, the B3LYP-parametrized MM3-2000 FF was used to provide reliable geometries and packing morphologies for disordered polymer chains.[87] The CFF91 force field was used to describe the interatomic interaction in poly(3-hexylthiophene) (P3HT) polymer and its derivatives.[195a,197a]

In these methods, the PBC are typically used to replicate simulation cells in 3-D and re-establish the continuity of molecules inside each cell. Because the side groups (e.g., alkyl chains) play a key role in the polymer packing determining the spatial distance between the chains, they are preserved during the MD simulation phase. Modeling of periodic cells with thousands of atoms is easily manageable with the FF/MD approach. However, this may be problematic for the DFT calculation phase. It is possible to replace the side chains with hydrogens or methyl groups, while preserving the MD-geometry of the main polymer backbone, thus reducing the number of atoms to about 800−1000, as illustrated in Figure 11b, allowing for DFT electronic structure calculations.[163c] Such simulations are typically conducted using a plane wave basis set, the core electrons are simulated using pseudopotentials, while all valence electrons are treated explicitly. Because of the large size of the simulation cells (about 3 nm on each side), a γ-point sampling of the Brillouin zone is adequate, as was shown in previous work.[163d] The GGA functionals, such as PBE and PW91, provide faster convergence as compared to hybrid and long-range corrected functionals, such as HSE, PBE0, and LC-ωPBE, which require much larger numerical expense.

These simulations result in a set of KS molecular orbitals for each amorphous sample. We emphasize that such approach relying on GGA models and single-particle picture of electronic excitation is extremely approximate for modeling, say, optical spectra dominated by tightly bound correlated excitonic states (see section 3.2). Use of the GGA functionals also leads to underestimated energy gap values as compared to experimental CP systems (e.g., Figure 4). However, examination of occupied (hole) and valence (electron) KS states allows one to single out disorder effects caused by molecular packing such as trap states in the gap. Moreover, these KS states may serve as an approximate basis for charge carriers in subsequent transport modeling.[197a] Overall the spatial distribution of KS states is weakly dependent on the DFT model in the limit of highly disordered CP systems. Recent DFT calculations of amorphous MEH-PPV and PFO oligomers confirm that the delocalization property of orbitals, which are responsible for formation of the trap state, is quite similar for both GGA, hybrid, and long-range corrected functionals,[163c] as illustrated in Figure 12.

4.2.2. Participation Ratio as a Measure of Localization of Electronic States. Quantitatively, localization properties of occupied and unoccupied electronic states, including those responsible for the trap states, can be conveniently characterized by the participation ratio (PR) and inverse participation ratio (IPR).[87,163c] The IPR (or PR) is widely used in solid-state physics as a measure of disorder and localization in a bulk semiconductor crystal of a volume[198] (V) or in a discrete space[199] (N atoms). For an ideally localized state on a single atom, PR = 1/IPR = 1. For a wave function uniformly distributed over all N atoms, PR = 1/IPR = N. To be applied for CPs, PR can be defined in a molecular basis as

$$\mathrm{PR}(m) = \frac{(\sum_n P_{mn})^2}{\sum_n P_{mn}} = \frac{1}{\sum_n P_{mn}^2} \quad (6)$$

DOI: 10.1021/acs.chemrev.5b00012
Chem. Rev. 2015, 115, 5929−5978

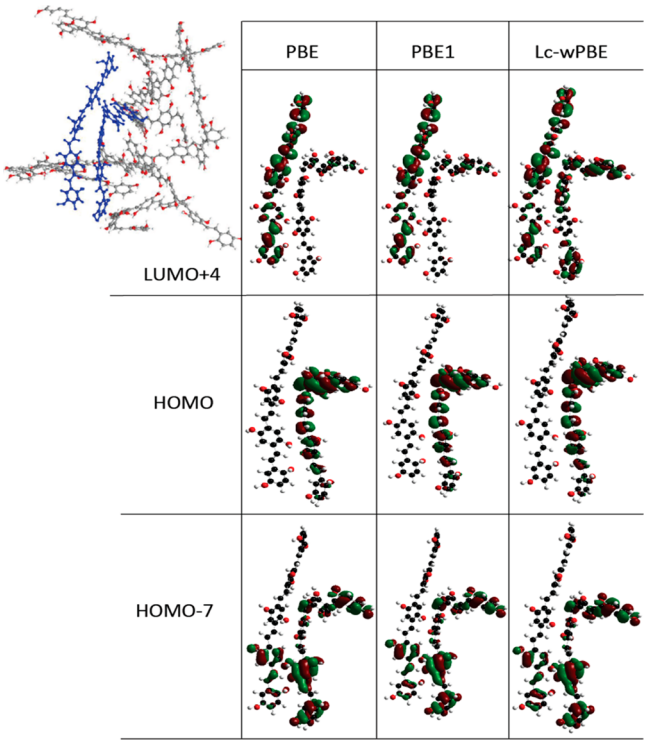

Figure 12. Selected MEH-PPV amorphous structure with the two marked oligomers with exactly the same confirmation they have in the amorphous MEH-PPV sample used for calculations of molecular orbitals by employing PBE, PBE0 (PBE1), and LC-wPBE functionals combined with 6-31G* basis set. Selected occupied and unoccupied molecular orbitals mostly have similar character of localization/delocalization properties of electronic states independent of the functional used. Reprinted and modified with permission from ref 163c. Copyright 2013 American Chemical Society.

where P_{mn} is a portion of the PR orbital m on the nth molecule. More details of the methodology used for PR calculations can be found elsewhere.[87,163c] According to this formula, an electronic state of a CP aggregate that is completely localized on a single chain has PR = 1, while the state delocalized over all N molecules in the cell has PR = N.

4.2.3. Origins of Trap States: Electron versus Hole Traps. Depending on the processing conditions, polymer chains in experimental samples are arranged either in an amorphous spaghetti-like structure or form ordered domains with amorphous regions at their boundaries. In each of these cases, there is a certain degree of disorder, which has a strong influence on the electronic properties of the material and consequently on the operation of organic electronic devices.[49a,51] Combined MD and DFT studies of amorphous PPV oligomers[163d] were able to distinguish between the effects of intramolecular disorder and intermolecular electronic interactions on the electronic structure of the densely packed oligomer clusters. In particular, intramolecular disorder originating from the oligomers not being straight and planar, but kinked and twisted, interrupts the conjugation of the π-orbitals, causing the electronic states to be more localized. As a result, such conformational deformations are responsible for the formation of electron trap states near the edges of the CB. In contrast, disorder in intermolecular interactions due to differences in the local packing of the oligomers governs the formation of hole trap states near the edge of the VB. In polymers with long side groups, such as MEH-PPV, intermolecular electronic interactions are reduced as compared to pristine PPV polymers. Thus, hole traps should be more dominant in pristine PPV, while electron traps are more dominant in MEH-PPV with long side chains, as was confirmed in further computational studies of MEH-PPV[163c] and PFO[87,163c] amorphous oligomers. This effect was also observed experimentally,[200] where blended MDMO-PPV with PCBM (chemically functionalized C_{60}) samples exhibit a 2 orders of magnitude increase in the hole mobility, as compared to pure MDMO-PPV. It has been found that the hole mobility reaches saturation beyond 67 wt % PCBM concentration in the samples;[201] likely, this threshold concentration of PCBM completely isolates one polymer chain from another eliminating the intermolecular interaction, so that further increase in the amount of PCBM does not affect the interchain interactions and does not contribute to the hole trap states.

Hybrid MD/DFT simulations[87,163c] also confirm that the alkyl side chains insignificantly affect the conformational disorder in amorphous polymers. However, the side groups significantly decrease the intermolecular interactions. Overall, it was found that the nature of the disorder and its impact on charge-carrier localization in amorphous polymers with alkyl side chains differ drastically from those of disordered polymers without side chains, such as PPVs. Thus, long-range intermolecular interactions and sparse packing are responsible for the formation of multiple, deep, highly localized trap states in amorphous MEH-PPVs and PFOs. This localization behavior, characterized by the PR values in Figure 13a,b, significantly differs from that observed in amorphous PPVs, as well as semiconductor disordered systems, such as hydrogenated amorphous silicon,[199] where the localized trap states are distributed mostly near the band gap edges, while the majority of states deep in the bands show significant delocalization.

Alternatively, for P3HT and its polyfluorene copolymer derivatives (APFO3), it was found that the alkyl chains act as spacers that reduce the electrostatic disorder introduced by the conformational distortions in main chains, while, on the other hand, they increase the insulating barriers between different chains that impede the charge carrier transport.[197a] The material based on the APFO3 monomers without side chains has a smaller mobility, due to the wider tail of the DOS near the band edge, as illustrated in Figure 13c–e. This effect prevails the effect of side groups acting as insulating barriers. Overall, all of these computational results suggest that a band- like description for mobility calculations may not be appropriate for amorphous CPs with long side chains. Calculations proved that in disordered CP materials, charge carrier wave functions of band edge states are localized at one–two polymer chains, taking a small region of space. As such, an electrical transport in amorphous CPs is controlled by carrier hopping between localized states.

4.3. Surface Functionalization and Chemical Defects in Carbon Nanotubes

A variety of low-dimensional materials are highly fluorescent. For example, CPs, QDs, and semiconductor nanorods may exhibit close to 100% quantum yield (QY). In this respect, semiconducting SWNTs are drastically different, typically showing less than 0.1% photoluminescence (PL) efficiency.[202] Such low PL of macroscopic SWNT samples is attributed to the presence of tube bundles, metallic tubes, and tubes with multiple defects, which quench emission. However, even the

DOI: 10.1021/acs.chemrev.5b00012
Chem. Rev. 2015, 115, 5929–5978

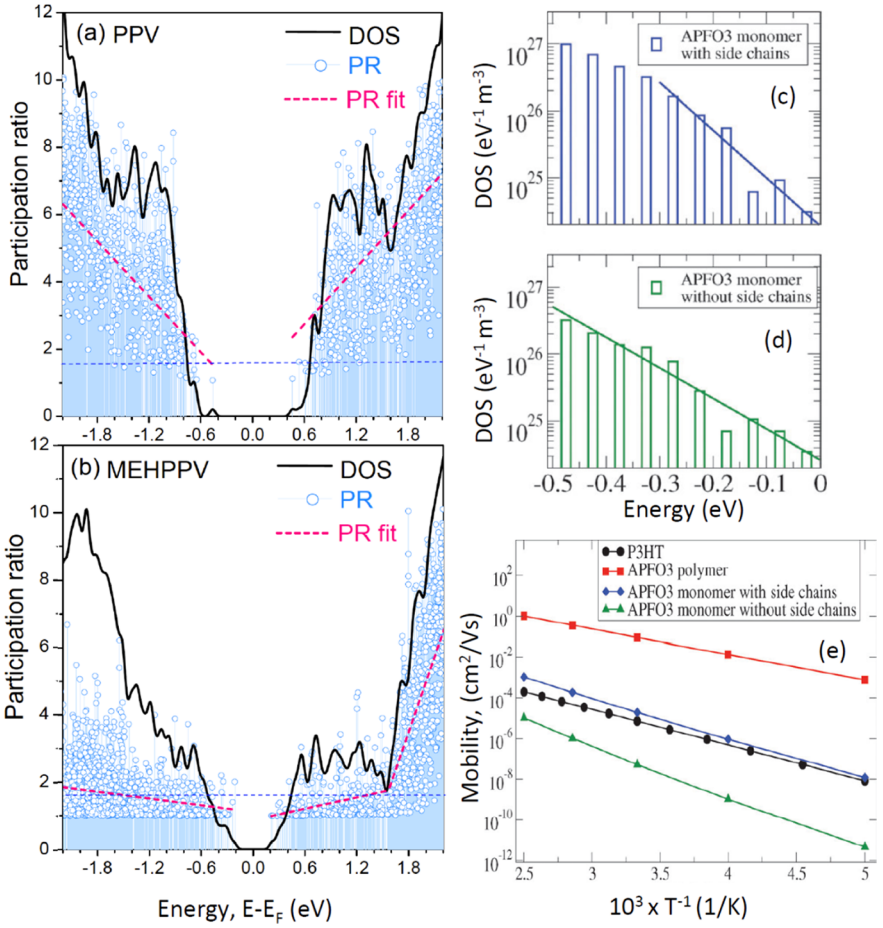

Figure 13. Calculated density of states (DOS) and participation ratios, calculated by eq 6, representing averaged data for 16−20 different equilibrium configurations of amorphous PPVs (a) and MEH-PPV aggregates (b), computed by DFT in plane-wave basis set with GGA PW91 functional. Reprinted and modified with permission from ref 163c. Copyright 2013 American Chemical Society. The PR distribution for each polymer is fitted to a linear dependence (dashed red lines). The smaller is the PR, the stronger is the localization of an electronic state. States with the PR < 2 correspond to the trap orbitals that are highly localized on a single polymer chain. Valence band of APFO3 monomers with (c) and without (d) alkyl side chains, and comparison of mobility of P3HT and APFO3 oligomers and monomers with and without side groups (c), computed by DFT with LDA. Reprinted and modified with permission from ref 197a. Copyright 2010 American Institute of Physics.

high-purity engineered samples of dispersed SWNTs protected from the nanotube environmental influences still have an overall low PL efficiency approaching about 10%.[34,203] This is explained by the intrinsic low-lying optically forbidden "dark" states trapping excitations and nonradiative recombination of freely diffusing 1D excitons at defect sites. As we discussed in section 3.2, the lower-energy optical excitations in SWNTs originate from four excitonic sub-bands[204] with at least one dark exciton residing below the first optically allowed bright E_{11} state,[30a,96b,174,176] as illustrated in Figure 5. Despite low PL efficiency, the optical properties of SWNTs have great advantages, such as photostability, the absence of blinking at room temperatures, near-IR fluorescence, and a narrow homogeneous line width.[205] Such robust photophysical features are important for a number of technological applications, including bioimaging and biosensing. Chemical functionalization of the nanotube surface offers an attractive route to change the selection rules controlling the optical activity in SWNTs and to tune their optical spectra. Functionalization of SWNTs can be achieved either through the formation of covalent bounds between the nanotube and an adsorbed molecule, the covalent functionalization, or through "stacking" and encapsulation, noncovalent functionalization.

4.3.1. Brightening of Carbon Nanotubes via Covalent Functionalization. In particular, covalent functionalization is expected to significantly change the optical properties of SWNTs. For example, recent experiments on individual SWNTs in water have revealed a significant increase in PL efficiency upon addition of reducing agents.[34] Other experimental studies have reported the appearance of low-energy satellite PL peaks in SWNT samples with adsorbed atomic gold,[35] hydrogen,[36] aryl salts,[23a] and oxygen.[37] These bright satellite peaks in PL have been associated with distortions of the nanotube structures due to local chemical defects that induce mixing between bright and dark excitons.[35,37,206] Alternative hypotheses have suggested the involvement of triplet states that provide bright red-shifted satellite peaks in emission.[35,36,207] In contrast, a significant reduction in the PL efficiency has been found for protonated SWNTs[208] and SWNT dispersions exposed to acidic environments.[209] The PL quenching has also been explained by chemical defects, which are assumed to introduce trap states for holes.[34] Overall, the mechanisms enabling optically forbidden transitions and the interplay between bright and dark excitons in SWNTs upon functionalization are still under debate. Part of the challenge from the modeling perspective is a frequent absence of precise

DOI: 10.1021/acs.chemrev.5b00012
Chem. Rev. 2015, 115, 5929−5978

binding/structural information on the chemical dopant site. Subsequently, simulations typically rely on chemical intuition and examine various binding energies to select preferable structures.[210]

Recent TD-DFT calculations have demonstrated that chemical functionalization of SWNTs by hydrogens and aryl molecules at low concentrations locally alters the π-conjugated network of the nanotube and leads to a spatial confinement of the excited wave functions.[38,101f] Depending on the adsorbant positions, the chemisorption significantly modifies the optical selection rules.[38,210a] Thus, chemical defects originating from hydrogen adsorption on a single carbon ring (insets in Figure 14a) perturb the low-energy excitonic band, allowing the lowest-lying excited state to moderately red shift and to gain substantial oscillator strength.[38,101f] This effect can be rationalized by an analogy with excited states of a molecular dimer in H-aggregate arrangement. One can impose this simplistic model onto SWNTs, where a degenerate two pairs of molecular orbitals appearing due to tube symmetry mix in pristine tubes leading to the lowest dark state (antisymmetric superposition) and the higher bright E_{11} state (symmetric superposition). Chemical defect that alters excited-state energies of one monomer may efficiently decouple states in the molecular dimer by breaking wave function superpositions, so that the resulting excited states would be localized back on their parent molecules and both would be optically active.[38] This is precisely what was observed in hydrogenated SWNTs, Figure 14.

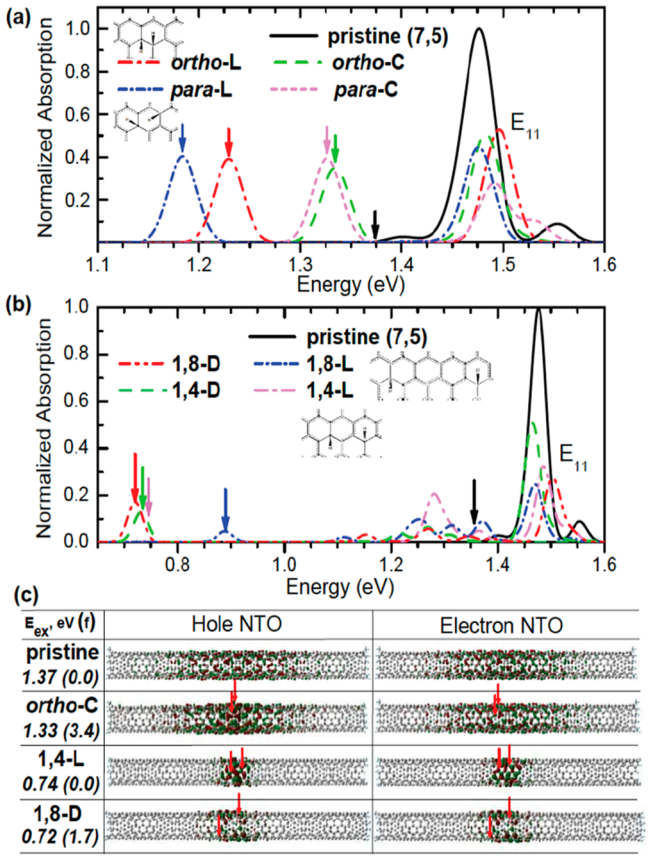

Figure 14. (a,b) Comparison of calculated absorption spectra of hydrogenated (at various position of H) and unmodified (7,5) SWNTs. Energy corresponding to the first excitation is indicated by an arrow. (c) Natural transition orbitals illustrating delocalization of excited states introduced by chemical dopant. Calculations of excited states have been performed with TD-DFT approach based on B3LYP functional and STO-3G basis set, using geometries optimized with AM1 method. Reprinted and modified with permission from ref 38. Copyright 2012 American Chemical Society.

In contrast to the above case, attachment of hydrogens to different carbon rings on the tube surface (1,4- and 1,8-defects) results in a significant red-shift of the lowest excitonic transition (Figure 14b), the wave function of which becomes highly localized with an electron and a hole being "trapped" between the two bonding hydrogen atoms,[38] as can be seen from the NTOs shown in Figure 14c. Such strong spatial localization explains the small oscillator strength of this transition, as compared to the *ortho*- and *para*-cases, and even complete darkening of the lowest state depending on the defect orientation. Computational data suggest that PL efficiency of semiconducting SWNTs can be controlled by selective chemical functionalization.[38,101f] All of these computational predictions well agree with the recent experimental findings of a bright emission peak in SWNTs with sp^3 defects that is red-shifted by as much as 254 meV from the original E_{11} excitonic transition.[206] Concurrent TD-DFT simulations of oxiden-doped carbon nanotubes[210b] have also identified a variety of deep and shallow traps leading to multiple sharp emission peaks at energies 50−300 meV red-shifted from the E_{11} bright exciton peak. These peaks are associated with trap states tied to different specific oxygen chemical adducts (e.g., ether-d, ether-l, and epoxide-l) with various wave function delocalization. Overall, specific chemical doping is a promising generalized route for direct control of carrier dynamics in SWNTs toward enhanced light emission properties for photonic applications.

4.3.2. Noncovalent Functionalization by Bio- and Conjugated Polymers. Noncovalent functionalization of SWNT materials such as wrapping the tube by CP or DNA chains and use of surfactants (e.g., sodium dodecylbenzenesulfonate, SDBS) proved to be a powerful approach allowing the separation of different tube chiralities and one to suspend and isolate individual species for subsequent characterization.[21,23a] Computation-wise, it is possible to use inexpensive FF MD/DFT combination described in section 4.2 to model morphology and mechanisms of interactions in composites of SWNTs. For example, the reduced structures of SWNTs wrapped in CPs[105b,211] and biopolymers like DNA[101e,105a] obtained from classical MD simulations were then used as an input for electronic structure and excited-state calculations. Particularly, for the SWNTs functionalized by conjugated polymers MM3-2000 FF,[57] parameters of carbon,[105b,163c] oxygen, and nitrogen atoms[211] have been modified to reproduce the geometry of the isolated PPV[105b] and carbazole[211] oligomers obtained from DFT calculations using the B3LYP functional with the 6-31G(d) basis set. Subsequent ZINDO calculations defined modifications in the excitonic structure of SWNT/PPV composites.[105b] To obtain structures of DNA-SWNTs hybrids, the CHARM27 force field was used to represent both the single-strand DNA and the aromatic carbon assigned to all C atoms on the SWNT[101e,105a] and graphene.[212]

It is expected that noncovalent interactions between CP (or DNA) chains and a SWNT occur via $\pi-\pi$ stacking. The mechanisms of SWNT interactions with CP and DNA have been predicted by molecular dynamics[105b,212,213] and Monte Carlo[214] simulations, unambiguously confirming a $\pi-\pi$ stacking with strong binding energy between the nanotube surface and

DOI: 10.1021/acs.chemrev.5b00012
Chem. Rev. 2015, 115, 5929−5978

the polymer backbone, with stronger DNA−SWNT interactions.[105a,212] Such strong CP−SWNTs and DNA−SWNTs interactions are expected to provide high stability of hybrids, so that a molecule is unlikely to unwrap from the nanotube surface under thermal fluctuations and other distortions.[101e] For some applications, such as drug delivery or biomarkers, the stability of polymer−SWNT hybrids is beneficial, because better-dispersed and fully coated functionalized SWNTs demonstrate an improved toxicological profile in medical studies.[215] In addition, morphology and, specifically, the alignment of a molecule with respect to the nanotube surface, which, indeed, rely on the polymer−SWNT interactions, affect all main properties of the polymer−SWNT interface in hybrid materials. Unfortunately, the current theoretical framework cannot explain the wide geometry variations in CP−SWNTs structures predicting different helical polymer wrapping,[216,217] as well as parallel alignment of a polymer along the nanotube axis. Nonetheless, most simulations predict stable CP/SWNT configurations only with relatively small wrapping angles (less than 20°),[105b] especially for CP with stiff backbones,[213a] rather than a strictly linear alignment on a nanotube surface, which agrees well with available experimental data.[218] Classical MD calculations[101e] have also established correlations between the most stable wrapping angles of SWNT−DNA hybrids and the most preferential DNA base orientations on the graphene with respect to its lattice vectors, which elucidate the sensitivity of SWNT−DNA interactions to the DNA sequence.[212] Trends in the dependence of SWNTs dispersion and bundling mechanisms on the type of the polycarbozole isomer, the polymer length, and the diameter of the nanotube have been also discussed on the basis of MD simulations.[211] Overall, noncovalent functionalization of SWNTs only weakly perturbs excited-state structure in nanotubes, resulting in small red-shifts (<30 meV) and broadening of the lowest-energy E_{11} and E_{22} absorption bands as seen in calculations[105b] and experiments.[218,219]

5. EXCITED-STATE POTENTIAL ENERGY SURFACES AND ELECTRON−VIBRATIONAL COUPLINGS

To this end, we have been discussing calculations and analysis of electronic properties for a given molecular structure, commonly, an equilibrium (optimal) geometry in the ground state being a minimum of the PES. Within the Born−Oppenheimer approximation, every electronic excitation has its own PES, generally different from that of the ground state. Subsequently, any electronic excitation results in perturbation of nuclei degrees of freedom raising electron−nuclei coupling phenomena. These electron−vibrational (in molecules) or electron−phonon (in solids) interactions result in vibronic effects, when the simultaneous changes in electronic and vibrational energy levels of a molecule occur, for instance, upon absorption or emission of a photon. Generally, the strength of the electron−phonon coupling inversely correlates with the extent of the respective electronic wave function; that is, delocalized electronic excitations produce only small changes of the electronic density "locally" with a minor effect on the force field.[220] Subsequently, the strength of electron−phonon coupling greatly increases with diminishing system size and an increase of quantum confinements, as illustrated in the examples below. Because of strong carrier confinement, a complete interplay between electronic correlations and electron−phonon couplings is a typical feature in low dimensional systems, such as conjugated organic[85a,221] and organometallic[222] polymers, mixed-valence chains,[223] and organic molecular materials.[224] Such effects frequently give rise to a spontaneous symmetry breaking or the Peierls distortions in many molecular materials. This leads to rich physical phenomena such as metal-to-semiconductor transitions in the electronic structure,[101c] exciton self-trapping, and formation of solitons, polarons, and breathers.[8,55b,170,225] However, these phenomena are expected to be less pronounced in inorganic materials, such as semiconductor QDs, nanorods, and nanowires, where strong ionic bonds arrange in rigid 3-D structures. These are weakly perturbed by the change of an electronic wave function, as compared to "soft" organic materials like CPs. The mechanisms of electron−phonon coupling, its strength, and dependence on the size and shape of nanostructures are important questions in investigations of ways of controlling photoexcited dynamics in nanomaterials to improve their efficiency in optoelectronic and photovoltaic applications.

The electronic confinement in nanomaterials effectively converges the continua bands of electronic and vibrational states of the bulk to discrete states. Therefore, nanostructures such as QDs and SWNTs can be considered as a large molecule rather than an infinite solid, with the difference being the mechanism and strength by which the electronic and vibrational states are coupled. Figure 15 schematically shows

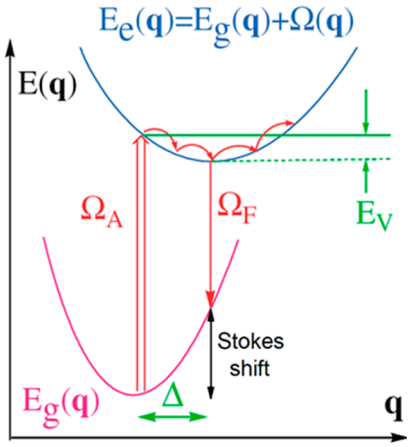

Figure 15. Schematic representation of ground $E_g(q)$ and excited $E_e(q)$ state molecular potential energy surfaces (PES) commonly characterized via nuclear coordinates q, displacements Δ, vibrational reorganization energy E_V, vertical absorption Ω_A, emission Ω_F, and Stokes shift $\Omega_A - \Omega_F$ energies. Reprinted and modified with permission from ref 91. Copyright 2002 American Physical Society.

two PESs corresponding to the ground and some excited states, which could be very complex in realistic materials. The minima can be characterized by a set of vibrational normal modes $\mathbf{q}_\alpha$, with their respective frequencies ω_α. Here, index α spans $3N - 6$ space, N being the total number of atoms in the molecule. Vibrational frequencies typically range from ∼100 to ∼3000 cm^{-1} forming dense bands across the entire spectrum for large molecules.[226] Vibrational normal modes are obtained by diagonalizing the Hessian for ground $(\partial^2 E_g(\mathbf{R})/\partial \mathbf{R}^2)$ or excited $(\partial^2 E_e(\mathbf{R})/\partial \mathbf{R}^2)$ states, where $\mathbf{R}$ denotes the set of Cartesian coordinates of the nuclei. The difference between ground- and excited-state PESs near minima is typically characterized by displacements Δ_α (reflecting different optimal geometries), different vibrational frequencies ω_α, and normal modes $\mathbf{q}_\alpha$

DOI: 10.1021/acs.chemrev.5b00012
Chem. Rev. 2015, 115, 5929−5978

(Duschinsky rotation). All three quantities leading to a variety of vibronic effects have been well explored for small molecules both experimentally[227] and theoretically.[31] This is often not the case for large systems, where calculations of vibrational spectra can be numerically intractable and only a few vibrational modes can be identified in the experimental spectra. Subsequently, a displaced oscillator model[151] accounting for displacements Δ_α only (which indeed captures the core differences between PESs in many cases) is typically implicitly assumed when discussing exciton−phonon coupling phenomena in nanostructures. For example, intensities of vibronic transitions in Raman spectra can be determined as the square of the overlap integral between the vibrational wave functions of the two states that are involved in the optical transition, so-called Franck−Condon (FC) overlaps.[228] The latter in the displaced oscillator model can be readily expressed via the respective Huang−Rhys factors $S_\alpha = \Delta_\alpha^2/2$, which are quantities most commonly used to characterize the strength of the electron−phonon coupling in a given system. Systems with $S > 1$ belong to the regime of strong electron−hole couplings, where the interactions between electronic and vibrational degrees of freedom cannot be treated as a small perturbation. Out of an overwhelming number of the discrete vibrational coordinates $\mathbf{q}$, it is a common case when only a few vibrational modes (or phonons) couple strongly to the electronic system.[170c] It is remarkable that for all systems in the focus of this Review, QDs, SWNTs, and CPs, usually there are only two types of vibrational motions ("fast" and "slow") responsible for the majority of vibronic effects. In the case of quantum dots, these are acoustic (∼50 cm^{-1}) and optical (∼300 cm^{-1}) phonons.[156,229,230] Carbon nanotubes have radial breathing mode, RBM (∼200 cm^{-1}), and G-mode (∼1500 cm^{-1}) relevant to the C−C bond stretching.[106] Conducting polymers feature torsional motion (∼100 cm^{-1}) and C−C stretching (∼1600 cm^{-1})[231] modes.

Computationally, even finding the excited-state optimal geometry can be a numerically demanding task. As in the ground-state case, direct minimization of the excited-state energy (e.g., steepest descent) or use of MD with damping (see eq 5) is a common strategy. It is critical to calculate gradients of the excited-state PES efficiently. Analytic gradients are available for all SCF and TD-SCF computational frameworks.[91,232] While the analytic second-order derivatives (Hessians) were available in the SCF approaches for a long time, these have been derived for TD-SCF methods only recently.[233] This advance is critical for the studies of excited-state vibrational spectra. In the single-electron picture, the excited-state geometry can readily be calculated by promoting one electron from the HOMO to the LUMO and optimizing the wave function with nonequilibrium state population; then keeping the electronic configuration fixed, relaxing the atomic positions.[234,235] This approach, for instance, provides a good approximation for the excited-state geometry of the QDs and inorganic solids, where the excitonic effects are small.

Atomistic simulations of excited-state geometry distortions and Huang−Rhys factors of nanosystems allow for investigations of the dependences of vibronic effects on the size, chemical composition, and the shape of nanosystems and help to reveal the intricate details of electron−phonon interactions in these systems in a presence of surface defects and passivating agents. Calculated observables, such as FC overlaps and Raman spectra, can be directly compared to measurements and provide important insights into interpretations of experimental data.[236] Vibronic effects can be also commonly characterized by spectroscopic parameters, such as Stokes shift frequently defined as the difference between absorption and emission maxima in experiments, which is roughly relevant to the difference between vertical absorption and fluorescence transition energies (see Figure 15). This should be distinguished from the Stokes shift of electronic origin, when the absorbing and emitting states have different electronic character. While the difference is obvious in the case of few level systems, it blurs out for large nanostructures with dense and overlapping electronic manifolds as exemplified below for QDs.

In addition, the FC overlaps and, consequently, the Huang−Rhys factors (see the relationship in ref 237) are directly connected to quantum dephasing of an excitation. Thus, the time-domain representation of the FC factor can be interpreted as a Fourier transform of the overlap of the vibrational wave packets evolving in the initial and final electronic states contributing to the excitation. Evolution of the vibrational wave packets in the electronic state can be obtained from MD coupled to DFT calculations of electronic subsystem, which allows for semiclassical treatment of phonons.[158b] As such, the obtained overlap provides the decoherence function,[220] which, in turn, gives the vibrationally induced decoherence (pure-dephasing) times.[158a,b] The last one can be compared to experimental values extracted from analyses of temperature dependences of shapes of absorption bands as $\Gamma = (1/T_2) = (1/2T_1) + (1/2T_2^*)$. Here, the intrinsic homogeneous line width is inversely proportional to the dephasing time, T_2. The latter includes the excited-state lifetime, T_1, and pure dephasing, T_2^*. For sufficiently long T_1, the line width is defined by T_2^*, which is associated with fluctuations and uncertainties of the energy levels occurring due to coupling to vibrational modes.[238]

5.1. Electron−Phonon Effects in Quantum Dots

The absorbed photon energy in the QDs is normally larger than the emitted energy resulting in the Stokes shift of mixed electronic and vibrational origin. Reported values of the Stokes shifts in CdX and PbX (X = S, Se, Te) QDs vary from 10 meV[239] to 100 meV[240] and even −10 meV[241] (anti-Stokes shift), depending on the composite, size, surface ligands, and shell thickness.[242] Such strong variations in the values are attributed to multiple contributions to the Stokes shift. Previous studies attributed the Stokes shift in QDs to size-distribution effects,[241] the variation of the valley−valley interactions,[18] electron−hole Coulomb and exchange interactions,[243] defect-related electron−hole recombination,[244] and the FC shifts.[234a,245] Only the latter is directly relevant to the electron−phonon couplings and has been shown to play an important role in small QDs.[118b,234b] For example, FC shifts were calculated as a difference between the electron−hole pair energies in the ground-state and excited-state geometries for PbSe, PbTe, and SnTe QDs of different sizes, as obtained from DFT using an occupation-number constraint to simulate excitation.[235] It was found that for QDs with diameters larger than 2 nm, the FC shifts are negligible. For all systems but PbSe QDs, the optical Stokes shifts were much larger than the FC shifts.[235] As such, the FC shift does not have the main contribution to the observed optical Stokes shift in many QDs. Only in some systems, such as 1 nm colloidal PbSe and Si QDs, was the FC shift found to dominate the Stokes shift between optical absorption and emission.[234b,235,246]

The Huang−Rhys factor, S, frequently taken as a measure of the strength of the exciton−phonon coupling, varies from 0.2

DOI: 10.1021/acs.chemrev.5b00012
Chem. Rev. 2015, 115, 5929−5978

to 0.7 for acoustic phonons in PbSe and CdSe QDs of 3−6 nm in diameter, increasing with the confinement.[244] Acoustic phonons correspond to low-frequency coherent movements of atoms of the lattice out of their equilibrium positions and most readily appear in low-temperature spectra of QDs.[229,230] Experimental values of S for optical phonons in the lowest excitonic transitions were found in the range of 0.02−0.5 for CdSe QDs,[247] being considerably smaller than those for bulk CdSe.[248] Optical phonons are out-of-phase movement of the atoms in the lattice giving characteristic vibrational replicas in QDs spectra. The coupling to both acoustic and, particularly, optical phonons has been found to be dependent on the excitonic state, becoming weaker for higher-lying states.[249] Overall, the values of $S < 1$ indicate a weak regime of exciton−phonon couplings in QDs. In contrast to bulk semiconductors, where longitudinal optical (LO) phonons govern the photoexcited electron dynamics, lower frequency acoustic phonons play a key role in dephasing[250] of the electronic transition in QDs and in the radiative properties of the lowest state transition in CdSe, CdTe, PbSe, and InAs QDs, independent of their composition and lattice symmetry.[244,251] For the same size and type QDs, the range of S values for the optical and acoustic phonons differs by at least an order of magnitude.[252] The smaller is the QD, the larger is the surface to volume ratio and the electron−phonon couplings,[246] especially to acoustic modes,[251] although more complicated size dependence has been also reported.[250]

Many discussions of electron−phonon couplings in QDs adopt a macroscopic picture, where phonons are treated as confined versions of the bulk crystal phonons.[253] However, such approach seems to be oversimplified. As compared to bulk semiconductors, the phonons no longer have well-defined wave vectors due to the confinement in QDs. As such, the selection rules for phonons in QDs should differ from those in bulk crystals. In addition, QDs have surface modes not present in the bulk, while a charge carrier confinement modifies the electronic transitions. Subsequently, the magnitudes and character of electron−phonon couplings in QDs are expected to differ from those in the bulk due to differences in both the phonons and the electron excitations. The strength of the exciton−phonon coupling correlates with matching between the wavelength of a vibrational mode and the spatial extent of the exciton. Therefore, highly delocalized excitonic states in bulk systems are much stronger coupled to the LO phonons with comparable wavelengths to the exciton size. However, the confinement of excitonic states in small QDs allows for coupling to smaller frequency vibrations, including the acoustic modes.[248] The presence of surface and defect states in the QDs with more localized character of the excitonic state is expected to result in a dominating role of acoustic phonons in electron−phonon couplings in QDs.

Different atomistic calculations confirm these predictions. For example, simulations of electron−phonon interactions in CdSe QDs based on an empirical FF combined with the effective mass approximations[254] reveal larger Huang−Rhys factors for the acoustic modes than for the optical modes in the lowest energy transitions and decrease with increasing crystal size from 2 to 4.5 nm. In contrast to acoustic modes, the optical mode couplings exhibit a weaker dependence on the QD size for both CdSe[254,255] and PbSe[230] QDs. The theoretically predicted reorganization energies of these systems, corresponding to the energy difference between the electronically excited configuration at the vertical (ground-state) geometry and at the relaxed excited-state geometry and relating to FC shifts, are in the range of 10−30 meV for acoustic phonons and 3−6 meV for optical phonons, as compared to 260 meV associated with LO phonons in bulk CdSe.[254] Thus, the overall electron−phonon couplings are smaller in QDs than in similar bulk crystals, while the coupling with acoustic modes is significantly increased in QDs due to confinement and surface effects. Adiabatic DFT-based molecular dynamics[132] of smaller CdSe and PbSe QDs of 1−1.8 nm in diameter also demonstrate that acoustic phonons with frequencies around 50 and 100 cm^{-1} dominate both electron and hole dynamics for PbSe and CdSe QDs, as shown in Figure 16. The optical modes with

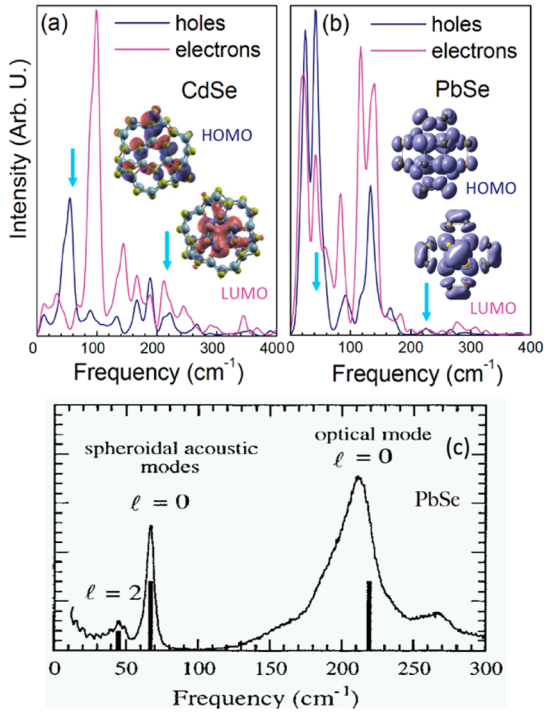

Figure 16. Fourier transforms of the time-evolving energies of initially photoexcited holes (HOMO) and electron (LUMO) states illustrating the hole− and electron−phonon couplings to the lowest energy excitation in $Cd_{33}Se_{33}$ (a) and $Pb_{68}Se_{68}$ QDs (b), computed using first-principles molecular dynamics with DFT and GGA (PW91) functional in plane wave basis. Reprinted and modified with permission from ref 132. Copyright 2011 American Chemical Society. For comparison, experimental Raman spectra of 6 nm PbSe are shown in (c). Reprinted with permission from ref 230. Copyright 1997 American Physical Society.

frequencies around 200−250 cm^{-1} are also clearly present in the spectra but with a smaller amplitude, indicating weaker coupling of both electrons and holes to optical modes. In this approach, thermal fluctuations of electronic levels depend directly on specific phonon modes coupled to these levels. Therefore, vibrational modes that most strongly modulate the energy levels create the largest coupling, appearing as well-pronounced peaks in the Fourier transform of the electronic state energy evolving in time along the trajectory on the ground-state adiabatic potential surface,[132] shown in Figure 16a,b.

The difference in electron−phonon couplings between acoustic and optical modes in QDs is rationalized by the fact that acoustic modes are modulated by QD size, shape, and surface, while atomic displacements of optical modes tend to

DOI: 10.1021/acs.chemrev.5b00012
Chem. Rev. 2015, 115, 5929−5978

average out due to thermal fluctuations. Such conclusion is supported by Raman[230,256] and photon-echo experiments[257,258] of PbS, PbSe, CdSe, and CdTe QDs. From these experimental observations, it was generalized that significantly enhanced acoustic phonon coupling in nanocrystals is indicated by both emission peak shift and large temperature-dependent homogeneous line shape. Strong interaction with acoustic phonons is also responsible for ultrafast dephasing in QDs. The pure-dephasing time was theoretically predicted to be ~10 fs for the lowest excitations in small PbSe QDs[158a] and ~35 fs in CdSe QDs[119a] of 1−1.8 nm in diameter. It was shown that dephasing slows with increasing QD size and is weakly dependent on the excitation energy, while occurring faster for biexcitons than single excitons.[160] In the collective description, low-frequency acoustic modes coupled to nonmetal ions in the QD's core contribute mostly to pure-dephasing. This finding is in agreement with the phenomenological elastic models,[246] predicting decreasing in dephasing time with increasing QD size. Overall, calculated dephasing times well reproduce the measured homogeneous fluorescence line widths in QDs.[259] Because electron−phonon couplings are relatively weak in QDs ($S < 1$), as compared to bulk semiconductors and molecular systems, ultrafast vibration-induced dephasing (<100 fs) is expected in all small semiconductor QDs, independent of their chemical composition.[260]

Changes in vibrational modes also can be used as fingerprints of surface reactions in QDs, for example, for characterizations of the chemical interactions taking place on the surface of the QDs during the formation of QD-Ru(II)-polybipyridine complex assemblies.[124c] IR spectroscopy and, in particular, attenuated total reflectance Fourier transform infrared spectroscopy (ATR-FTIR) have been shown to be a powerful tool in studies of the surface properties of NCs.[124c] These experiments have demonstrated that the Ru(II)-complex adsorption to the CdSe QD surface is associated with a loss of a proton from the anchoring carboxylic group,[124c] which is associated with well-pronounced symmetric and asymmetric COO stretching vibrational frequencies of dye/QD composites, as illustrated in Figure 17a. Overall, three modes of attachment for these complexes to the QD surfaces are possible: unidentate, where one oxygen of the carboxylate linker is bound to one metal ion of the QD surface, chelating, where both oxygens of the carboxylate are coordinated with one metal ion, and bridging, where each oxygen of the carboxylate is bound to metal sites of the QD surface, shown in Figure 17b. Each of these binding modes is characterized by its specific range of the separation, $\Delta\nu = \nu_{as} - \nu_{s}$, between the asymmetric and symmetric stretch of the carboxylate group. These $\Delta\nu$ values have been effectively used as an empirical guideline for distinguishing between binding modes of carboxylic acids to various metal oxide surfaces.[261] For the complex **2**, $\Delta\nu \approx 210$ cm^{-1} is consistent with an attachment via a bridging mode[262] (see Figure 17b). The DFT and TD-DFT simulations of $Cd_{33}Se_{33}$ clusters passivated with carboxylate groups result in the largest absolute values of the binding energies between the QD and the carboxylate in its bridging position,[124c] while $\Delta\nu$ gave the values of 289, 140, and 55 cm^{-1} for the unidentate, bridging, and chelating geometries, respectively, following the experimental trends. These calculations[124c] support the conclusion obtained from ATR-FTIR spectra for the dye-functionalized CdSe QDs that the complex **2** attaches exclusively to the cadmium sites of the QD surface via a bridging geometry, with the carboxylic acid anchoring group

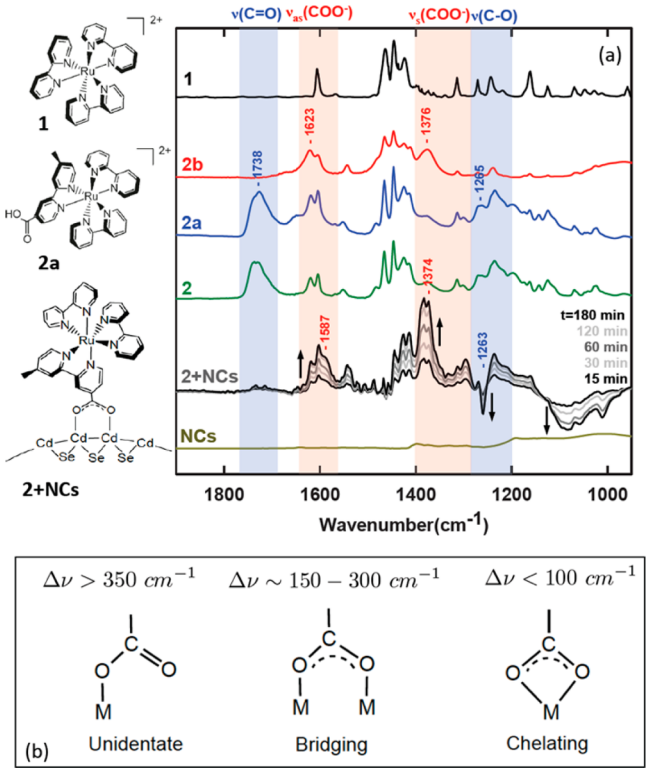

Figure 17. ATR-FTIR spectra observed following exposure of CdSe nanocrystal (NC) film to 10^{-3} M acetonitrile solution of complex **2** (**2**+NCs), recorded at indicated delay (gray lines). For references, the spectra of independently prepared films comprising complexes **1** and **2** and its protonated (**2a**) and deprotonated (**2b**) forms, and the film of NCs are also shown in (a) with schematic structures of studied systems represented in the left column. (b) Possible modes of attachment of the carboxylic acids to semiconductor surfaces and corresponding difference in frequencies of symmetric and asymmetric stretches of the carboxylic acid group, computed by DFT with B3LYP functional and LANL2DZ basis set using CPCM for solvent model by Gaussian 09 software. Reprinted and modified with permission from ref 124c. Copyright 2011 American Chemical Society.

being deprotonated in the process. Similar results have been recently obtained for 1−1.8 nm PbSe and ZnO QDs supporting that the most stable QD-Ru(II)-complex structures occur through binding of the complex in a bridging mode to the QD surface.[119c,159]

5.2. Huang−Rhys Factors and Excitation Self-Trapping in Conjugated Systems

It is well established that exciton−vibrational interactions are strong and practically define the entire photoinduced dynamics of CPs[85a,169a,221] and conjugated molecular systems.[224a,b,263] For instance, pronounced ~0.1−0.5 eV Stokes shifts in optical spectra of CPs generally have predominantly vibronic origin due to vibrational relaxation of the lowest singlet S_1 state PES. The latter leads to a significant distortion of the molecular geometry,[91] exemplified in Figure 18 for PPV systems. As shown in section 4.2, the ground-state structure of PPV is not planar; weak perturbations such as impurities and intermolecular interactions may lead to a significant torsional disorder. The situation is very different for the excited-state S_1. Here, the energy profile is no longer shallow with respect to the torsional motion and has its global minimum at a planar structure shown in Figure 18a.[85a,231] The BLA parameter introduced in section 2.1 is an important feature of a conjugated oligomer's geometry

DOI: 10.1021/acs.chemrev.5b00012
Chem. Rev. 2015, 115, 5929−5978

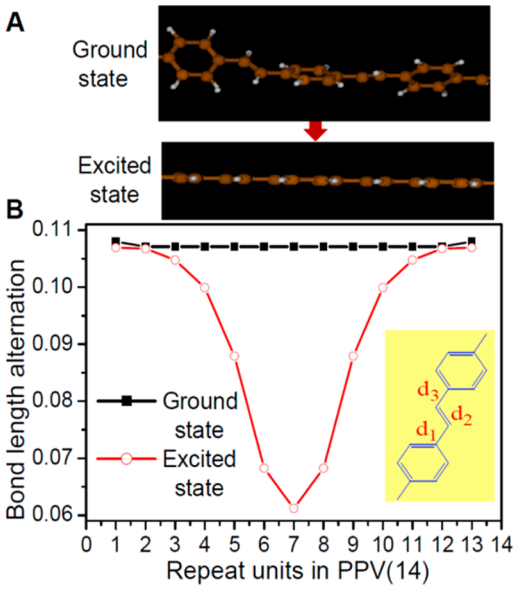

Figure 18. Geometry relaxation along the excited-state surface from the ground to the lowest excited-state equilibrium geometry of PPV(14) oligomer. The excited-state structure shows reduced torsional disorder (planar geometry) (A) and reduced bond-length alternation $(d_1 - d_3)/2 - d_2$ in the middle of the molecule (B), as compared to the ground-state geometry. Simulations have been conducted using AM1/CIS representation of excited states. Reprinted and modified with permission from ref 91. Copyright 2002 American Physical Society.

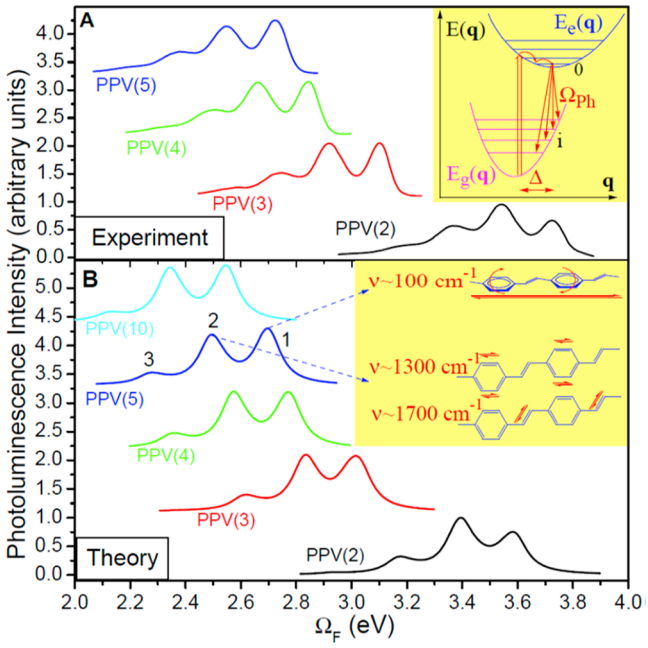

Figure 19. Experimental (A) and calculated (B) photoluminescence spectra of PPV oligomers. Inset in (A) schematically displays emission processes between vibrational levels of the excited and ground states controlled by magnitudes of the corresponding Franck–Condon factors. Inset in (B) shows dominant nuclear motions leading to vibrational structure of the fluorescence line shape. Simulations have been conducted using AM1/CIS representation of excited states. Reprinted and modified with permission from ref 91. Copyright 2002 American Physical Society.

reflecting the uneven distribution of the π-electrons over the bonds associated with the effect of spontaneous symmetry breaking also known as Peierls distortion.[264] In half-filled zone materials, Peierls distortion leads to gap opening at the Fermi level, the metal–semiconductor transition.[264] Polyacetylene provides an example of such transition with the gap opening of about 2 eV.[221] As shown in Figure 18b, the BLA parameter in the adjacent vinylene linkages of PPV(14) is constant along the chain for the ground-state geometry and noticeably reduced in the middle of the molecule for the excited-state geometry. Such vibronic activities frequently lead to the spatial confinement of the excited-state wave function (exciton self-trapping)[91,265] as discussed below and appear across many experimental measurements such as IR/Raman or UV–vis spectra, time-resolved spectroscopic probes, and molecular conductance.[266] For example, a characteristic progression signifying coupling of specific vibrational modes to the electronic system with Huang–Rhys factors $S \approx 1-2$ for CPs is frequently observed in absorption and emission spectra and can be well captured with electronic structure simulations[267] (see Figure 19 for the PPV case).

Similar to CPs, various signatures of electron–phonon interactions in the photophysics of SWNTs have been evidenced in various experiments, including vibronic resonances in the photoluminescence excitation spectra,[205b] vibrational progression in absorption/fluorescence line shapes,[268] Raman spectroscopy,[269] coherent phonon excitation experiments,[106] transport measurements,[270] as well as theoretical studies.[95a,99c,101b–d] However, nanotubes have more rigid structure, as compared to organic molecules and CPs. As such, vibronic effects in SWNTs are expected to differ from those in the above systems, while also being very sensitive to the tube's diameter and chirality. Quantitative measurements of electron–phonon coupling constants and Huang–Rhys factors from the analysis of experimental Raman profiles[271] and calculations[101b,272] place SWNTs in a regime of weak coupling strength as compared to typical molecular systems. In fact, Huang–Rhys factors for SWNTs of about 1 nm in diameter have been found in the range of 0.01–0.02 for the lower frequency radial breathing mode (RBM) associated with acoustic phonons.[101a,b] Conformational changes induced by the C–C bond stretching, the longitudinal G-mode, are stronger, as compared to RBM modes. Typical Huang–Rhys factors along E_{11} PES for G-modes are 0.1–0.4, respectively, for SWNTs with diameter of about 1 nm.[106,271b] Despite the weak electron–phonon coupling regime, sophisticated vibronic phenomena have been experimentally detected, such as anharmonic coupling between RBM and G-mode appearing in the excited-state potential,[106] ultrafast bandgap oscillations upon intense short optical pulses via the generation of coherent phonons,[273] and exciton self-trapping.[274]

Electronic structure calculations can quantify the differences in geometries of ground (GS) and E_{11} excited (ES) states. Figure 20 compares the GS and ES structures of several SWNTs. The GS geometry contains the corrugation of a tube surface appearing as sharp peaks in the radial dependence in Figure 20a,b. These surface corrugations are associated with the BLA parameter making some bonds shorter (more like a double bond) and some bonds longer (more like a single bond) in the hexagonal cell of both zigzag and chiral nanotubes.[101c] Because of the rigid structure, the respective nanotube BLA is about 0.01–0.02 Å, which is about 10 times smaller than those in CPs (see Figure 18b).[101a] This geometric distortion, caused by interactions of σ- and π-orbitals induced by the curvature,

DOI: 10.1021/acs.chemrev.5b00012
Chem. Rev. 2015, 115, 5929–5978

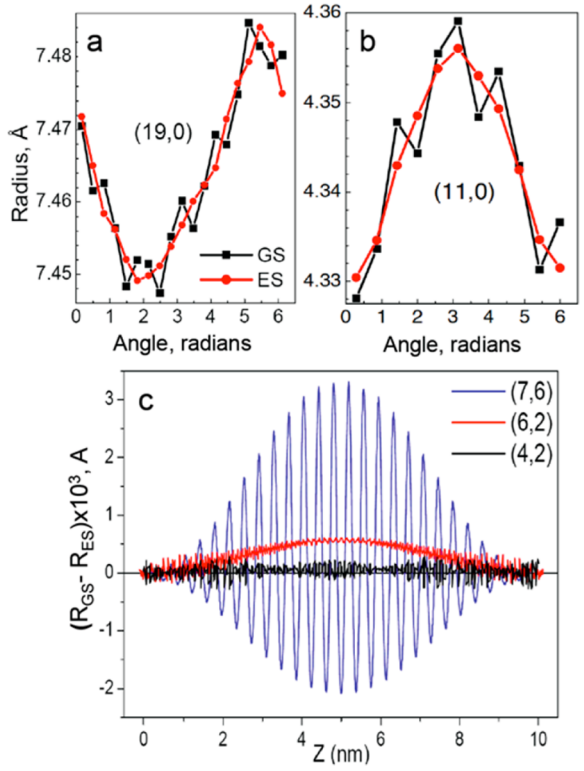

Figure 20. Variation of tube radius at the ground (GS) and E_{11} excited-state (ES) geometries as a function of azimuthal angle (a,b) and the tube axis Z (c) showing a change in corrugation of the tube surface in the ground versus excited states. GS geometry is corrugated for all considered tubes, while ES geometry exhibits smoother surface shape and, thus, decreased Peierls distortion. The narrower is a nanotube, the less difference is observed between the GS and ES distortions. Reprinted and modified with permission from refs 101a and 101c. Copyright 2007 Elsevier (a,b) and 2007 American Chemical Society (c).

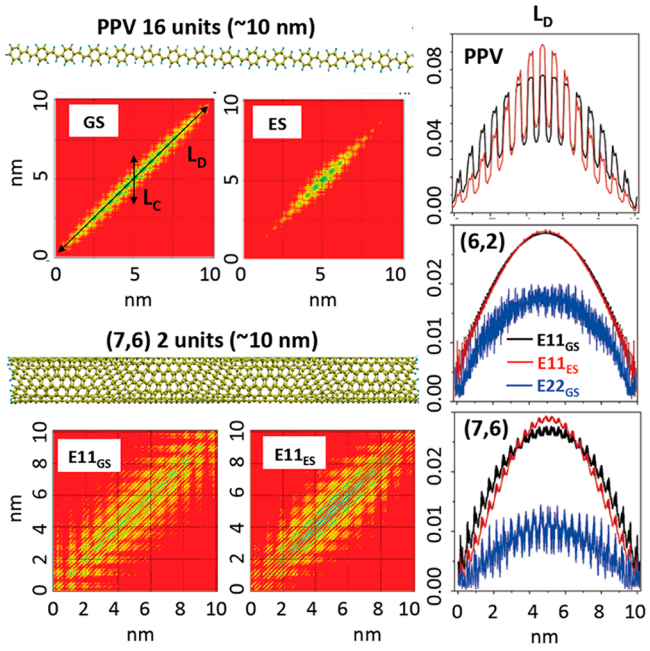

Figure 21. Comparison of transition density matrices from the ground state to the lowest optically active excited state (E_{11}) of various SWNTs and the PPV polymer of similar length. The first and second columns display two-dimensional contour plots of transition density matrices for E_{11} excitons at the GS and ES optimal geometries, respectively, as a function of electron (Y-axis, nm) and hole (X-axis, nm) coordinates. Transition density magnitude scales from red (0) to violet (1) through the natural rainbow color sequence. The right column shows the diagonal slice (L_D) of the E_{11} and E_{22} transition density matrix as a function of electron−hole pair position along a tube illustrating delocalization patterns of excited states. Similar to the PPV, SWNTs with larger diameter exhibit higher localization of the E_{11} exciton in the middle of a tube (self-trapping) at ES geometries as compared to the GS profile. Computations are completed by TD-HF approximation combined with the AM1 Hamiltonian. Reprinted and modified with permission from ref 101c. Copyright 2007 American Chemical Society.

has many similarities with Peierls distortion phenomenon.[264] However, in contrast to CPs, the produced band gap in the metallic SWNTs is smaller than the energy of thermal fluctuations,[275] rationalized by much weaker local distortions in nanotubes. Despite a small value of BLA, its change in the ES is well noticeable: The BLA nearly diminishes at the ES geometries, making the nanotube surface locally less distorted, as seen in Figure 20a,b. The periodic oscillations in the difference between the radial distances of carbon atoms along the tube length in the GS and ES geometries (Figure 20c) reflect the decrease of radial difference upon relaxation of photoexcitation, with the largest geometric changes developing in the middle of the tubes. Overall, zigzag tubes show larger ES structural relaxation than chiral tubes.[101a] This vibrational relaxation vanishes in the limit of very narrow tubes[101c] due to disruption of π-conjugation and curvature induced strain. The vibronic relaxation increases and reaches a maximum for tubes with diameters close to 1 nm. For tubes with a diameter >1 nm, the radial difference becomes smaller and approaches zero in the graphene limit.

Structural changes in the excited state (Figures 18 and 20) manifest concomitant localization of the exciton in the center of the system, known as exciton self-trapping detected both in CPs[91] and SWNTs.[101c] Figure 21 signifies similarities of this phenomenon for both cases by examining the diagonal size L_D of transition density matrices corresponding to the lowest singlet electronic excitations, which quantify the spatial extent of excited-state wave function. As expected, the self-trapping effect of the lowest exciton in CPs is significantly stronger than those in SWNTs, as illustrated in Figure 21 for the PPV case, due to much stronger electron−phonon couplings. The trend in the exciton trapping in SWNTs follows the magnitude of lattice distortions: it vanishes for narrow nanotubes with diameter less than 1 nm (e.g., (6,2) as shown in Figure 21) and becomes most pronounced in SWNTs with diameter of about 1 nm (like (7,6) in Figure 21).

An important and interesting phenomenon resulting from electron−vibrational coupling and spatial redistribution of the excitonic wave function is violation of the so-called Condon approximation.[276] The latter states that the dipole moment should be independent of the vibrational coordinates and has been successfully used in modeling and analysis of vibrational spectra, particularly of small molecules.[277] However, the validity of the Condon approximation in the world of nanostructures should be carefully considered. For example, an extremely strong violation of this approximation has been recently observed[210b] in the case of cycloparaphenylenes ([n]CPP),[278] which consist of n-phenyl units connected in a conjugated periodic chain. Unique circular geometries of CPPs ensure a variety of interesting physicochemical and electronic properties

DOI: 10.1021/acs.chemrev.5b00012
Chem. Rev. 2015, 115, 5929−5978

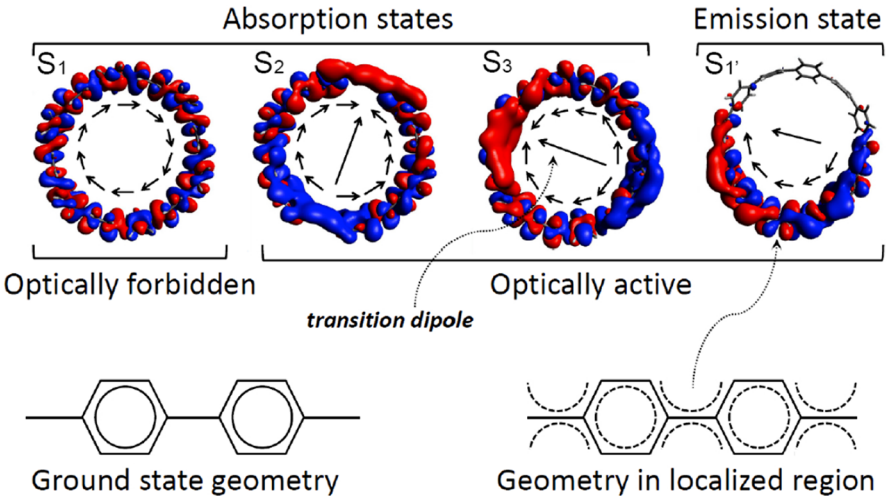

Figure 22. Top: Orbital distribution of transition density and schematic of transition dipole for S_1, S_2, S_3, and S_1 transitions in [12]CPP molecule. Bottom: Torsionally distorted geometry in the ground state locally planarizes due to vibronic relaxation. In the ground-state geometry, S_2 and S_3 states are optically active, whereas S_1 state is optically forbidden due to symmetry. Exciton self-trapping of S_1 leads to the appearance of transition dipole and strong fluorescence. Computations were performed using CAM-B3LYP/6-31G* model chemistry coupled with CPCM solvent model. Reprinted and modified with permission from ref 279. Copyright 2014 American Chemical Society.

valuable for many applications in materials science and technology such as photovoltaic, photoelectronic, and light-emission technologies. Here, in contrast to the linear CP chains, the lowest S_1 state is optically forbidden as shown in Figure 22. The next electronic states S_2 and S_3 are degenerate and strongly optically allowed with perpendicular polarization emerging from the orthogonal transition dipole moments, making the CPPs good light absorbers. A significant transition dipole moment (and oscillator strength) appears in the lowest excited state during its equilibration[279] due to exciton self-trapping, making this class of chromophores excellent light emitters[278a] due to violation of Condon approximation.[228]

Non-Condon effects may also appear in SWNTs resulting in nontrivial profiles of Raman spectra. Resonant Raman experiments of single-chirality enriched SWNT samples reveal strong asymmetry in intensities of the resonance coupling of G-mode to incident and scattered photons for the second excitonic band E_{22}.[280] The observed asymmetry can be attributed to violation of the Condon approximation. Quantum chemistry calculations at the level of CIS coupled to semiempirical Hamiltonian determined the degree to which displacement along the G-mode coordinate affects the transition dipole moment of the E_{22} band in (7,6) and (9,4) SWNTs.[101d] For both tubes, excitonic band E_{22} demonstrates redistribution of intensities between the most optically active and optically weak transitions in tubes with geometries disturbed by displacement parameter along the G-mode. The simulated change in the intensity of E_{22} as a function of the displacement along the G-mode confirms the non-Condon behavior of SWNTs. Significant non-Condon contribution to Raman response was also experimentally detected for E_{33} and E_{44} bands in (8,6), (9,4), and (10.5) SWNTs.[281] However, alternative interpretation of the asymmetric Raman profiles of G-modes has been suggested recently[269b] within the framework of the quantum-field third-order model for Raman scattering and perturbation theory. This model described the observed asymmetry in Raman profile of G-mode to the contribution of van Hove singularities in the optical transitions and to the wave-vector dependence of the matrix elements of the Raman-scattering process in SWNTs.[269b]

5.3. Electron–Vibrational Couplings and Polarons in Conjugated Polymers

The previous section has focused on the role of electron–phonon coupling in delocalization of optically active excitations (singlet states) in organic materials. Similar effects appear also for other significant electronic excitations such as charge and spin states. Ultimately, interactions of energy (excitons) and charge (polarons) carriers[282,283] and their delocalization properties define optoelectronic properties of CPs being strongly affected by materials morphology.[47a] For example, charge carriers anion and cation in organic CPs are typically localized on a segment of a π-conjugated polymer creating a local distortion in the structure.[284] Frequently, such quasiparticles are denoted as polarons, where dressing is provided by interactions of a charge with the lattice. Notably, when considering charge states, the role of dielectric environment should not be overlooked. Both experimental and theoretical studies revealed that polarization effects play an important role in polaron formation.[285,286] As such, there are two distinct origins leading to self-localization (or self-trapping) of electronic excitations in low-dimensional semiconducting polymers. First is the distortion of molecular geometry, which may create a spatially localized potential energy well where the state wave function self-traps. Second, even in the absence of geometric relaxation and vibrational dynamics, the electronic excitation may become spatially confined due to energy stabilization caused by polarization effects from the surrounding dielectric medium. These origins are challenging to separate experimentally, while atomistic quantum chemistry calculations are in a better position to get insights into this question.[94,287]

Computationally, there is a great sensitivity of the results to the choice of model chemistry.[285,288] For example, pure DFT functionals such as BLYP within unrestricted Kohn–Sham scheme are unable to reproduce charge localization by overestimating delocalization of polarons in PPVs and its derivatives.[288,289] As was the case for excitonic effects (see section 3.2), a quantitative description of the polaronic states strongly depends on the amount of orbital exchange included in the DFT functionals.[166a,b,290] The larger is the HF portion in

DOI: 10.1021/acs.chemrev.5b00012
Chem. Rev. 2015, 115, 5929–5978

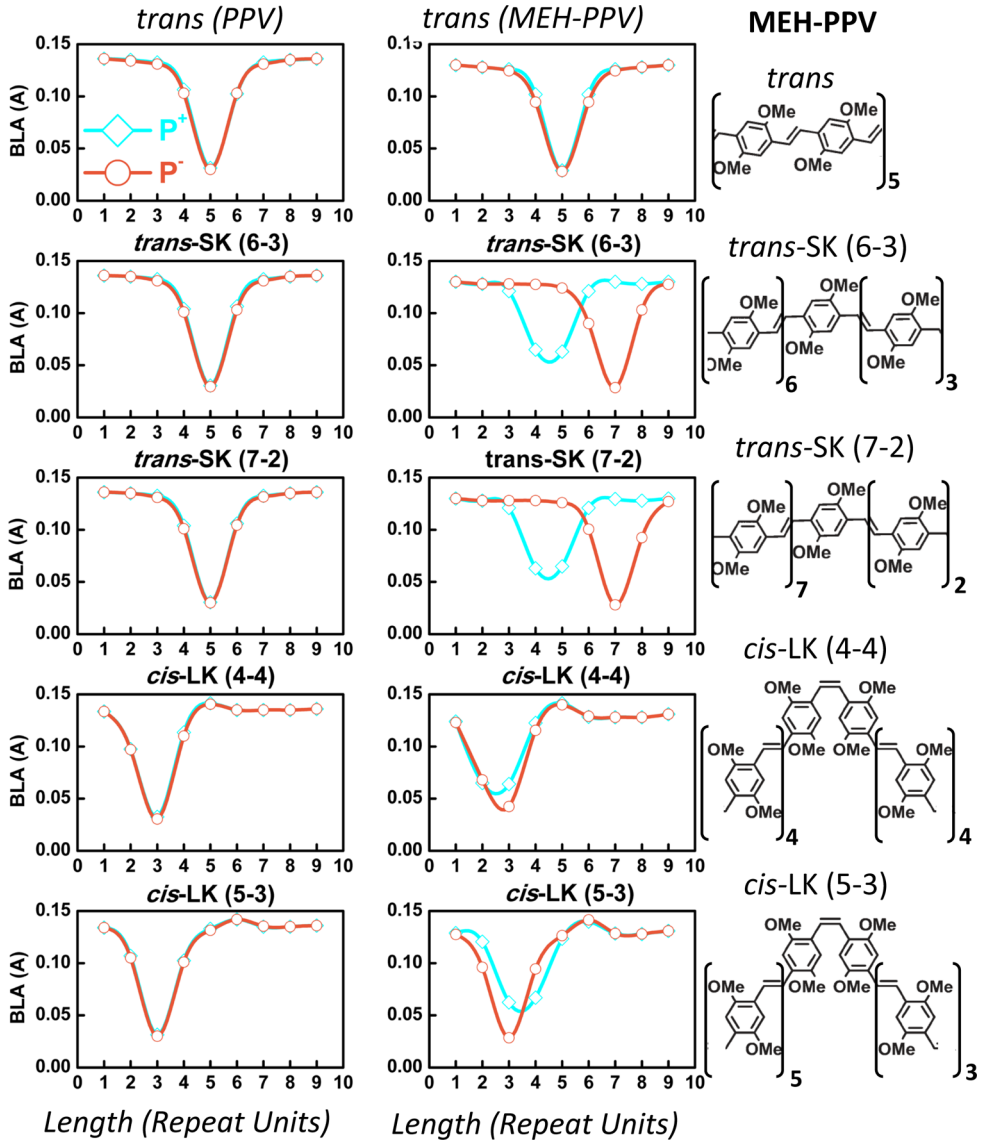

Figure 23. BLA defined in Figure 18 along the length of the PPV (left column) and MEH-PPV (middle column) chains with *trans*- and *cis*-defects for charged species. The dip in the BLA distribution corresponds to the self-trapping region of P^+ and P^- polarons. Depending on the type of the *trans*- and *cis*-defects (right column), polarons attract or repel from it. Notably, symmetry between P^+ and P^- excitations is broken in MEH-PPV. Computations were performed using LC-wPBE/6-31G* model chemistry coupled with CPCM solvent model. Reprinted and modified with permission from ref 287a. Copyright 2013 John Wiley & Sons, Inc.

hybrid functional, the stronger is the spatial localization of both polarons and excitons, while polaron's localization significantly increases when a polar continuum environment is introduced into calculations.[94] According to the results of refs 94 and 287, however, only long-range corrected functionals such as LC-wPBE are able to reproduce the extent of the polaronic spin density in MEH-PPV (2−3 repeat units) consistent with experimental estimates.[291,292]

Finally, we illustrate complex relationships between polaronic localization and CP morphology resulting in breaking symmetry between conduction and valence bands present, for example, in an ideal chain. Indeed, previous experimental[200] and theoretical[87,163d,293] studies observe a strong dependence of the optical response of the opposite carriers on the molecular structure. Asymmetry in response of the opposite charged polarons was optically detected in magnetic resonance response of MEH-PPV.[294] It is important to note that in experimental samples both torsion disorder and *cis*- and *trans*-defects are present. The latter have been shown to differently affect the electron and energy transfer properties in PPV derivatives with various side-chain substitutions.[295,296] The fluorescence intensity of the optoelectronic devices was shown to improve by the introduction of *cis*-defects into the backbone of the PPV derivatives.[297−299] Further, in a theoretical study,[300] the hole and electron transport properties were observed to be markedly different for *cis* conformations of PPV derivatives in comparison to the *trans* ones. TD-DFT calculations confirm that the introduction of weak-trans defects along the MEH-PPV chain results in asymmetry of positive P^+ and negative P^- polarons, while preserving their symmetry in PPV chains, as illustrated in Figure 23. Self-trapping of P^+ and P^- polarons signified by BLA occurs for both PPV and MEH-PPV polymers in the middle of the chain for their undistorted *trans* geometries. However, *trans*-defects in MEH-PPV shift the P^- state closer to the defect position, whereas P^+ stays away from it. In contrast, *cis*-distortion does not contribute to the asymmetry between P^+

DOI: 10.1021/acs.chemrev.5b00012
Chem. Rev. 2015, 115, 5929−5978

and P^- polarons in MEH-PPV, while slightly shifting them from the center to the edge of the oligomer. Similar behavior is observed in PPV with a strong *cis*-distortion, while *trans*-defects do not affect the position of both polarons. The difference in polaron self-trapping between PPV and MEH-PPV is attributed to the presence of the alkoxy groups (OCH_3) on the phenyl rings in the latter, distributing a complex set of local dipoles along the molecular backbone.[287a] The difference between P^+ and P^- locations in the presence of *trans*-defects in MEH-PPV originates from the existence of two energy minima for opposite charged carriers, with the energy barriers of ~13 meV ($<k_BT_{room}$) for P^+ and 55 meV for P^- polaron in the *trans*-SK(6−3) configuration. The lower energy difference between the two wells of positive polaron provides a higher drift mobility of holes in weakly defected *trans* MEH-PPV geometries than the electrons, which well agrees with the lower reorganization energies in these systems[301] and experimental findings.[294]

As compared to CPs, interplay of electron−phonon coupling and charge carrier localization has been explored to a much lesser extent in SWNT and QD materials. In inorganic semiconductors, including QDs, the density of charge carriers is typically delocalized over the entire lattice[124a] or getting fully localized on the surface state or dopant atom.[122c,302] Charge carriers in SWNTs are extremely mobile. However, experimental evidence of charge states localized on the nanometer-scale in carbon nanotubes was reported recently.[303] This phenomenon was attributed to an enhanced electron−vibrational coupling and distortion of the tube surface similar to the exciton−phonon features discussed in Figures 20 and 21.

6. NONADIABATIC DYNAMICS AND NONRADIATIVE RELAXATION

Prediction of photoexcited dynamics at molecular- and nanoscales is fundamental to a myriad of technological applications, ranging from sensing, imaging, solar energy harvesting, to future optoelectronic devices. After a molecule absorbs light quantum, a typical scenario includes relaxation of the initial excitation via phonon/vibronic mechanisms through multiple excited states (intraband relaxation), leading to spatial energy transfer, excitation localization/delocalization, and/or charge separation phenomena, schematically illustrated in Figure 24a. Understanding and control over these processes (photoinduced pathways) lies in the heart of all of our efforts to design functional photoactive materials for many technological applications. Modern time-resolved ultrafast spectroscopy is a major tool to study such dynamics.[151]

The simplest but practical models describing the rate k of transitions between initial (i) and final (f) electronic states is based on the celebrated Fermi golden rule $k_{i\to f} = (2\pi/\hbar)|V_{if}|^2\rho_f$, where V_{if} is coupling between states and ρ_f is the density of final states. Examples of such models include Foerster theory[304] describing energy (excitation) transfer,[305] Marcus theory describing charge transport,[301] and Landau−Zener tunneling in the case of nonradiative transitions between two electronic terms.[306] The key quantities to all of these models such as electronic couplings and spectral overlaps (Forster theory) or electronic couplings and reorganization energies (Marcus theory) can be extracted from quantum chemical methods,[130,169a,307,308] which have been discussed in the previous sections. Such approaches do provide a prototype framework for first-principle simulation of transport or relaxation phenomena. However, frequently common cases already

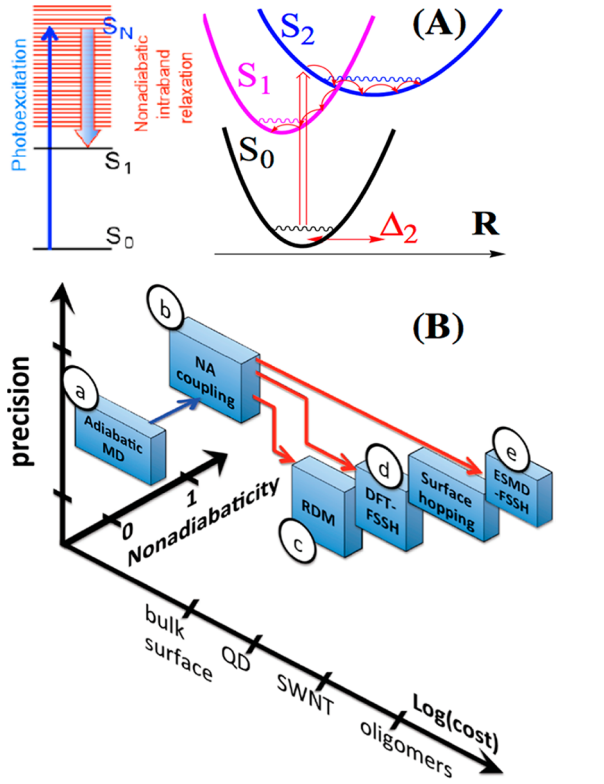

Figure 24. (A) The main aspects of photoexcited dynamics: Electronic excitation from the ground-state surface S_0 to an excited-state S_N follows by nonadiabatic intraband relaxation with typical time scales from ~100 fs to ~10 ps. This relaxation involves complex electron−vibrational dynamics where transition probabilities depend on nonadiabatic couplings between states. (B) Schematic overview of methods for photoexcited dynamics applicable to atomistic modeling of nanosized systems. Methods are grouped by contributions of nonadiabatic (NA) electronic transitions (nonadiabaticity), numerical cost, and precision. Adiabatic electronic states calculated along MD trajectories (a) serve as a reference point. Methods including quantum electronic transitions (marked by red arrows) use first-order NA couplings (b) computed using MD trajectories. Time evolution of an excitation is based on density matrix (c) or surface hopping within the ground-state (d) or excited-state (e) trajectories.

feature multiple photoexcited pathways difficult to describe with a phenomenological few-level systems. Moreover, association of initial (i) and final (f) states with specific electronic transitions or molecular fragments, is frequently unclear and ambiguous.

This calls for direct atomistic modeling of photoexcited electronic processes, which is much more challenging as compared to adiabatic Born−Oppenheimer MD on a single-state PES,[91,232a,309] as discussed in section 5. The main problem is treatment of nonadiabatic electron−phonon processes allowing changing PESs and wave functions (i.e., quantum transitions) in the course of dynamics. This requires consideration of electronic and nuclear interactions beyond Born−Oppenheimer approximation[310−312] with inclusions of quantum features in the vicinity of the level crossing.[313] Methods providing quantum mechanical/semiclassical dynamics in such cases exist, for example, path-integral techniques[314] or multiconfigurational time-dependent Hartree (MCTDH)[315] techniques solving the time evolution of the nuclear wave packet. The ab initio multiple spawning (AIMS)[313b,c,316] simultaneously solves nuclear dynamics (via evolution of frozen

DOI: 10.1021/acs.chemrev.5b00012
Chem. Rev. 2015, 115, 5929−5978

Gaussian wavepackets) and electronic structure problems. While being accurate enough, these approaches, however, are not feasible for applications to extended systems of hundreds of atoms in size, due to tremendous computational cost.

Mixed quantum-classical dynamics approaches[317] are numerically easier. The relative simplicity in these approaches comes at the expense of built-in severe approximations underlying inconsistencies between quantum and classical mechanics.[317] Here, we briefly outline the main approaches used in the field and refer the interested reader to comprehensive reports.[318] The time-dependent wave function is typically presented on the basis of adiabatic excited-state wave functions ϕ_i as

$$|\Psi(\mathbf{r}, \mathbf{R}, t)\rangle = \sum_i C_i(t)|\varphi_i(\mathbf{r}; \mathbf{R})\rangle \tag{7}$$

where $\mathbf{r}(\mathbf{R})$ corresponds to electronic (nuclear) degrees of freedom and the expansion coefficients $C_i(t)$ satisfy the equation of motion (time-dependent Schrodinger equation):

$$i\hbar\frac{\partial}{\partial t}C_i(t) = C_i(t)E_i - i\hbar\sum_j C_j(t)\dot{\mathbf{R}}\mathbf{d}_{ij} \tag{8}$$

with the first term corresponding to the adiabatic state with the energy E_i. The main ingredients driving quantum transitions between adiabatic states are the first-order nonadiabatic (NA) derivative couplings (the second term in eq 8):

$$V_{ij} = \langle\varphi_i|\partial/\partial t|\varphi_j\rangle = \sum_I d_{ij,I}\dot{R}_I = \mathbf{d}_{ij}\dot{\mathbf{R}} \tag{9}$$

$$\mathbf{d}_{ij} = \langle\varphi_i|\nabla_{\mathbf{R}}|\varphi_j\rangle \tag{10}$$

Here, indices i, j refer to electronic states, whereas I labels nuclei degrees of freedom. The Ehrenfest (or mean field) dynamics propagates nuclei using an average force corresponding to the electronic subsystem being in a linear combination (superposition) of adiabatic states according to eq 8. It can be considered as an intermediate step from adiabatic to nonadiabatic MD.[319] However, the Ehrenfest method suffers from the same deficiency as all mean field approximations; that is, classical motion follows a single average path.[320] This deficiency is critical in modeling systems, where different excited-state PESs vary dramatically from each other and from the ground state, and when there are multiple products.

Surface hopping approaches (such as fewest switches surface hopping (FSSH) algorithm) typically average over a family of classical trajectories, where quantum transitions among states are allowed.[321,322] These techniques address the deficiency of the Ehrenfest dynamics by allowing a trajectory to split into branches, so that each quantum state gives rise to a different branch governed by state-specific forces and weighted by the quantum state probability. For example, in the FSSH, the probability for a quantum transition from the current electronic state i to all of the other states j is proportional to the NA couplings V_{ij}, calculated at each integration step along the classical MD trajectory following Tully's algorithm minimizing the number of hops between electronic states.[322−324] Overall, the FSSH can be interpreted as a quantum master equation for electron dynamics, in which state-to-state transition rates nonperturbatively depend on time through couplings to explicit phonon dynamics simulated at the atomistic level.[322,323]

The FSSH-type approaches are the most common nonadiabatic MD schemes with various implementations ranging from ab initio methods[325,326] to DFT[318a] and TD-DFT[56b] to semiempirical models[327] to reduced Hamiltonian problems.[328,329] Figure 24 schematically represents methods of different level of complexity dictated by used approximations, which are commonly employed in simulations of photoexcited dynamics of large systems. To make the FSSH feasible for large systems, a series of approximations were made to lighten the computational load.[318a,323,330] The most severe is the classical path approximation, which assumes that nuclei behave according to classical Hellman−Feynman forces, which are equal for the ground and excited electronic states, due to negligible variations in the ground versus excited-state total densities. In this case, either a single ground-state or excited-state adiabatic trajectory can be used as input for the NA simulations. Such strong approximation is justified for inorganic solids, QDs, and SWNTs, having relatively rigid structures and small Franck−Condon factors pointing to weak distortions of their lattices by absorbed light, as we discussed in section 5. Additional drastic approximation is neglecting electron−hole correlations, so that the excited states are described as single-electron excitations between KS orbitals as discussed in section 3.[331−333] This time-domain KS (TD-KS) framework (d-method in Figure 24) has been found to work well for describing the energy relaxation process in semiconductor surfaces,[330,334] as well as bare,[318a] ligated,[158c] and doped[335] quantum dots, and also SWNTs.[95b,97]

Such approximations, however, may not be suitable for organic conjugated materials featuring strong excitonic effects and large electron−vibrational couplings. In this case, the NA excited-state MD (NA-ESMD)[85a,141,336,337] (e-method in Figure 24) relies on the FSSH and describes excited states using the configuration interaction singles (CIS) formalism with a semiempirical model Hamiltonian accounting for excitonic effects. Furthermore, the use of state-specific gradients for propagation of nuclei on the native excited-state PES eliminates the need for the classical path approximation. Efficient computation of analytic NA couplings[338−341] and gradients[139a,141] allows for NA-ESMD considerations for hundreds of atoms on ∼10 ps time scales by simulating a few hundreds of classical trajectories with various initial conditions to be propagated along different excited-state PESs. The computational compromise here is usage of numerically efficient semiempirical models with limited quantitative accuracy.

One of the major drawbacks of the FSSH method is the lack of decoherence and description of interference phenomena in the electronic wave function due to independent trajectory framework. To overcome this problem, various decoherence corrections were implemented to the FSSH algorithms.[328,342−344] For example, the method proposed in refs 345−347 includes phase corrections to the electronic propagation and does not require the specification of a decoherence time or simultaneously running trajectories on multiple electronic PESs.[328] The decoherence-induced surface hopping (DISH) algorithm coupled with the time-domain DFT has been developed by Prezhdo's group.[348] Recently developed, the semiclassical Monte Carlo (SCMC) approach[266,349] accumulates phase information characterizing each classical trajectory, which is further used to perform "postprocessing" evaluation of multidimensional integrals while retaining the FSSH simplicity in applications to the realistic systems.

Decoherence between excited states and relaxation of an excitation to the thermal equilibrium can be also computed in terms of reduced density matrix (RDM),[350] an analytically

DOI: 10.1021/acs.chemrev.5b00012
Chem. Rev. 2015, 115, 5929−5978

derived method complementary to the surface hopping algorithm. Here, dynamics is efficiently described by averaging over the NA couplings, $V_{ij}(t)$, obtained at a short period of the adiabatic trajectory and providing time-independent NA couplings as a parameter for each electronic transition. This parametrization follows from decomposition of a molecule into a system (electronic degrees of freedom) and bath (nuclear motion) parts, as implemented in the multilevel Redfield theory.[351,352] Upon average over the ensemble, the influence of nuclei on electrons is represented by the autocorrelation functions of NA coupling.[353] Such autocorrelation functions decay instantly, thus justifying use of the master equation with time-independent coefficients, in contrast to the FSSH procedure. A time average of the autocorrelation function of NA couplings provides time-independent Redfield coefficients of electronic transitions that enter into the equation of motion for the electronic degrees of freedom to get evolution of the state population[318d,354] (c-method, in Figure 24). Being less accurate but still consistent with the FSSH,[355] the RDM is faster and works well for the semiconductor bulk and surfaces.[318d,356−358]

6.1. Photoexcited Dynamics in Quantum Dots

Because of the much higher surface/volume ratio as compared to bulk materials, surfaces play a critical role in defining light-driven charge transport and energy relaxation processes in QDs. Effects of the surface ligands and dopants on the radiative and nonradiative dynamics of QDs have been experimentally studied for several decades.[180,239,359] However, questions of controlling the surface chemistry are still open, mainly because of a lack of suitable experimental and theoretical tools for quantitative characterization of the surfaces of nanostructures. Some progress has been achieved in simulation of relaxation processes in small bare PbSe and CdSe QDs.[118a,119a,b,132,158b] Most of these simulations address the question why QDs demonstrate ultrafast electron relaxation similar to bulk materials (a few picoseconds). Strong confinement in QDs is expected to result in a significant mismatch between the electronic and vibrational energy quanta, which should slow the rates of energy relaxation through electron−phonon interactions and, thus, significantly reduce the loss of photoexcitation to heat.[360] Known as phonon-bottleneck, the effect remains elusive, except the cases where the emitting central core of the QD is isolated from a surface environment by shells of other semiconductor structures, like, in "giant" QDs.[10,361] Several mechanisms have been suggested to explain the absence of the phonon-bottleneck in QDs: (i) many-phonon interactions, (ii) the Auger process, when the excited electron exchanges its energy with the coupled hole, and the hole then relaxes fast through its denser manifold of states,[17,362] and (iii) surface processes, including surface impurities, defects, and passivating ligands.[15b,363] Experimentally, it is almost impossible to decouple these processes. The exception is the giant QDs, where several shells of different thicknesses and compositions (CdS, ZnS, or ZnSe) surround the core (CdSe or PbSe) of the QD.[10] These shells protect the QD core from a surface environment and decouple electrons from holes, thus minimizing both relaxation mechanisms.[359b] When both types of relaxation channels are suppressed, the energy relaxation time could be as long as 1 ns, revealing the phonon bottleneck.[361] To complement insights into experimental observables, nonadiabatic MD simulations provide the necessary details on efficiency and interplay between each of these processes.[364]

For example, TD-KS modeling reveals a dense distribution of electronic levels near the energy gap (E_g) in PbSe[119a,b] and CdSe[118a] QDs due to surface reconstructions and the lack of absolute spherical symmetry of the QD. The ratio of the number of such surface states to the number of core states is growing with decrease in the QDs size. Most of these states are optically dark and are not seen in absorption spectra, but they do couple to phonons and facilitate carrier relaxation processes.[118a] This explains why the measured relaxation rates in small QDs are faster than in larger nanocrystals.[365] It was also found that NA coupling between nearest states is nearly twice larger than the coupling averaged over all other pairs of states, for both electrons and holes independent of their initial excitation energies.[132] As such, neighboring transitions govern the carrier relaxation in QDs. For both PbSe and CdSe QDs, holes exhibit stronger NA couplings than electrons,[118a,132] rationalizing faster relaxation times for holes, especially in CdSe where the holes are much heavier than electrons, which agrees with experimental data.[359a] These simulations also demonstrate enhancement of multiphonon processes in small QDs.[119b,132]

Although relaxation through several phonons is typically inefficient in bulk semiconductors,[359a,366,367] the localization of wave functions due to surface defects plus strong NA electron−phonon coupling in small QDs make multiphonon processes highly probable, particularly for acoustic phonons coupled to the lowest energy electronic states in small QDs.[119a,132] Using TD-KS calculations, Kamisaka et al.[158a] also have predicted ultrafast dephasing times (10−30 fs) of excitations in QDs rationalizing it by strong interactions between excitons and acoustic phonons, as was later proved by experiments.[257] Overall, nonadiabatic MD simulations demonstrate that the phonon bottleneck in QDs can be efficiently avoided through two relaxation pathways: surface states and multiphonon processes. In the close proximity to the band gap, the multiphonon mechanism governs the relaxation, and a signature of the phonon bottleneck is seen for the lowest energy transitions.[118a]

Similar TD-KS approaches have elucidated the role of surface ligands in the phonon-mediated energy relaxation in CdSe QDs.[158c] It is found that at the excitation energies larger than 2.5 times the QD's energy gap (>2.5E_g), relaxation occurs about twice as fast in CdSe QDs ligated by phosphine oxides and amines than in ligand-free QDs, as illustrated in Figure 25. At high excitation energy, the ligands introduce to the electronic structure of the QD a new manifold of hybridized orbitals, for which the electronic density is spread over both the QD and the ligands.[124a] Such hybridized orbitals are characterized by increased electron−phonon couplings to the high frequency vibrations of the ligands, thus opening new relaxation channels allowing for faster relaxation rates. Extrapolation of the simulated results to different QD sizes and ligand densities suggests that for commonly used in experiment CdSe nanocrystals with 4−7 nm diameters, surface ligands can increase relaxation rates by 3−4 times at photoexcitation energies higher than 3 times of the QD's energy gap, and become a competing mechanism to other relaxation processes. Overall, this computational work[158c] provides energy-resolved relaxation rates across the broad excitation region (which can be further used for analytical models, such as effective mass approximation), clarifies the effect of ligands on intraband carrier relaxation, including the

DOI: 10.1021/acs.chemrev.5b00012
Chem. Rev. 2015, 115, 5929−5978

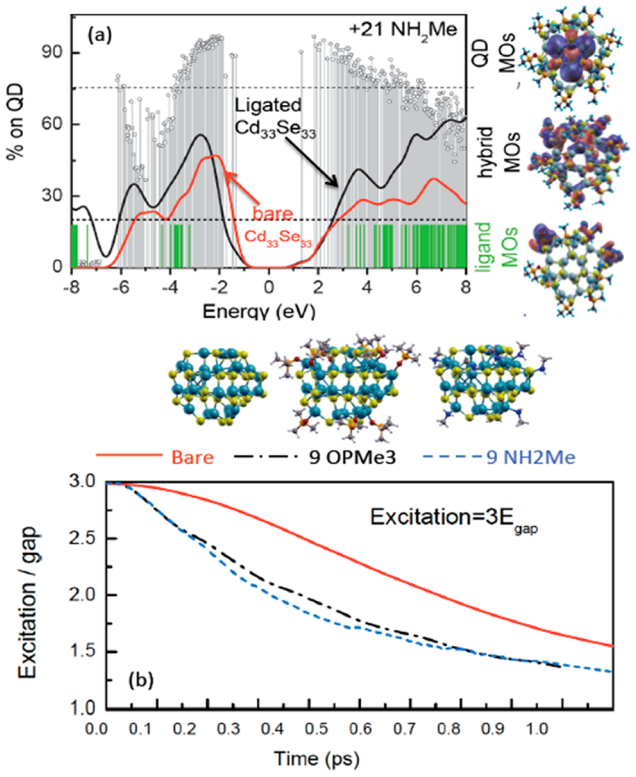

Figure 25. Strong surface−ligand interactions in QDs lead to formation of hybridized states manifold (top). This opens new relaxation channels for high energy photoexcitations resulting in faster rates at ligated QDs (bottom). Data are presented for the models of atomic models of $Cd_{33}Se_{33}$ in vacuum and covered by ligands, methylamine (NH_2Me) and trimethylphosphine oxide ($OPMe_3$) used as models for primary amines and trioctylphosphine oxide (TOPO), respectively. Nine ligands are attached only to two-coordinated Cd atoms. Reprinted and modified with permission from refs 124a and 158c. Copyright 2009 American Chemical Society 2012 American Chemical Society.

dependence on the excitation energy, and intends to stimulate experimental efforts in measuring the intraband relaxation rates in the high-energy domain, which are now scarce. Additionally, this generates an understanding of the conditions necessary to achieve and control the phonon-bottleneck experimentally via chemical manipulations of the QD's shells, ligands, and dopants, for example, due to the recently established relationship between the phonon-bottleneck and the quantum Zeno effect.[158b]

Fischer et al. have used the TD-KS approach to study formation of a metal-to-ligand charge transfer (MLCT) states in a Mn(II)-doped ZnO QD clusters.[335a] Simulations elucidate that MLCT state population occurs on an ultrafast time scale (<10 fs), which is beneficial for photomagnetization and zero-reabsorption luminescence. However, calculated lifetime of the MLCT state is not long enough to allow for spin-ordering, although relaxation in ZnO QDs is noticeably slowed upon addition of a Mn(II). Because of the effect of surface ligands, QD size, and the type and location of the dopant on the MLCT state lifetime and finite-temperature, inhomogeneous broadening of peaks in the absorption spectra of dilute magnetic semiconductor nanocrystals is complex and nontrivial.[335] The effect of p- and n-doping on the radiative and nonradiative pathways of energy relaxation in Si QDs has been investigated using combinations of TD-KS and RDM approaches.[368] Previously, it was shown that only the initially excited and band edge levels experience noticeable population changes during NA dynamics in QDs.[132] As such, intermediate levels exhibit small changes in population and serve an auxiliary role. This allows for an explicit description of only the first and last levels, while the rest effectively couple these two states, as implemented in the RDM technique.[368,369] With this method, the time-resolved emission spectra of codoped Si QDs are simulated providing information on the nature and lifetime of emission states in doped nanosystems. Obtained computational insights into pathways and mechanisms of relaxation dynamics in silicon nanostructures could be useful in specifying mechanisms of both radiative and nonradiative process and might help in interpretations of spectroscopy results.[370]

6.2. Charge Transfer in Functionalized Carbon Nanotubes

Efficient use of SWNTs in photoelectronic applications is limited by quantum efficiencies and lifetimes of quantum states involved in photoluminescence, which affect charge transfer and carrier mobility. Simulations of photoexcitation dynamics opens an opportunity to elucidate mechanisms of exciton relaxation and estimate characteristic lifetimes of excited state to be compared to the relaxation rates in SWNTs. These questions become extremely important for interacting and chemically functionalized SWNTs. To reduce computational cost, most applications of FSSH and RDM techniques to excited-state dynamics in SWNTs are made within independent electron and hole approximation.[95a] Using the TD-KS method, computations of hot carrier relaxation in (7,0) nanotube have revealed slower hole relaxation with multiple time-scales as compared to a faster single exponential electron dynamics, as illustrated in Figure 26a. Although simulation results qualitatively agree with experimental data,[371] they are surprisingly taking into account that VB (hole states) has higher DOS than CB (electron states). This is rationalized by the dominant role of high frequency phonons (G-mode) to electron relaxation, while RBM mostly contributes to hole dynamics, resulting in weaker NA coupling for holes.[63c] Nonadiabatic electronic dynamics provides answers to important questions on formation time scales of charge transfer states, where experimental measurements are not readily available. Qualitatively important insights in analyzing dynamics of charge transfer between closely packed nanotubes of different diameters have been recently reported in ref 372 (see Figure 26b). Interacting (6,4) and (8,4) SWNTs show ultrafast formation of dark charge-transfer state excitons with energy lesser than the lowest excitation in the original isolated nanotubes providing the nonradiative relaxation pathways and trapping of the photoexcitation in tube bundles. RBM phonons are found to distort the SWNT geometry, induce crossings of electronic states, and modulate coupling between SWNTs.

Another key process is the dynamics of charge transfer states at the interface of SWNT and substrate or functional groups. Such charge transfer dynamics was simulated by RDM for zigzag SWNTs, $(n,0)$ with n = 7, 10, 13, 16, 19, passivated by dinitromethane molecules ($CH_2N_2O_4$) acting as electron-withdrawing groups,[371] as presented in Figure 26c. It was found that initial photoexcitations at the SWNT trigger the intraband relaxation for both electrons and holes, followed by an electron transfer from the nanotube to the adsorbate, thus leaving a hole on the nanotube surface (see Figure 26d). The photoinduced charge transfer completes in about 10 fs in all reported models. Electron and hole relaxation times depend on

DOI: 10.1021/acs.chemrev.5b00012
Chem. Rev. 2015, 115, 5929−5978

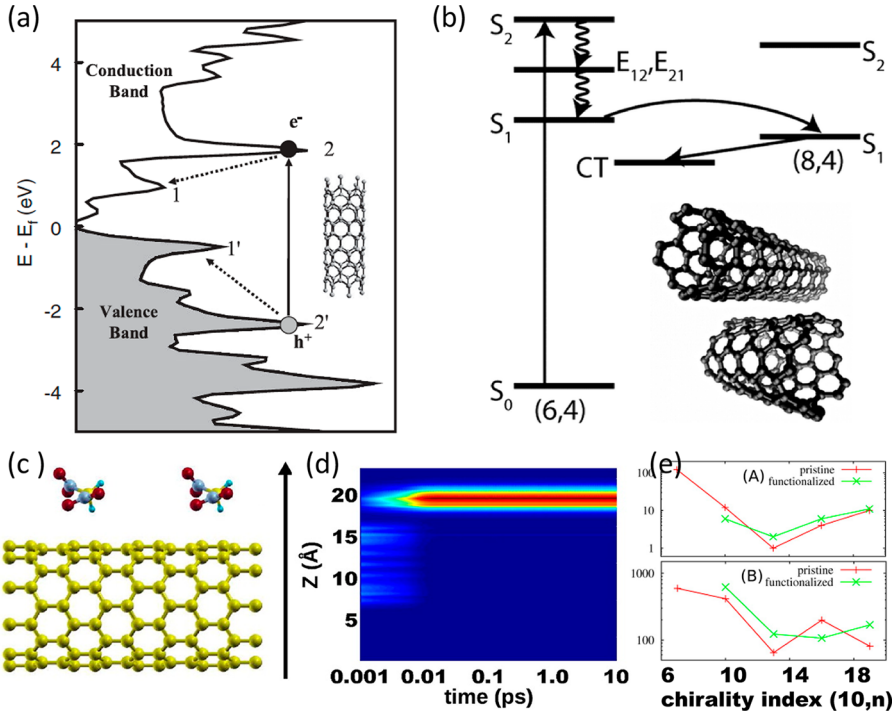

Figure 26. Excited-state dynamics in SWNTs. (a) Calculated DOS and pathways of nonradiative relaxation from E_{22} to E_{11} manifold of photoexcitation in (7,0) SWNT. Reprinted and modified with permission from ref 95a. Copyright 2006 American Physical Society. (b) Schematic representation of the charge transfer between closely packed (6,4) and (8,4) nanotubes. Reprinted and modified with permission from ref 372. Copyright 2014 American Chemical Society. (c–e) Dynamics of charge transfer in (10,0) SWNT functionalized by dinitromethane molecules $H_2C(NO_2)_2$ that noncovalently dope the SWNT and provide states into the gap. Reprinted and modified with permission from ref 371. Copyright 2013 American Chemical Society. (c) Reduced nanotube model with noncovalent electron acceptor ($CH_2(NO_2)_2$) in the vicinity of (10,0) SWNT. (d) Visualization of photoinduced electron dynamics in space along the direction from tube to the adsorbate (*Y*-axis). *X*-axis shows the logarithmic scale for relaxation time. Colors ranging from blue to red correspond to electron density with values from zero to maximum. During the first 10 fs, electron density is localized on the tube, while at later time the electron migrates to the acceptor, demonstrating formation of charge transfer state. (e) Dependence of the relaxation rate of a hot hole on the tube diameter. *Y*-axis stays for time in femtoseconds.

tube diameter and are minimal for the (13,0) SWNT due to electronic energy subgaps achieving resonance with phonon modes frequencies (see Figure 26e). Simulated mechanisms of excited-state relaxation in SWNTs and pathways of charge carrier dynamics at their interfaces complement experimental measurements, as well as static or adiabatic computations. Computed lifetimes, rates, and direction of charge transfer are critical components in design and characterization of new SWNT-based materials for photoelectronic applications.

6.3. Internal Conversion and Energy Transfer in Conjugated Macromolecules

Similar to successful applications of TD-KS and RDM methods in QDs and semiconducting surfaces, the NA-ESMD technique has been broadly used to simulate nonradiative relaxation and accompanying energy transfer processes in conjugated organic materials.[373−379] For example, this technique has been successfully applied to study ultrafast conformational planarization in polyfluorenes where the rate of torsional relaxation can be controlled on the basis of the initial excitation.[318b,380] Figure 27 illustrates dynamical aspects of exciton self-trapping leading to a violation of Condon approximation in CPPs discussed in section 5 (Figure 22).[279] The NA-ESMD simulations of internal conversion to the emission S_1 state after photoexcitation to S_2/S_3 states show that this process completes within 200 fs in all systems, being slightly faster in the larger hoops due to smaller S_2/S_1 gaps. Transition density plots for all trajectories (representative examples are shown as insets in Figure 27a) at the beginning and end of the dynamics have the same structures as those calculated with TD-DFT for S_2/S_3 (delocalized exciton) and S_1 (self-trapped exciton) states in Figure 22, respectively. A quantitative measure of excitonic delocalization is provided by participation ratio P_{ring} showing on average over how many phenyl rings the excitonic wave function is delocalized. Even in the ideal uniform geometry, the wavefuction is distributed nonuniformly over carbon atoms of the phenyl ring, so that P_{ring} is always smaller than the number of phenyls in the CPP hoop, Figure 27b. Calculated time-evolution of this quantity exemplifies that within 50 fs excitation becomes localized from about 7 to 5 rings in all large hoops, which fully agrees with the static TD-DFT simulations in Figure 22.

The NA-ESMD studies[318b] of energy transfer between conjugated chromophores show multiple competing processes/pathways and electronic states involved, going well beyond the Foerster theory.[318b,327] A detailed picture of energy transfer in conjugated (phenylene ethynylene) (PPE) dendrimers has been obtained with the NA-ESMD by considering photoexcited dynamics in various model segments (Figure 28a,b). As shown in Figure 28b, meta-branching localizes excitations within each fragment.[318b] Dendrimers of these building blocks have been shown to undergo highly efficient and unidirectional electronic and vibrational energy transfer schematically illustrated in Figure 28a. Explicit NA-ESMD simulations allowed one to identify the *shishiodoshi* unidirectional energy transfer mechanism representing a concerted

DOI: 10.1021/acs.chemrev.5b00012
Chem. Rev. 2015, 115, 5929−5978

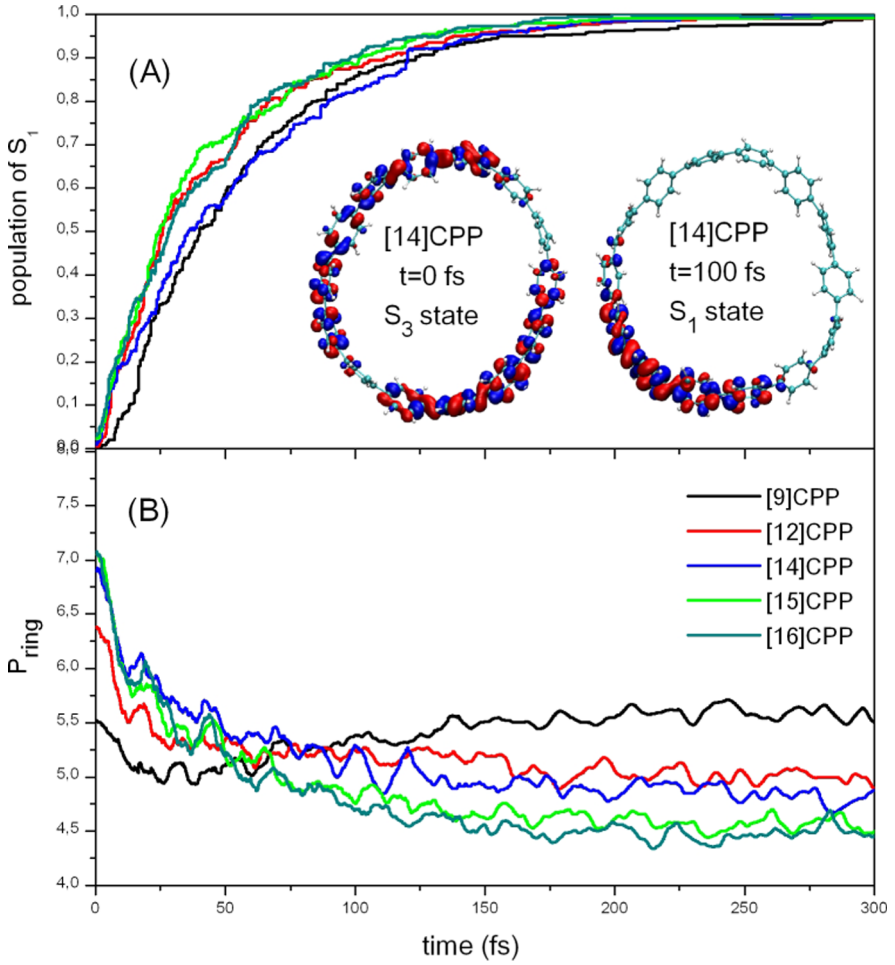

Figure 27. Nonadiabatic dynamics simulations of internal conversion at room temperature T = 300 K in [9], [12], [14], [15], and [16] CPP molecules after an excitation to S_2 and S_3 states. (a) Percentage of population in S_1 state calculated from the number of trajectories in it at a given time showing rapid relaxation within 200 fs in all CPP molecules; (b) time-dependence of the average participation number of phenyl ring demonstrating ultrafast spatial localization of photoexcitation within 50 fs. Simulations have been conducted using AM1/CIS representation of excited states. Reprinted and modified with permission from ref 279. Copyright 2014 American Chemical Society.

electronic and vibrational process: excitation transport through a chain of excited states with descending order of energies is found to be enhanced by vibronic relaxation bringing intermediate states into resonance condition (Figure 27a,b), an effect beyond the classical path approximation.

The effect of photoisomerization in stilbene and azobenzene has been recently investigated using NA-MD.[318e] Exploration of photoexcited dynamics of a stilbene and azobenzene exhibits correlation between electronic state and nuclear configuration. Dynamical relaxation of system from excited-state S_1 to S_0 provides substantial modification of the geometry from *cis*- to *trans*-isomers, as illustrated in Figure 28e and f. Time evolution of dihedral angles to smaller values is interpreted as a photoisomerization for both stilbene and azobenzene.[318e]

7. CONCLUSION, OUTLOOK, AND PERSPECTIVES

Despite significant technological and fabrication progress, the field of electronics based on nanostructured organic, inorganic, and hybrid materials stands at a critical junction and faces a situation similar to the early days of inorganic semiconductors when basic material and device principles were recognized but before the ability to design complex structures such as heterojunction diode lasers and integrated circuits. As such, theoretical simulation of complex materials is an important counterpart to experimental studies facilitating a quantitative understanding of matter at the nanoscale. In this Review, we consider quantum chemical modeling of three classes of nanomaterials: quantum dots, carbon nanotubes, and conjugated polymers focusing on their structural, electronic, transport, optical, and photodynamical properties. Various computational approaches from DFT and semiempirical model Hamiltonians to TD-SCF (allowing description of excitonic effects), to adiabatic and nonadiabatic MD (providing vibronic effects and nonradiative relaxation) have been overviewed and shown to be instrumental in complementing synthetic fabrication and experimental characterization efforts aimed to design novel nanostructures with improved and enhanced properties for various technological applications. For example, recent advances in DFT simulations, including the development of new long-range corrected density functionals, allow for filling some gaps in understanding of both the structural and the electronic properties of nanomaterials originating from their surface chemistry and interfaces that are important for applications, but are challenging to obtain through experimental characterization. In particular, recent DFT calculations bring important insights into the surface structure and stoichiometry of different types of semiconductor QDs, and the strength and mechanism of interactions between the QD and specific

DOI: 10.1021/acs.chemrev.5b00012
Chem. Rev. 2015, 115, 5929−5978

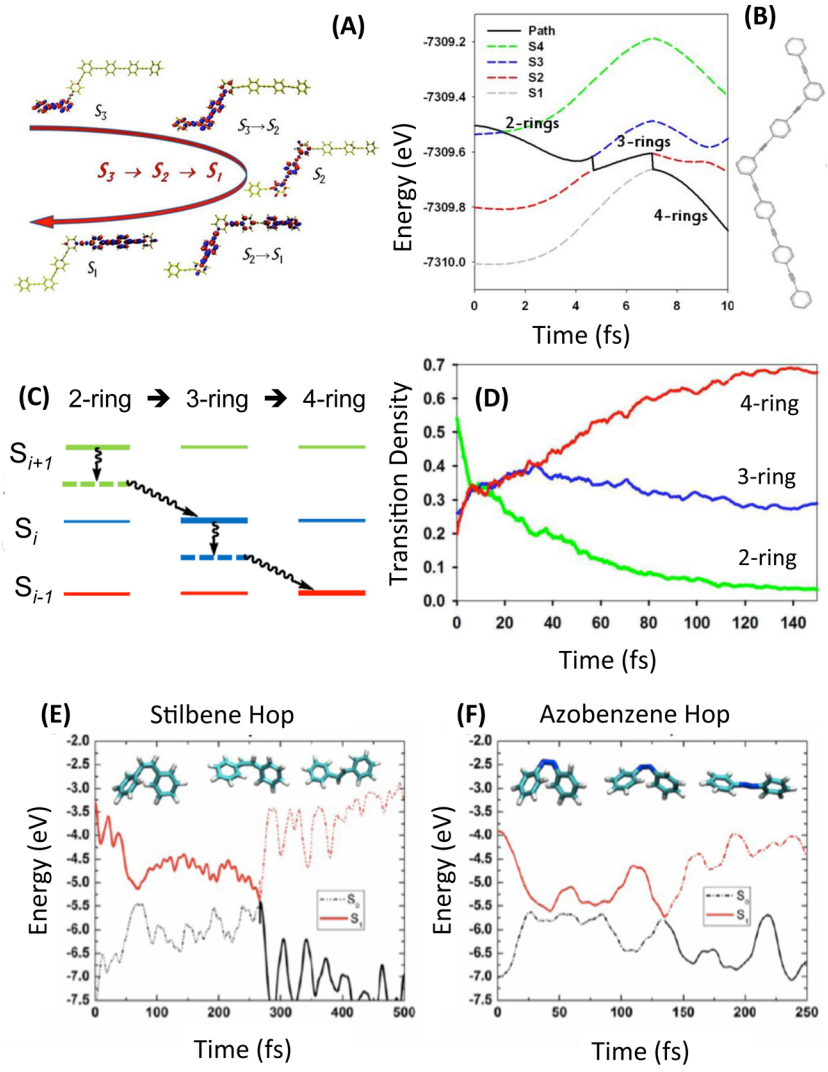

Figure 28. Excited-state dynamics in conjugated polymers and oligomers. (A) Observed sequence of unidirectional energy transfer events revealed by the transition density localization in PPE chromophores. (B) Dashed lines illustrate dynamics of PESs energies parametrized by time; solid line stands for a single trajectory and indicates which of the PESs are occupied. Vertical fragments of this occupation trajectory stand for hops. Inset illustrates meta-linked PPE oligomers. (C) Schematic of the *shishiodoshi* unidirectional energy transfer mechanism. Simulations have been conducted using AM1/CIS representation of excited states. (D) Evolution of the transition density localized in each segment during NA-ESMD simulations illustrating spatial energy flow. Reprinted and modified with permission from ref 318b. Copyright 2014 American Chemical Society. (E) Photoexcitation in *cis*-stilbene is followed by electronic relaxation and twist of dihedral angle, leading to change of the isomer to *trans*-stilbene. (F) Photoisimerization effect observed for azobenzene. Computations were performed by NAMD methodology using the fewest switches surface-hopping (FSSH) algorithm within an ab initio local orbital DFT framework at the non-equilibrium population with BLYP functional and localized basis set. Reprinted and modified with permission from ref 318e. Copyright 2014 American Chemical Society.

passivating ligands and adsorbents. These properties have been shown to define the offset of frontier energy levels and localized/delocalized characters of surface-associated trap states in QD composites, and, thus, are important for designing favorable conditions for charge and energy transfer in these materials used in energy applications.

An important part of this Review is dedicated to defining applicability ranges of applied quantum chemistry methods in describing specific electronic properties of a considered material. For instance, it is shown that a single-particle approach (noninteracting electron−hole pairs) is a valid approximation in the qualitative description of photoexcitations in QDs, while it fails in the case of π-conjugated systems such as SWNTs and CPs, due to strong excitonic effects in these materials. For these systems, optical spectra calculated with TD-SCF methods demonstrate good agreement with experimental data, while the choice of the density functional (with an appropriate portion of the orbital exchange and, especially, with long-range corrections) is critical for realistic description of size-scaling of observables and localization of excitonic and polaronic states in CPs and SWNTs.

The electronic confinement in nanomaterials renders the continua bands of electronic and vibrational states of the bulk to discrete states. Therefore, similar to CPs, nanostructures such as QDs and SWNTs can be treated as large molecules, rather than as an infinite solid. In our Review, we have shown that applications of such "molecular" approach to finite-size SWNTs (~10 nm in length) are validated by the much smaller size of excitons (~2−3 nm) as compared to the length of the modeled nanotubes. Thus, results obtained for 10−15 nm nanotubes can be extrapolated to the longer SWNTs used in experimental samples. For example, TD-DFT calculations of

DOI: 10.1021/acs.chemrev.5b00012
Chem. Rev. 2015, 115, 5929−5978

finite-size SWNTs provide qualitatively similar energy alignments of optically dark and bright excitons consistent with many-body GW/BSE results for SWNTs with periodic boundary conditions. Both approaches reveal that optically inactive states are lower in energy than the bright excitons, which, along with a fast photoexcitation quenching due to exceptional excitonic diffusion, explains the low intensity of photoemission in nanotubes. In addition, TD-DFT calculations predict possible control of luminescence intensity of SWNTs via covalent functionalization. In our Review, we have exemplified that the adsorbent type, its position, and concentration can modify the optical selection rules of SWNTs. These results explain and rationalize recent experimental data on emission spectroscopy of chemically doped SWNTs and suggest that enhanced emission efficiency of nanotubes can be achieved via selective chemical functionalization.

Nevertheless, for large systems with up to 1000 atoms in size, such as ligated QDs, chemically functionalized SWNTs, and amorphous aggregates of CPs, modeling of structural conformations is limited due to numerically expensive quantum chemistry calculations. Therefore, lower-level methods are needed. For example, classical force field and MD calculations have been shown to provide reasonable structural morphologies for both CPs and SWNTs functionalized by bio- or conjugated polymers. For instance, this allows us to establish structure−property relationships of the polymer−nanotube interface important for understanding conditions controlling SWNT dispersion and chirality separation via chemical functionalization. Combinations of FF (for geometries and packing of large molecules) with DFT (for the electronic structure calculations) allow for understanding of the role of inter- versus intramolecular disorder in the formation of deep electronic/hole trap states in amorphous CPs, information on which is scarce in experimental measurements. However, such approaches are challenging for QDs, where FF parametrization for inorganic composites is not well developed.

Photoexcited dynamics in these systems is even more challenging to address computationally, because electronic and nuclear degrees of freedom experience significant interactions, which are not negligible and often cannot be treated perturbatively for excited states, for example, as quantified by displacement and reorganization of nuclear degrees of freedom as reflected in large Huang−Rhys factors of CPs. Within the Born−Oppenheimer approximation, the MD at the excited state demonstrates complex contributions of vibronic features and electron−phonon interactions to the photophysics of isolated conjugated oligomers and SWNTs. Joined experimental and computational studies define the Huang−Rhys factors in SWNTs to be about 10 times smaller than those in CPs, placing SWNTs in a weak electron−phonon coupling regime. However, calculations have revealed that, similar to the CPs, the local distortions of the nanotube surface during vibronic relaxation, the Peierls distortions, lead to experimentally detectable phenomena, such as coherent phonon dynamics and exciton self-trapping effects, mostly pronounced in SWNTs of about 1 nm in the diameter. Another important and interesting phenomenon resulting from electron−vibrational coupling and spatial redistribution of the excitonic wave function is violation of the Franck−Condon approximation in cycloparaphenylenes and SWNTs. These computational predictions have been already experimentally confirmed by nontrivial optical and Raman spectra of these systems.

Direct computational modeling of excited-state dynamics and internal conversion beyond Born−Oppenheimer regime is always numerically expensive, subject to many approximations, and is tractable only for relatively small systems (up to a few hundreds of atoms in size). However, such simulations deliver important information in many cases, where direct experimental measurements are problematic. One example is monitoring dynamics of formation of charge transfer states, which are optically dark. For instance, we have discussed qualitative insights into dynamics of charge transfer between closely packed nanotubes of different diameters and between the SWNT and adsorbed organic molecules. Another example is decomposing complex energy transfer processes into distinct pathways with different efficiency allowing one to formulate the respective synthetic strategies. In some cases, excited-state dynamics can be approximated by the ground-state MD with nonequilibrium electronic state population. This is possible in materials such as inorganic solids and QDs where vibronic phenomena are less pronounced (stronger ionic bonds assume more rigid structures, which are weakly perturbed by the change of an electronic wave function). The ground-state approximation and neglect of electron−hole correlations allow for computationally inexpensive and very practical approaches to nonadiabatic phonon-mediated dynamics in pristine, doped, and ligated QDs. Overall, this approach resulted in the identification of conditions affecting radiative and nonradiative pathways of energy and charge relaxation in QDs and semiconductor surfaces, simulations of the time-resolved emission spectra of different types of QDs, revealing the role of surface defects and passivating ligands in ultrafast loss of photoexcitation to heat rationalizing the absence of the phonon bottleneck in QDs, and establishing a connection between slow energy relaxation (the phonon bottleneck) and Zeno effect in QDs. Consequently, results of the TD-KS nonadiabatic dynamics provide insights on how to control solar energy conversion via manipulations of the QD's surface shells, dopants, and ligands. However, this approach becomes inaccurate for describing excited-state dynamics in conjugated systems such as CPs and SWNTs due to excitonic effects and a failure of the classical path approximation. The NA-ESMD methodology based on semiempirical CIS framework bypasses the above approximations and offers a computationally tractable route for simulating hundreds of atoms on ∼10 ps time scales where multiple coupled excited states are involved. Demonstrated in this Review is ultrafast dynamical localization of photoexcitations in cycloparaphenylenes on ∼200 fs time scales confirming violation of Condon approximation. In another example, ultrafast unidirectional energy transfer in dendrimers composed of poly(phenylene ethynylene) chromophores is controlled by specific differential nuclear motion favoring downhill energy transfer.

Overall, reviewed computational results are important steps toward understanding complicated photophysical properties at the nanometer scale manifested by the presence of conformational disorder, defects, impurities, and complex interactions between different (e.g., organic−inorganic) components of nanostructures. Despite significant progress, many additional computational studies are needed for further demonstrations on how theoretically predicted properties can be realized in realistic experimental samples and then utilized in various applications. Potentially such theoretical simulations can

DOI: 10.1021/acs.chemrev.5b00012
Chem. Rev. 2015, 115, 5929−5978

substantially accelerate the completion of proof-of-concept development stage and facilitate practical usage of nanostructured materials to produce efficiently operating optoelectronic devices, solar cells, sensors, biolabels, etc. For practical devices, binding and blending nanomaterials into organized interfaces is expected to drastically modify their properties by, for example, introducing interfacial charge transfer states and such. Study of interfaces from atomistic to macro-level is a very ambitious task for electronic structure simulations in the next decade. Notably, any progress in the study of interfaces is not possible until sufficient and satisfactory understanding of basic properties of stand-alone nanoblocks is achieved. So, this Review scans through properties of three main classes of nanomaterials and suggests "possible" and "impossible" routes in addressing open challenges on the way. Moreover, by placing these seemingly distinct materials (frequently requiring different theoretical methodologies) in direct comparison, this Review aims to provide sufficient background information required to approach computational modeling of photophysics and dynamics in various hybrid (e.g., organic−inorganic) materials and interfaces.

In the big picture, this Review targets the goal of helping experimental scientists and computational chemists to synergistically address open challenges in the field of applied nanoscience. However, as a rule, computational modeling cannot provide universally exhaustive and accurate information for all cases involving large molecular systems by acting as a black box tool. Instead, specific model chemistry has to be applied to a well-defined and focused problem with a deep understanding of manifold of approximations that were used to reach a desired compromise between accuracy and numerical cost. This frequently provides only narrow-range qualitative descriptions of a targeted process in extended nanosystems. While direct comparison of computational results with their experimental counterparts constitutes an important task of benchmarking and validation of specific theoretical technique (e.g., DFT model), it is usually only feasible only for simple well-defined systems. In contrast, here we have outlined multiple examples demonstrating to the reader that the main benefit of reported computational approaches for realistic complex structures is recognition of physical mechanisms, structure−property relationships, and trends in observables. In this way, quantum chemistry simulations have potentials to get insight into the most important processes taking place at atomistic and molecular levels of realistic materials and bring applied and fundamental research closer together.

AUTHOR INFORMATION

Corresponding Author

*E-mail: serg@lanl.gov.

Notes

The authors declare no competing financial interest.

Biographies

Svetlana Kilina received her undergraduate education (1994) and M.S. degree in Physics (1996) at the Belarusian State University, Minsk, Belarus. Her research interests were further shaped during her Ph.D. studies in Chemistry at the University of Washington, Seattle (2003−2007). She joined the group of Prof. Oleg Prezhdo and mastered the formalism of nonadiabatic dynamics in nanomaterials. In January 2008, after she completed her Ph.D., she was awarded the Director's Postdoctoral Fellowship and worked at Los Alamos National Laboratory under the supervision of Dr. Sergei Tretiak. Since August 2010, she holds an appointment as an Assistant Professor at Chemistry and Biochemistry Department, North Dakota State University (NDSU). Her current research is on the frontiers of modern quantum chemistry and nanoscale material science with a particular focus on inorganic−organic interfaces in novel hybrid, functionalized nanomaterials. This includes understanding how the bio and organic functional groups, such as organic dyes, conjugated polymers, DNA, etc., affect electronic and optical properties, radiative and nonradiative dynamics, and charge and energy transfer in semiconductor quantum dots and carbon nanotubes.

Dmitri Kilin completed undergraduate (1994) and masters degrees (1996) in Physics from Belarus State University, (Minsk, Belarus) and received the doctoral degree from the Chemnitz University of Technology (Chemnitz, Germany) in 2000. After subsequent postdoctoral internships at research groups of Prof. Jeffery A. Cina at the University of Oregon, Prof. Oleg Prezhdo at the University of Washington, and Prof. David Micha at the University of Florida, he joined the Department of Chemistry at the University of South Dakota as a faculty member. His current research interests are focused on modeling the photoinduced dynamic processes of charge transfer, nonradiative charge carrier relaxation, and surface reactions at catalytic sites and interfaces of metal and semiconductor nanomaterials for photovoltaic and photocatalytic solar energy conversion.

DOI: 10.1021/acs.chemrev.5b00012
Chem. Rev. 2015, 115, 5929−5978

Sergei Tretiak received his M.Sc. degree (1994) from Moscow Institute of Physics and Technology (Russia) and his Ph.D. degree in Chemistry (1998) from the University of Rochester, NY where he worked with Prof. Shaul Mukamel. He was then a Director's Postdoctoral Fellow in Theoretical Division at Los Alamos National Laboratory (LANL) and became a LANL staff scientist in 2001. Since 2006, he is a staff scientist at Center for Integrated Nanotechnologies (CINT), a DOE user facility. His research interests include development of computational methods for optical properties in nanoscale materials such as conjugated polymers, carbon nanotubes, semiconductor nanoparticles, and molecular aggregates; nonlinear optical response of organic chromophores; adiabatic and nonadiabatic molecular dynamics of excited states; and charge and energy transfer in biological and artificial antenna complexes.

ACKNOWLEDGMENTS

This work was supported by the U.S. Department of Energy and Los Alamos LDRD funds. Los Alamos National Laboratory is operated by Los Alamos National Security, LLC, for the National Nuclear Security Administration of the U.S. Department of Energy under contract DE-AC5206NA25396. S.K. acknowledges financial support of the U.S. Department of Energy (DOE) Early Career Research grant DE-SC008446 for the work on QDs, and D.K. together with S.K. thank NSF grant CHE-1413614 for financial support of studies of functionalized SWNTs. We acknowledge support from the Center for Integrated Nanotechnologies (CINT) and the Center for Nonlinear Studies (CNLS) at LANL. S.K. acknowledges support of the Alfred P. Sloan Research Fellowship BR2014-073 for polymer work.

REFERENCES

(1) Martin, C. R. Nanomaterials – a Membrane-Based Synthetic Approach. *Science* **1994**, *266*, 1961−1966.
(2) Moriarty, P. Nanostructured Materials. *Rep. Prog. Phys.* **2001**, *64*, 297−381.
(3) Klimov, V. I. *Semiconductor and Metal Nanocrystals: Synthesis and Electronic and Optical Properties*; Taylor & Francis: UK, 2003.
(4) Dresselhaus, M.; Dresselhaus, G.; Avouris, P. *Carbon Nanotubes: Synthesis, Structure, Properties and Applications*; Springer-Verlag: Berlin, Germany, 2001.
(5) Saeki, A.; Koizumi, Y.; Aida, T.; Seki, S. Comprehensive Approach to Intrinsic Charge Carrier Mobility in Conjugated Organic Molecules, Macromolecules, and Supramolecular Architectures. *Acc. Chem. Res.* **2012**, *45*, 1193−1202.
(6) Rogach, A. L.; Eychmueller, A.; Hickey, S. G.; Kershaw, S. V. Infrared-Emitting Colloidal Nanocrystals: Synthesis, Assembly, Spectroscopy, and Applications. *Small* **2007**, *3*, 536−557.
(7) Yoffe, A. D. Semiconductor Quantum Dots and Related Systems: Electronic, Optical, Luminescence and Related Properties of Low Dimensional Systems. *Adv. Phys.* **2001**, *50*, 1−208.
(8) Gierschner, J.; Cornil, J.; Egelhaaf, H.-J. Optical Bandgaps of Pi-Conjugated Organic Materials at the Polymer Limit: Experiment and Theory. *Adv. Mater.* **2007**, *19*, 173−191.
(9) Weisman, R. B.; Bachilo, S. M. Dependence of Optical Transition Energies on Structure for Single-Walled Carbon Nanotubes in Aqueous Suspension: An Empirical Kataura Plot. *Nano Lett.* **2003**, *3*, 1235−1238.
(10) Chen, Y.; Vela, J.; Htoon, H.; Casson, J. L.; Werder, D. J.; Bussian, D. A.; Klimov, V. I.; Hollingsworth, J. A. "Giant" Multishell CdSe Nanocrystal Quantum Dots with Suppressed Blinking. *J. Am. Chem. Soc.* **2008**, *130*, 5026−5027.
(11) Howes, P. D.; Chandrawati, R.; Stevens, M. M. Colloidal Nanoparticles as Advanced Biological Sensors. *Science* **2014**, *346*, 247390.
(12) Sameer, S.; Nanda, J.; Pietryga, J. M.; Hollingsworth, J. A.; Sarma, D. D. Unraveling Internal Structures of Highly Luminescent Pbse Nanocrystallites Using Variable-Energy Synchrotron Radiation Photoelectron Spectroscopy. *J. Phys. Chem. B* **2006**, *110*, 15244−15250.
(13) Winkler, U.; Eich, D.; Chen, Z. H.; Fink, R.; Kulkarni, S. K.; Umbach, E. Detailed Investigation of CdS Nanoparticle Surfaces by High-Resolution Photoelectron Spectroscopy. *Chem. Phys. Lett.* **1999**, *306*, 95−102.
(14) Ip, A. H.; Thon, S. M.; Hoogland, S.; Voznyy, O.; Zhitomirsky, D.; Debnath, R.; Levina, L.; Rollny, L. R.; Carey, G. H.; Fischer, A.; Kemp, K. W.; Kramer, I. J.; Ning, Z.; Labelle, A. J.; Chou, K. W.; Amassian, A.; Sargent, E. H. Hybrid Passivated Colloidal Quantum Dot Solids. *Nat. Nanotechnol.* **2012**, *7*, 577−582.
(15) (a) Liu, I. S.; Lo, H. H.; Chien, C. T.; Lin, Y. Y.; Chen, C. W.; Chen, Y. F.; Su, W. F.; Liou, S. C. Enhancing Photoluminescence Quenching and Photoelectric Properties of CdSe Quantum Dots with Hole Accepting Ligands. *J. Mater. Chem.* **2008**, *18*, 675−682. (b) Guyot-Sionnest, P.; Wehrenberg, B.; Yu, D. Intraband Relaxation in CdSe Nanocrystals and the Strong Influence of the Surface Ligands. *J. Chem. Phys.* **2005**, *123*, 074709. (c) Talapin, D. V.; Rogach, A. L.; Kornowski, A.; Haase, M.; Weller, H. Highly Luminescent Monodisperse CdSe and CdSe/ZnS Nanocrystals Synthesized in a Hexadecylamine-Trioctylphosphine Oxide-Trioctylphospine Mixture. *Nano Lett.* **2001**, *1*, 207−211.
(16) Cooney, R. R.; Sewall, S. L.; Anderson, K. E. H.; Dias, E. A.; Kambhampati, P. Breaking the Phonon Bottleneck for Holes in Semiconductor Quantum Dots. *Phys. Rev. Lett.* **2007**, *98*, 177403.
(17) Klimov, V. I.; Mikhailovsky, A. A.; McBranch, D. W.; Leatherdale, C. A.; Bawendi, M. G. Mechanisms for Intraband Energy Relaxation in Semiconductor Quantum Dots: The Role of Electron-Hole Interactions. *Phys. Rev. B* **2000**, *61*, 13349−13352.
(18) (a) Efros, A. L.; Rosen, M.; Kuno, M.; Nirmal, M.; Norris, D. J.; Bawendi, M. Band-Edge Exciton in Quantum Dots of Semiconductors with a Degenerate Valence Band: Dark and Bright Exciton States. *Phys. Rev. B* **1996**, *54*, 4843−4856. (b) Makarov, N. S.; Lau, P. C.; Olson, C.; Velizhanin, K. A.; Solntsev, K. M.; Kieu, K.; Kilina, S.; Tretiak, S.; Norwood, R. A.; Peyghambarian, V.; Perry, J. W. Two-Photon Absorption in CdSe Colloidal Quantum Dots Compared to Organic Molecules. *ACS Nano.* **2014**, *18*, 12572−12586.
(19) Kamat, P. V. Boosting the Efficiency of Quantum Dot Sensitized Solar Cells through Modulation of Interfacial Charge Transfer. *Acc. Chem. Res.* **2012**, *45*, 1906−1915.
(20) (a) Krasheninnikov, A. V.; Lehtinen, P. O.; Foster, A. S.; Nieminen, R. M. Bending the Rules: Contrasting Vacancy Energetics and Migration in Graphite and Carbon Nanotubes. *Chem. Phys. Lett.* **2006**, *418*, 132−136. (b) Hunt, S. R.; Fuller, E. J.; Corso, B. L.; Collins, P. G. Distinguishing Carbon Nanotube Defect Chemistry Using Scanning Gate Spectroscopy. *Phys. Rev. B* **2012**, *85*, 235418.
(21) Tu, X.; Manohar, S.; Jagota, A.; Zheng, M. DNA Sequence Motifs for Structure-Specific Recognition and Separation of Carbon Nanotubes. *Nature* **2009**, *460*, 250−253.

DOI: 10.1021/acs.chemrev.5b00012
Chem. Rev. 2015, 115, 5929−5978

(22) Samanta, S. K.; Fritsch, M.; Scherf, U.; Gomulya, W.; Bisri, S. Z.; Loi, M. A. Conjugated Polymer-Assisted Dispersion of Single-Wall Carbon Nanotubes: The Power of Polymer Wrapping. *Acc. Chem. Res.* **2014**, *47*, 2446−2456.
(23) (a) Lin, S.; Hilmer, A. J.; Mendenhall, J. D.; Strano, M. S.; Blankschtein, D. Molecular Perspective on Diazonium Adsorption for Controllable Functionalization of Single-Walled Carbon Nanotubes in Aqueous Surfactant Solutions. *J. Am. Chem. Soc.* **2012**, *134*, 8194−8204. (b) Khripin, C. Y.; Tu, X.; Heddleston, J. M.; Silvera-Batista, C.; Walker, A. R. H.; Fagan, J.; Zheng, M. High-Resolution Length Fractionation of Surfactant-Dispersed Carbon Nanotubes. *Anal. Chem.* **2013**, *85*, 1382−1388.
(24) Toshimitsu, F.; Nakashima, N. Semiconducting Single-Walled Carbon Nanotubes Sorting with a Removable Solubilizer Based on Dynamic Supramolecular Coordination Chemistry. *Nat. Commun.* **2014**, *5*, 5041.
(25) Iliafar, S.; Mittal, J.; Vezenov, D.; Jagota, A. Interaction of Single-Stranded DNA with Curved Carbon Nanotube Is Much Stronger Than with Flat Graphite. *J. Am. Chem. Soc.* **2014**, *136*, 12947−12957.
(26) (a) Usmani, F. A.; Hasan, M. Carbon Nanotube Field Effect Transistors for High Performance Analog Applications: An Optimum Design Approach. *Microelectron. J.* **2010**, *41*, 395−402. (b) Wind, S. J.; Appenzeller, J.; Avouris, P. Lateral Scaling in Carbon-Nanotube Field-Effect Transistors. *Phys. Rev. Lett.* **2003**, *91*, 058301.
(27) (a) Byon, H. R.; Choi, H. C. Network Single-Walled Carbon Nanotube-Field Effect Transistors (Swnt-Fets) with Increased Schottky Contact Area for Highly Sensitive Biosensor Applications. *J. Am. Chem. Soc.* **2006**, *128*, 2188−2189. (b) Koh, J.; Yi, M.; Lee, B. Y.; Kim, T. H.; Lee, J.; Jhon, Y. M.; Hong, S. Directed Assembly of Carbon Nanotubes on Soft Substrates for Use as a Flexible Biosensor Array. *Nanotechnology* **2008**, *19*, 505502.
(28) Singh, I.; Madhwal, D.; Verma, A.; Kumar, A.; Rait, S.; Kaur, I.; Bharadwaj, L. M.; Bhatia, C. S.; Bhatnagar, P. K.; Mathur, P. C. Enhanced Luminance of Meh-Ppv Based Pleds Using Single Walled Carbon Nanotube Composite as an Electron Transporting Layer. *J. Lumin.* **2010**, *130*, 2157−2160.
(29) Gomulya, W.; Gao, J.; Loi, M. A. Conjugated Polymer-Wrapped Carbon Nanotubes: Physical Properties and Device Applications. *Eur. Phys. J. B* **2013**, *86*, 1−13.
(30) (a) Perebeinos, V.; Tersoff, J.; Avouris, P. Radiative Lifetime of Excitons in Carbon Nanotubes. *Nano Lett.* **2005**, *5*, 2495−2499. (b) Shaver, J.; Kono, J.; Portugall, O.; Krstic, V.; Rikken, G. L. J. A.; Miyauchi, Y.; Maruyama, S.; Perebeinos, V. Magnetic Brightening of Carbon Nanotube Photoluminescence through Symmetry Breaking. *Nano Lett.* **2007**, *7*, 1851−1855. (c) Zaric, S.; Ostojic, G. N.; Shaver, J.; Kono, J.; Portugall, O.; Frings, P. H.; Rikken, G. L. J. A.; Furis, M.; Crooker, S. A.; Wei, X.; Moore, V. C.; Hauge, R. H.; Smalley, R. E. Excitons in Carbon Nanotubes with Broken Time-Reversal Symmetry. *Phys. Rev. Lett.* **2006**, *96*, 016406.
(31) Mukamel, S.; Tretiak, S.; Wagersreiter, T.; Chernyak, V. Electronic Coherence and Collective Optical Excitations of Conjugated Molecules. *Science* **1997**, *277*, 781−787.
(32) (a) Cognet, L.; Tsyboulski, D. A.; Rocha, J.-D. R.; Doyle, C. D.; Tour, J. M.; Weisman, R. B. Stepwise Quenching of Exciton Fluorescence in Carbon Nanotubes by Single-Molecule Reactions. *Science* **2007**, *316*, 1465−1468. (b) Crochet, J. J.; Duque, J. G.; Werner, J. H.; Doorn, S. K. Photoluminescence Imaging of Electronic-Impurity-Induced Exciton Quenching in Single-Walled Carbon Nanotubes. *Nat. Nanotechnol.* **2012**, *7*, 126−132.
(33) Singh, P.; Campidelli, S.; Giordani, S.; Bonifazi, D.; Bianco, A.; Prato, M. Organic Functionalisation and Characterisation of Single-Walled Carbon Nanotubes. *Chem. Soc. Rev.* **2009**, *38*, 2214−2230.
(34) Lee, A. J.; Wang, X. Y.; Carlson, L. J.; Smyder, J. A.; Loesch, B.; Tu, X. M.; Zheng, M.; Krauss, T. D. Bright Fluorescence from Individual Single-Walled Carbon Nanotubes. *Nano Lett.* **2011**, *11*, 1636−1640.
(35) Harutyunyan, H.; Gokus, T.; Green, A. A.; Hersam, M. C.; Allegrini, M.; Hartschuh, A. Defect-Induced Photoluminescence from Dark Excitonic States in Individual Single-Walled Carbon Nanotubes. *Nano Lett.* **2009**, *9*, 2010−2014.
(36) Nagatsu, K.; Chiashi, S.; Konabe, S.; Homma, Y. Brightening of Triplet Dark Excitons by Atomic Hydrogen Adsorption in Single-Walled Carbon Nanotubes Observed by Photoluminescence Spectroscopy. *Phys. Rev. Lett.* **2010**, *105*, 157403.
(37) Ghosh, S.; Bachilo, S. M.; Simonette, R. A.; Beckingham, K. M.; Weisman, R. B. Oxygen Doping Modifies near-Infrared Band Gaps in Fluorescent Single-Walled Carbon Nanotubes. *Science* **2010**, *330*, 1656−1659.
(38) Kilina, S.; Ramirez, J.; Tretiak, S. Brightening of the Lowest Exciton in Carbon Nanotubes Via Chemical Functionalization. *Nano Lett.* **2012**, *12*, 2306−2312.
(39) Ortmann, F.; Bechstedt, F.; Hannewald, K. Charge Transport in Organic Crystals: Theory and Modelling. *Phys. Status Solidi B* **2011**, *248*, 511−525.
(40) Dong, H.; Fu, X.; Liu, J.; Wang, Z.; Hu, W. 25th Anniversary Article: Key Points for High-Mobility Organic Field-Effect Transistors. *Adv. Mater.* **2013**, *25*, 6158−6182.
(41) Yeh, N.; Yeh, P. Organic Solar Cells: Their Developments and Potentials. *Renewable Sustainable Energy Rev.* **2013**, *21*, 421−431.
(42) Hartel, M. J.; Subbiah, J.; So, F. Interlayers for Efficient Electron Injection in Polymer Leds. *J. Disp. Technol.* **2013**, *9*, 469−475.
(43) Hangarter, C. M.; Chartuprayoon, N.; Hernandez, S. C.; Choa, Y.; Myung, N. V. Hybridized Conducting Polymer Chemiresistive Nano-Sensors. *Nano Today* **2013**, *8*, 39−55.
(44) Nicholson, P. G.; Castro, F. A. Organic Photovoltaics: Principles and Techniques for Nanometre Scale Characterization. *Nanotechnology* **2010**, *21*, 492001.
(45) (a) Graham, K. R.; Cabanetos, C.; Jahnke, J. P.; Idso, M. N.; El Labban, A.; Ndjawa, G. O. N.; Heumueller, T.; Vandewal, K.; Salleo, A.; Chmelka, B. F.; Amassian, A.; Beaujuge, P. M.; McGehee, M. D. Importance of the Donor: Fullerene Intermolecular Arrangement for High-Efficiency Organic Photovoltaics. *J. Am. Chem. Soc.* **2014**, *136*, 9608−9618. (b) Sun, Y.; Welch, G. C.; Leong, W. L.; Takacs, C. J.; Bazan, G. C.; Heeger, A. J. Solution-Processed Small-Molecule Solar Cells with 6.7% Efficiency. *Nat. Mater.* **2012**, *11*, 44−48. (c) Heeger, A. J. Semiconducting Polymers: The Third Generation. *Chem. Soc. Rev.* **2010**, *39*, 2354−2371. (d) Mayer, A. C.; Toney, M. F.; Scully, S. R.; Rivnay, J.; Brabec, C. J.; Scharber, M.; Koppe, M.; Heeney, M.; McCulloch, I.; McGehee, M. D. Bimolecular Crystals of Fullerenes in Conjugated Polymers and the Implications of Molecular Mixing for Solar Cells. *Adv. Funct. Mater.* **2009**, *19*, 1173−1179.
(46) Moon, J. S.; Lee, J. K.; Cho, S.; Byun, J.; Heeger, A. J. "Columnlike" Structure of the Cross-Sectional Morphology of Bulk Heterojunction Materials. *Nano Lett.* **2009**, *9*, 230−234.
(47) (a) Reid, O. G.; Pensack, R. D.; Song, Y.; Scholes, G. D.; Rumbles, G. Charge Photogeneration in Neat Conjugated Polymers. *Chem. Mater.* **2014**, *26*, 561−575. (b) Okamoto, T.; Nakahara, K.; Saeki, A.; Seki, S.; Oh, J. H.; Akkerman, H. B.; Bao, Z.; Matsuo, Y. Aryl-Perfluoroaryl Substituted Tetracene: Induction of Face-to-Face Pi-Pi Stacking and Enhancement of Charge Carrier Properties. *Chem. Mater.* **2011**, *23*, 1646−1649.
(48) (a) Guo, J. M.; Ohkita, H.; Benten, H.; Ito, S. Near-Ir Femtosecond Transient Absorption Spectroscopy of Ultrafast Polaron and Triplet Exciton Formation in Polythiophene Films with Different Regioregularities. *J. Am. Chem. Soc.* **2009**, *131*, 16869−16880. (b) Jiang, X. M.; Osterbacka, R.; Korovyanko, O.; An, C. P.; Horovitz, B.; Janssen, R. A. J.; Vardeny, Z. V. Spectroscopic Studies of Photoexcitations in Regioregular and Regiorandom Polythiophene Films. *Adv. Funct. Mater.* **2002**, *12*, 587−597.
(49) (a) Adachi, T.; Brazard, J.; Ono, R. J.; Hanson, B.; Traub, M. C.; Wu, Z.-Q.; Li, Z.; Bolinger, J. C.; Ganesan, V.; Bielawski, C. W.; Bout, D. A. V.; Barbara, P. F. Regioregularity and Single Polythiophene Chain Conformation. *J. Phys. Chem. Lett.* **2011**, *2*, 1400−1404. (b) Bolinger, J. C.; Traub, M. C.; Adachi, T.; Barbara, P. F. Ultralong-Range Polaron-Induced Quenching of Excitons in Isolated Conjugated Polymers. *Science* **2011**, *331*, 565−567.

DOI: 10.1021/acs.chemrev.5b00012
Chem. Rev. 2015, 115, 5929−5978

(50) (a) Kloc, C.; Tan, K. J.; Toh, M. L.; Zhang, K. K.; Xu, Y. P. Purity of Rubrene Single Crystals. *Appl. Phys. A: Mater. Sci. Process.* **2009**, *95*, 219−224. (b) Pflaum, J.; Niemax, J.; Tripathi, A. K. Chemical and Structural Effects on the Electronic Transport in Organic Single Crystals. *J. Chem. Phys.* **2006**, *325*, 152−159.
(51) Da Como, E.; Becker, K.; Feldmann, J.; Lupton, J. M. How Strain Controls Electronic Linewidth in Single Beta-Phase Polyfluorene Nanowires. *Nano Lett.* **2007**, *7*, 2993−2998.
(52) (a) Peverati, R.; Truhlar, D. G. Quest for a Universal Density Functional: The Accuracy of Density Functionals across a Broad Spectrum of Databases in Chemistry and Physics. *Philos. Trans. R. Soc., A* **2014**, *372*, 20120476. (b) Perdew, J. P.; Burke, K. Comparison Shopping for a Gradient-Corrected Density Functional. *Int. J. Quantum Chem.* **1996**, *57*, 309−319. (c) Fiolhais, C.; Nogueira, F.; Marques, M. A. L. *A Primer in Density Functional Theory*; Springer: New York, 2003. (d) Engel, E.; Dreizler, R. M. *Density Functional Theory: An Advanced Course*; Springer: New York, 2011.
(53) Draxl, C.; Nabok, D.; Hannewald, K. Organic/Inorganic Hybrid Materials: Challenges for Ab Initio Methodology. *Acc. Chem. Res.* **2014**, *47*, 3225−3232.
(54) (a) Casida, M. E.; Huix-Rotllant, M. Progress in Time-Dependent Density-Functional Theory. *Annu. Rev. Phys. Chem.* **2012**, *63*, 287−323. (b) Gulans, A.; Kontur, S.; Meisenbichler, C.; Nabok, D.; Pavone, P.; Rigamonti, S.; Sagmeister, S.; Werner, U.; Draxl, C. Exciting: A Full-Potential All-Electron Package Implementing Density-Functional Theory and Many-Body Perturbation Theory. *J. Phys.: Condens. Matter* **2014**, *26*, 363202.
(55) (a) Scholes, G. D. Insights into Excitons Confined to Nanoscale Systems: Electron-Hole Interaction, Binding Energy, and Photodissociation. *ACS Nano* **2008**, *2*, 523−537. (b) Scholes, G. D. Rumbles, G. Excitons in Nanoscale Systems. *Nat. Mater.* **2006**, *5*, 683−696.
(56) (a) Neukirch, A. J.; Hyeon-Deuk, K.; Prezhdo, O. V. Time-Domain Ab Initio Modeling of Excitation Dynamics in Quantum Dots. *Coord. Chem. Rev.* **2014**, *263*, 161−181. (b) Tapavicza, E.; Bellchambers, G. D.; Vincent, J. C.; Furche, F. Ab Initio Non-Adiabatic Molecular Dynamics. *Phys. Chem. Chem. Phys.* **2013**, *15*, 18336−18348.
(57) Lii, J. H.; Allinger, N. L. Directional Hydrogen Bonding in the Mm3 Force Field: Ii. *J. Comput. Chem.* **1998**, *19*, 1001−1016.
(58) Hornak, V.; Abel, R.; Okur, A.; Strockbine, B.; Roitberg, A.; Simmerling, C. Comparison of Multiple Amber Force Fields and Development of Improved Protein Backbone Parameters. *Proteins: Struct., Funct., Bioinf.* **2006**, *65*, 712−725.
(59) Denning, E. J.; Priyakumar, U. D.; Nilsson, L.; Mackerell, A. D., Jr. Impact of 2 '-Hydroxyl Sampling on the Conformational Properties of Rna: Update of the Charmm All-Atom Additive Force Field for Rna. *J. Comput. Chem.* **2011**, *32*, 1929−1943.
(60) Dewar, M. J. S.; Zoebisch, E. G.; Healy, E. F.; Stewart, J. J. P. The Development and Use of Quantum-Mechanical Molecular-Models 0.76. AM1 - a New General-Purpose Quantum-Mechanical Molecular-Model. *J. Am. Chem. Soc.* **1985**, *107*, 3902−3909.
(61) Dewar, M. J. S.; Fox, M. A.; Campbell, K. A.; Chen, C. C.; Friedheim, J. E.; Holloway, M. K.; Kim, S. C.; Liescheski, P. B.; Pakiari, A. M.; Tien, T. P.; Zoebisch, E. G. Calculation of Energies of Excited-States Using Mndo. *J. Comput. Chem.* **1984**, *5*, 480−485.
(62) Stewart, J. P. Optimization of Parameters for Semiempirical Methods Vi: More Modifications to the Nddo Approximations and Re-Optimization of Parameters. *J. Mol. Model.* **2013**, *19*, 1−32.
(63) (a) Grimme, S. Calculation of the Electronic Spectra of Large Molecules. *Rev. Comp. Chem.* **2004**, *20*, 153−218. (b) Dreuw, A.; Head-Gordon, M. Single-Reference Ab Initio Methods for the Calculation of Excited States of Large Molecules. *Chem. Rev.* **2005**, *105*, 4009−4037. (c) Tretiak, S. Triplet State Absorption in Carbon Nanotubes: A Td-Dft Study. *Nano Lett.* **2007**, *7*, 2201−2206.
(64) Heyd, J.; Scuseria, G. E.; Ernzerhof, M. Hybrid Functionals Based on a Screened Coulomb Potential. *J. Chem. Phys.* **2003**, *118*, 8207−8215.
(65) Vydrov, O. A.; Scuseria, G. E. Importance of Short-Range Versus Long-Range Hartree-Fock Exchange for the Performance of Hybrid Density Functionals. *J. Chem. Phys.* **2006**, *125*, 074106.
(66) (a) Rohrdanz, M. A.; Herbert, J. M. Simultaneous Benchmarking of Ground- and Excited-State Properties with Long-Range-Corrected Density Functional Theory. *J. Chem. Phys.* **2008**, *129*, 034107. (b) Kronik, L.; Stein, T.; Refaely-Abramson, S.; Baer, R. Excitation Gaps of Finite-Sized Systems from Optimally Tuned Range-Separated Hybrid Functionals. *J. Chem. Theory Comput.* **2012**, *8*, 1515−1531.
(67) Phillips, H.; Geva, E.; Dunietz, B. D. Calculating Off-Site Excitations in Symmetric Donor−Acceptor Systems Via Time-Dependent Density Functional Theory with Range-Separated Density Functionals. *J. Chem. Theory Comput.* **2012**, *8*, 2661−2668.
(68) (a) Angyan, J. G.; Gerber, I. C.; Savin, A.; Toulouse, J. Van Der Waals Forces in Density Functional Theory: Perturbational Long-Range Electron-Interaction Corrections. *Phys. Rev. A* **2005**, *72*, 012510. (b) Grimme, S. Accurate Description of Van Der Waals Complexes by Density Functional Theory Including Empirical Corrections. *J. Comput. Chem.* **2004**, *25*, 1463−1473. (c) Tkatchenko, A.; Scheffler, M. Accurate Molecular Van Der Waals Interactions from Ground-State Electron Density and Free-Atom Reference Data. *Phys. Rev. Lett.* **2009**, *102*, 073005.
(69) Tomasi, J.; Mennucci, B.; Cammi, R. Quantum Mechanical Continuum Solvation Models. *Chem. Rev.* **2005**, *105*, 2999−3093.
(70) Klamt, A.; Jonas, V.; Burger, T.; Lohrenz, J. C. W. Refinement and Parametrization of Cosmo-Rs. *J. Phys. Chem. A* **1998**, *102*, 5074−5085.
(71) Takano, Y.; Houk, K. N. Benchmarking the Conductor-Like Polarizable Continuum Model (Cpcm) for Aqueous Solvation Free Energies of Neutral and Ionic Organic Molecules. *J. Chem. Theory Comput.* **2005**, *1*, 70−77.
(72) Cossi, M.; Rega, N.; Scalmani, G.; Barone, V. Energies, Structures, and Electronic Properties of Molecules in Solution with the C-Pcm Solvation Model. *J. Comput. Chem.* **2003**, *24*, 669−681.
(73) Bussi, G.; Zykova-Timan, T.; Parrinello, M. Isothermal-Isobaric Molecular Dynamics Using Stochastic Velocity Rescaling. *J. Chem. Phys.* **2009**, *130*, 074101.
(74) Uberuaga, B. P.; Anghel, M.; Voter, A. F. Synchronization of Trajectories in Canonical Molecular-Dynamics Simulations: Observation, Explanation, and Exploitation. *J. Chem. Phys.* **2004**, *120*, 6363−6374.
(75) Lin, H.; Truhlar, D. G. Qm/Mm: What Have We Learned, Where Are We, and Where Do We Go from Here? *Theor. Chem. Acc.* **2007**, *117*, 185−199.
(76) Frisch, M. J.; Trucks, G. W.; Schlegel, H. B.; Scuseria, G. E.; Robb, M. A.; Cheeseman, J. R.; Scalmani, G.; Barone, V.; Mennucci, B.; Petersson, G. A.; Nakatsuji, H.; Caricato, M.; Li, X.; Hratchian, H. P.; Izmaylov, A. F.; Bloino, J.; Zheng, G.; Sonnenberg, J. L.; Hada, M.; Ehara, M.; Toyota, K.; Fukuda, R.; Hasegawa, J.; Ishida, M.; Nakajima, T.; Honda, Y.; Kitao, O.; Nakai, H.; Vreven, T.; Montgomery, J. A., Jr.; Peralta, J. E.; Ogliaro, F.; Bearpark, M. J.; Heyd, J.; Brothers, E. N.; Kudin, K. N.; Staroverov, V. N.; Kobayashi, R.; Normand, J.; Raghavachari, K.; Rendell, A. P.; Burant, J. C.; Iyengar, S. S.; Tomasi, J.; Cossi, M.; Rega, N.; Millam, N. J.; Klene, M.; Knox, J. E.; Cross, J. B.; Bakken, V.; Adamo, C.; Jaramillo, J.; Gomperts, R.; Stratmann, R. E.; Yazyev, O.; Austin, A. J.; Cammi, R.; Pomelli, C.; Ochterski, J. W.; Martin, R. L.; Morokuma, K.; Zakrzewski, V. G.; Voth, G. A.; Salvador, P.; Dannenberg, J. J.; Dapprich, S.; Daniels, A. D.; Farkas, Ö.; Foresman, J. B.; Ortiz, J. V.; Cioslowski, J.; Fox, D. J. *Gaussian*; Gaussian, Inc.: Wallingford, CT, 2009.
(77) Kong, J.; White, C. A.; Krylov, A. I.; Sherrill, D.; Adamson, R. D.; Furlani, T. R.; Lee, M. S.; Lee, A. M.; Gwaltney, S. R.; Adams, T. R.; Ochsenfeld, C.; Gilbert, A. T. B.; Kedziora, G. S.; Rassolov, V. A.; Maurice, D. R.; Nair, N.; Shao, Y. H.; Besley, N. A.; Maslen, P. E.; Dombroski, J. P.; Daschel, H.; Zhang, W. M.; Korambath, P. P.; Baker, J.; Byrd, E. F. C.; Van Voorhis, T.; Oumi, M.; Hirata, S.; Hsu, C. P.; Ishikawa, N.; Florian, J.; Warshel, A.; Johnson, B. G.; Gill, P. M. W.; Head-Gordon, M.; Pople, J. A. Q-Chem 2.0: A High-Performance Ab

DOI: 10.1021/acs.chemrev.5b00012
Chem. Rev. 2015, 115, 5929−5978

Initio Electronic Structure Program Package. *J. Comput. Chem.* **2000**, *21*, 1532−1548.
(78) Ahlrichs, R.; Bar, M.; Haser, M.; Horn, H.; Kolmel, C. Electronic-Structure Calculations on Workstation Computers - the Program System Turbomole. *Chem. Phys. Lett.* **1989**, *162*, 165−169.
(79) te Velde, G.; Bickelhaupt, F. M.; Baerends, E. J.; Guerra, C. F.; Van Gisbergen, S. J. A.; Snijders, J. G.; Ziegler, T. Chemistry with Adf. *J. Comput. Chem.* **2001**, *22*, 931−967.
(80) Schmidt, M. W.; Baldridge, K. K.; Boatz, J. A.; Elbert, S. T.; Gordon, M. S.; Jensen, J. H.; Koseki, S.; Matsunaga, N.; Nguyen, K. A.; Su, S. J.; Windus, T. L.; Dupuis, M.; Montgomery, J. A. General Atomic and Molecular Electronic-Structure System. *J. Comput. Chem.* **1993**, *14*, 1347−1363.
(81) Kresse, G.; Furthmuller, J. Efficient Iterative Schemes for Ab Initio Total-Energy Calculations Using a Plane-Wave Basis Set. *Phys. Rev. B* **1996**, *54*, 11169−11186.
(82) Valiev, M.; Bylaska, E. J.; Govind, N.; Kowalski, K.; Straatsma, T. P.; Van Dam, H. J. J.; Wang, D.; Nieplocha, J.; Apra, E.; Windus, T. L.; de Jong, W. Nwchem: A Comprehensive and Scalable Open-Source Solution for Large Scale Molecular Simulations. *Comput. Phys. Commun.* **2010**, *181*, 1477−1489.
(83) Stewart, J. J. P. Special Issue - Mopac - a Semiempirical Molecular-Orbital Program. *J. Comput.-Aided Mol. Des.* **1990**, *4*, 1−45.
(84) Papas, B. N.; Schaefer, H. F., III. Concerning the Precision of Standard Density Functional Programs: Gaussian, Molpro, Nwchem, Q-Chem, and Gamess. *J. Mol. Struct. (THEOCHEM)* **2006**, *768*, 175−181.
(85) (a) Tretiak, S.; Mukamel, S. Density Matrix Analysis and Simulation of Electronic Excitations in Conjugated and Aggregated Molecules. *Chem. Rev.* **2002**, *102*, 3171−3212. (b) Bredas, J. L.; Beljonne, D.; Coropceanu, V.; Cornil, J. Charge-Transfer and Energy-Transfer Processes in Pi-Conjugated Oligomers and Polymers: A Molecular Picture. *Chem. Rev.* **2004**, *104*, 4971−5003. (c) Bredas, J. L.; Cornil, J.; Beljonne, D.; dos Santos, D.; Shuai, Z. G. Excited-State Electronic Structure of Conjugated Oligomers and Polymers: A Quantum-Chemical Approach to Optical Phenomena. *Acc. Chem. Res.* **1999**, *32*, 267−276. (d) Tretiak, S.; Chernyak, V.; Mukamel, S. Chemical Bonding and Size Scaling of Nonlinear Polarizabilities of Conjugated Polymers. *Phys. Rev. Lett.* **1996**, *77*, 4656−4659. (e) Schulz, M.; Tretiak, S.; Chernyak, V.; Mukamel, S. Size Scaling of Third-Order Off-Resonant Polarizabilities. Electronic Coherence in Organic Oligomers. *J. Am. Chem. Soc.* **2000**, *122*, 452−459.
(86) Hutchison, G. R.; Zhao, Y. J.; Delley, B.; Freeman, A. J.; Ratner, M. A.; Marks, T. J. Electronic Structure of Conducting Polymers: Limitations of Oligomer Extrapolation Approximations and Effects of Heteroatoms. *Phys. Rev. B* **2003**, *68*, 035204.
(87) Kilina, S.; Batista, E. R.; Yang, P.; Tretiak, S.; Saxena, A.; Martin, R. L.; Smith, D. L. Electronic Structure of Self-Assembled Amorphous Polyfluorenes. *ACS Nano* **2008**, *2*, 1381−1388.
(88) Bredas, J. L. Relationship between Band-Gap and Bond Length Alternation in Organic Conjugated Polymers. *J. Chem. Phys.* **1985**, *82*, 3808−3811.
(89) (a) Oda, M.; Nothofer, H. G.; Scherf, U.; Sunjic, V.; Richter, D.; Regenstein, W.; Neher, D. Chiroptical Properties of Chiral Substituted Polyfluorenes. *Macromolecules* **2002**, *35*, 6792−6798. (b) Donley, C. L.; Zaumseil, J.; Andreasen, J. W.; Nielsen, M. M.; Sirringhaus, H.; Friend, R. H.; Kim, J. S. Effects of Packing Structure on the Optoelectronic and Charge Transport Properties in Poly(9,9-Di-N-Octylfluorene-Alt-Benzothiadiazole). *J. Am. Chem. Soc.* **2005**, *127*, 12890−12899.
(90) Sony, P.; Shukla, A. Large-Scale Correlated Calculations of Linear Optical Absorption and Low-Lying Excited States of Polyacenes: Pariser-Parr-Pople Hamiltonian. *Phys. Rev. B* **2007**, *75*, 155208.
(91) Tretiak, S.; Saxena, A.; Martin, R. L.; Bishop, A. R. Conformational Dynamics of Photoexcited Conjugated Molecules. *Phys. Rev. Lett.* **2002**, *89*, 097402.
(92) (a) Koerzdoerfer, T.; Bredas, J.-L. Organic Electronic Materials: Recent Advances in the DFT Description of the Ground and Excited States Using Tuned Range-Separated Hybrid Functionals. *Acc. Chem. Res.* **2014**, *47*, 3284−3291. (b) Autschbach, J.; Srebro, M. Delocalization Error and "Functional Tuning" in Kohn-Sham Calculations of Molecular Properties. *Acc. Chem. Res.* **2014**, *47*, 2592−2602.
(93) Sutton, C.; Koerzdoerfer, T.; Gray, M. T.; Brunsfeld, M.; Parrish, R. M.; Sherrill, C. D.; Sears, J. S.; Bredas, J.-L. Accurate Description of Torsion Potentials in Conjugated Polymers Using Density Functionals with Reduced Self-Interaction Error. *J. Chem. Phys.* **2014**, *140*, 054310.
(94) Nayyar, I. H.; Batista, E. R.; Tretiak, S.; Saxena, A.; Smith, D. L.; Martin, R. L. Role of Geometric Distortion and Polarization in Localizing Electronic Excitations in Conjugated Polymers. *J. Chem. Theory Comput.* **2013**, *9*, 1144−1154.
(95) (a) Habenicht, B. F.; Craig, C. F.; Prezhdo, O. V. Time-Domain Ab initio Simulation of Electron and Hole Relaxation Dynamics in a Single-Wall Semiconducting Carbon Nanotube. *Phys. Rev. Lett.* **2006**, *96*, 187401. (b) Habenicht, B. F.; Kamisaka, H.; Yarnashita, K.; Prezhdo, O. V. Ab Initio Study of Vibrational Dephasing of Electronic Excitations in Semiconducting Carbon Nanotubes. *Nano Lett.* **2007**, *7*, 3260−3265. (c) Barone, V.; Peralta, J. E.; Wert, M.; Heyd, J.; Scuseria, G. E. Density Functional Theory Study of Optical Transitions in Semiconducting Single-Walled Carbon Nanotubes. *Nano Lett.* **2005**, *5*, 1621−1624.
(96) (a) Spataru, C. D.; Ismail-Beigi, S.; Benedict, L. X.; Louie, S. G. Excitonic Effects and Optical Spectra of Single-Walled Carbon Nanotubes. *Phys. Rev. Lett.* **2004**, *92*, 077402. (b) Maultzsch, J.; Pomraenke, R.; Reich, S.; Chang, E.; Prezzi, D.; Ruini, A.; Molinari, E.; Strano, M. S.; Thomsen, C.; Lienau, C. Exciton Binding Energies in Carbon Nanotubes from Two-Photon Photoluminescence. *Phys. Rev. B* **2005**, *72*, 241402. (c) Maiti, A.; Svizhenko, A.; Anantram, M. P. Electronic Transport through Carbon Nanotubes: Effects of Structural Deformation and Tube Chirality. *Phys. Rev. Lett.* **2002**, *88*, 126805.
(97) Habenicht, B. F.; Prezhdo, O. V. Nanotube Devices: Watching Electrons in Real Time. *Nat. Nanotechnol* **2008**, *3*, 190−191.
(98) Chang, E.; Bussi, G.; Ruini, A.; Molinari, E. Excitons in Carbon Nanotubes: An Ab Initio Symmetry-Based Approach. *Phys. Rev. Lett.* **2004**, *92*, 196401.
(99) (a) Osika, E. N.; Mrenca, A.; Szafran, B. Tight-Binding Simulations of Electrically Driven Spin-Valley Transitions in Carbon Nanotube Quantum Dots. *Phys. Rev. B* **2014**, *90*, 125302. (b) Yang, L.; Han, J. Electronic Structure of Deformed Carbon Nanotubes. *Phys. Rev. Lett.* **2000**, *85*, 154−157. (c) Perebeinos, V.; Tersoff, J.; Avouris, P. Electron-Phonon Interaction and Transport in Semiconducting Carbon Nanotubes. *Phys. Rev. Lett.* **2005**, *94*, 086802. (d) Jiang, J.; Saito, R.; Samsonidze, G. G.; Jorio, A.; Chou, S. G.; Dresselhaus, G.; Dresselhaus, M. S. Chirality Dependence of Exciton Effects in Single-Wall Carbon Nanotubes: Tight-Binding Model. *Phys. Rev. B* **2007**, *75*, 035407.
(100) Blase, X.; Benedict, L. X.; Shirley, E. L.; Louie, S. G. Hybridization Effects and Metallicity in Small Radius Carbon Nanotubes. *Phys. Rev. Lett.* **1994**, *72*, 1878−1881.
(101) (a) Kilina, S.; Tretiak, S. Excitonic and Vibrational Properties of Single-Walled Semiconducting Carbon Nanotubes. *Adv. Funct. Mater.* **2007**, *17*, 3405−3420. (b) Shreve, A. P.; Haroz, E. H.; Bachilo, S. M.; Weisman, R. B.; Tretiak, S.; Kilina, S.; Doorn, S. K. Determination of Exciton-Phonon Coupling Elements in Single-Walled Carbon Nanotubes by Raman Overtone Analysis. *Phys. Rev. Lett.* **2007**, *98*, 037405. (c) Tretiak, S.; Kilina, S.; Piryatinski, A.; Saxena, A.; Martin, R. L.; Bishop, A. R. Excitons and Peierls Distortion in Conjugated Carbon Nanotubes. *Nano Lett.* **2007**, *7*, 86−92. (d) Duque, J. G.; Chen, H.; Swan, A. K.; Shreve, A. P.; Kilina, S.; Tretiak, S.; Tu, X.; Zheng, M.; Doorn, S. K. Violation of the Condon Approximation in Semiconducting Carbon Nanotubes. *ACS Nano* **2011**, *5*, 5233−5241. (e) Kilina, S.; Yarotski, D. A.; Talin, A. A.; Tretiak, S.; Taylor, A. J.; Balatsky, A. V. Unveiling Stability Criteria of DNA-Carbon Nanotubes Constructs by Scanning Tunneling Microscopy and Computational Modeling. *J. Drug Delivery* **2011**, *2011*, 415621. (f) Ramirez, J.; Mayo, M. L.; Kilina, S.; Tretiak, S. Electronic

DOI: 10.1021/acs.chemrev.5b00012
Chem. Rev. 2015, 115, 5929−5978

Structure and Optical Spectra of Semiconducting Carbon Nanotubes Functionalized by Diazonium Salts. *Chem. Phys.* **2013**, *413*, 89−101. (g) Kilina, S.; Tretiak, S.; Doorn, S. K.; Luo, Z.; Papadimitrakopoulos, F.; Piryatinski, A.; Saxena, A.; Bishop, A. R. Cross-Polarized Excitons in Carbon Nanotubes. *Proc. Natl. Acad. Sci. U.S.A.* **2008**, *105*, 6797−6802. (h) Araujo, P. T.; Doorn, S. K.; Kilina, S.; Tretiak, S.; Einarsson, E.; Maruyama, S.; Chacham, H.; Pimenta, M. A.; Jorio, A. Third and Fourth Optical Transitions in Semiconducting Carbon Nanotubes. *Phys. Rev. Lett.* **2007**, *98*, 067401.

(102) (a) Lueer, L.; Hoseinkhani, S.; Polli, D.; Crochet, J.; Hertel, T.; Lanzani, G. Size and Mobility of Excitons in (6,5) Carbon Nanotubes. *Nat. Phys.* **2009**, *5*, 54−58. (b) Kislitsyn, D. A.; Gervasi, C. F.; Allen, T.; Palomaki, P. K. B.; Hackley, J. D.; Maruyama, R. Spatial Mapping of Sub-Bandgap States Induced by Local Nonstoichiometry in Individual Lead Sulfide Nanocrystals. *J. Phys. Chem. Lett.* **2014**, *5*, 3701−3707.

(103) (a) Wohlgenannt, M.; Tandon, K.; Mazumdar, S.; Ramasesha, S.; Vardeny, Z. V. Formation Cross-Sections of Singlet and Triplet Excitons in Pi-Conjugated Polymers. *Nature* **2001**, *409*, 494−497. (b) Zhao, H.; Mazumdar, S.; Sheng, C. X.; Tong, M.; Vardeny, Z. V. Photophysics of Excitons in Quasi-One-Dimensional Organic Semiconductors: Single-Walled Carbon Nanotubes and Pi-Conjugated Polymers. *Phys. Rev. B* **2006**, *73*, 075403.

(104) Kilina, S.; Badaeva, E.; Piryatinski, A.; Tretiak, S.; Saxena, A.; Bishop, A. R. Bright and Dark Excitons in Semiconductor Carbon Nanotubes: Insights from Electronic Structure Calculations. *Phys. Chem. Chem. Phys.* **2009**, *11*, 4113−4123.

(105) (a) Yarotski, D. A.; Kilina, S. V.; Talin, A. A.; Tretiak, S.; Prezhdo, O. V.; Balatsky, A. V.; Taylor, A. J. Scanning Tunneling Microscopy of DNA-Wrapped Carbon Nanotubes. *Nano Lett.* **2009**, *9*, 12−17. (b) Furmanchuk, A. O.; Leszczynski, J.; Tretiak, S.; Kilina, S. V. Morphology and Optical Response of Carbon Nanotubes Functionalized by Conjugated Polymers. *J. Phys. Chem. C* **2012**, *116*, 6831−6840.

(106) Gambetta, A.; Manzoni, C.; Menna, E.; Meneghetti, M.; Cerullo, G.; Lanzani, G.; Tretiak, S.; Piryatinski, A.; Saxena, A.; Martin, R. L.; Bishop, A. R. Real-Time Observation of Nonlinear Coherent Phonon Dynamics in Single-Walled Carbon Nanotubes. *Nat. Phys.* **2006**, *2*, 515−520.

(107) Ekimov, A. I.; Hache, F.; Schanneklein, M. C.; Ricard, D.; Flytzanis, C.; Kudryavtsev, I. A.; Yazeva, T. V.; Rodina, A. V.; Efros, A. L. Absorption and Intensity-Dependent Photoluminescence Measurements on CdSe Quantum Dots - Assignment of the 1st Electronic-Transitions. *J. Opt. Soc. Am. B* **1993**, *10*, 100−107.

(108) (a) Pokrant, S.; Whaley, K. B. Tight-Binding Studies of Surface Effects on Electronic Structure of CdSe Nanocrystals: The Role of Organic Ligands, Surface Reconstruction, and Inorganic Capping Shells. *Eur. Phys. J. D* **1999**, *6*, 255−267. (b) Frenzel, J.; Joswig, J. O.; Sarkar, P.; Seifert, G.; Springborg, M. The Effects of Organisation, Embedding and Surfactants on the Properties of Cadmium Chalcogenide (CdS, CdSe and CdS/CdSe) Semiconductor Nanoparticles. *Eur. J. Inorg. Chem.* **2005**, 3585−3596.

(109) (a) Wang, L. W.; Zunger, A. Pseudopotential Calculations of Nanoscale Cdse Quantum Dots. *Phys. Rev. B* **1996**, *53*, 9579−9582. (b) Elward, J. M.; Chakraborty, A. Effect of Dot Size on Exciton Binding Energy and Electron-Hole Recombination Probability in CdSe Quantum Dots. *J. Chem. Theory Comput.* **2013**, *9*, 4351−4359. (c) Franceschetti, A.; Zunger, A. Direct Pseudopotential Calculation of Exciton Coulomb and Exchange Energies in Semiconductor Quantum Dots. *J. Phys. Rev. Lett.* **1997**, *78*, 915−918.

(110) Reboredo, F. A.; Zunger, A. Surface-Passivation-Induced Optical Changes in Ge Quantum Dots. *Phys. Rev. B* **2001**, *63*, 235314.

(111) (a) Schapotschnikow, P.; Hommersom, B.; Vlugt, T. J. H. Adsorption and Binding of Ligands to CdSe Nanocrystals. *J. Phys. Chem. C* **2009**, *113*, 12690−12698. (b) Schapotschnikow, P.; van Huis, M. A.; Zandbergen, H. W.; Vanmaekelbergh, D.; Vlugt, T. J. H. Morphological Transformations and Fusion of PbSe Nanocrystals Studied Using Atomistic Simulations. *Nano Lett.* **2010**, *10*, 3966−3971.

(112) Nguyen, K. A.; Day, P. N.; Pachter, R. Understanding Structural and Optical Properties of Nanoscale CdSe Magic-Size Quantum Dots: Insight from Computational Prediction. *J. Phys. Chem. C* **2010**, *114*, 16197−16209.

(113) Zanjani, M. B.; Lukes, J. R. Size Dependent Elastic Moduli of CdSe Nanocrystal Superlattices Predicted from Atomistic and Coarse Grained Models. *J. Chem. Phys.* **2013**, *139*, 144702.

(114) (a) Zaiats, G.; Yanover, D.; Vaxenburg, R.; Tilchin, J.; Sashchiuk, A.; Lifshitz, E. PbSe-Based Colloidal Core/Shell Heterostructures for Optoelectronic Applications. *Materials* **2014**, *7*, 7243−7275. (b) Pichaandi, J.; van Veggel, F. C. J. M. Near-Infrared Emitting Quantum Dots: Recent Progress on Their Synthesis and Characterization. *Coord. Chem. Rev.* **2014**, *263*, 138−150. (c) Smith, C.; Binks, D. Multiple Exciton Generation in Colloidal Nanocrystals. *Nanomaterials* **2014**, *4*, 19−45.

(115) (a) Dolai, S.; Nimmala, P. R.; Mandal, M.; Muhoberac, B. B.; Dria, K.; Dass, A.; Sardar, R. Isolation of Bright Blue Light-Emitting CdSe Nanocrystals with 6.5 Kda Core in Gram Scale: High Photoluminescence Efficiency Controlled by Surface Ligand Chemistry. *Chem. Mater.* **2014**, *26*, 1278−1285. (b) Wang, Y.; Zhang, Y.; Wang, F.; Giblin, D. E.; Hoy, J.; Rohrs, H. W.; Loomis, R. A.; Buhro, W. E. The Magic-Size Nanocluster (Cdse)(34) as a Low-Temperature Nucleant for Cadmium Selenide Nanocrystals; Room-Temperature Growth of Crystalline Quantum Platelets. *Chem. Mater.* **2014**, *26*, 2233−2243.

(116) Gao, B.; Shen, C.; Yuan, S.; Yang, Y.; Chen, G. Synthesis of Highly Emissive CdSe Quantum Dots by Aqueous Precipitation Method. *J. Nanomater.* **2013**, *2013*, 138526.

(117) Evans, C. M.; Guo, L.; Peterson, J. J.; Maccagnano-Zacher, S.; Krauss, T. D. Ultrabright PbSe Magic-Sized Clusters. *Nano Lett.* **2008**, *8*, 2896−2899.

(118) (a) Kilina, S. V.; Kilin, D. S.; Prezhdo, O. V. Breaking the Phonon Bottleneck in PbSe and CdSe Quantum Dots: Time-Domain Density Functional Theory of Charge Carrier Relaxation. *ACS Nano* **2009**, *3*, 93−99. (b) Puzder, A.; Williamson, A. J.; Grossman, J. C.; Galli, G. Computational Studies of the Optical Emission of Silicon Nanocrystals. *J. Am. Chem. Soc.* **2003**, *125*, 2786−2791. (c) Kryjevski, A.; Kilina, S.; Kilin, D. Amorphous Silicon Nanomaterials: Quantum Dots Versus Nanowires. *J. Renewable Sustainable Energy* **2013**, *5*, 043120−043116. (d) Mavros, M. G.; Micha, D. A.; Kilin, D. S. Optical Properties of Doped Silicon Quantum Dots with Crystalline and Amorphous Structures. *J. Phys. Chem. C* **2011**, *115*, 19529−19537.

(119) (a) Kamisaka, H.; Kilina, S. V.; Yamashita, K.; Prezhdo, O. V. Ab Initio Study of Temperature- and Pressure Dependence of Energy and Phonon-Induced Dephasing of Electronic Excitations in CdSe and PbSe Quantum Dots. *J. Phys. Chem. C* **2008**, *112*, 7800−7808. (b) Kilina, S. V.; Craig, C. F.; Kilin, D. S.; Prezhdo, O. V. *Ab Initio* Time-Domain Study of Phonon-Assisted Relaxation of Charge Carriers in a PbSe Quantum Dot. *J. Phys. Chem. C* **2007**, *111*, 4871−4878. (c) Hedrick, M. M.; Mayo, M. L.; Badaeva, E.; Kilina, S. First-Principles Studies of the Ground- and Excited-State Properties of Quantum Dots Functionalized by Ru(II)-Polybipyridine. *J. Phys. Chem. C* **2013**, *117*, 18216−18224.

(120) (a) Isborn, C. M.; Kilina, S. V.; Li, X.; Prezhdo, O. V. Generation of Multiple Excitons in PbSe and CdSe Quantum Dots by Direct Photoexcitation: First-Principles Calculations on Small PbSe and CdSe Clusters. *J. Phys. Chem. C* **2008**, *112*, 18291−18294. (b) Chung, S. Y.; Lee, S.; Liu, C.; Neuhauser, D. Structures and Electronic Spectra of CdSe-Cys Complexes: Density Functional Theory Study of a Simple Peptide-Coated Nanocluster. *J. Phys. Chem. B* **2009**, *113*, 292−301. (c) Inerbaev, T. M.; Masunov, A. E.; Khondaker, S. I.; Dobrinescu, A.; Plamada, A.-V.; Kawazoe, Y. Quantum Chemistry of Quantum Dots: Effects of Ligands and Oxidation. *J. Chem. Phys.* **2009**, *131*, 044106. (d) Yang, P.; Tretiak, S.; Masunov, A. E.; Ivanov, S. Quantum Chemistry of the Minimal CdSe Clusters. *J. Chem. Phys.* **2008**, *129*, 074709. (e) Proshchenko, V.; Dahnovsky, Y. Spectroscopic and Electronic Structure Properties of CdSe Nanocrystals: Spheres and Cubes. *Phys. Chem. Chem. Phys.* **2014**, *16*, 7555−7561. (f) Sigalas, M. M.; Koukaras, E. N.; Zdetsis, A. D. Size

DOI: 10.1021/acs.chemrev.5b00012
Chem. Rev. 2015, 115, 5929−5978

Dependence of the Structural, Electronic, and Optical Properties of (CdSe)(N), N=6−60, Nanocrystals. *RSC Adv.* **2014**, *4*, 14613−14623.
(121) Nguyen, K. A.; Pachter, R.; Day, P. N. Computational Prediction of Structures and Optical Excitations for Nanoscale Ultrasmall ZnS and CdSe Clusters. *J. Chem. Theory Comput.* **2013**, *9*, 3581−3596.
(122) (a) del Puerto, M. L.; Tiago, M. L.; Chelikowsky, J. R. Ab Initio Methods for the Optical Properties of CdSe Clusters. *Phys. Rev. B* **2008**, *77*, 045404. (b) del Puerto, M. L.; Tiago, M. L.; Chelikowsky, J. R. Excitonic Effects and Optical Properties of Passivated CdSe Clusters. *Phys. Rev. Lett.* **2006**, *97*, 096401. (c) Badaeva, E.; Isborn, C. M.; Feng, Y.; Ochsenbein, S. T.; Gamelin, D. R.; Li, X. S. Theoretical Characterization of Electronic Transitions in Co^{2+}- and Mn^{2+}-Doped ZnO Nanocrystals. *J. Phys. Chem. C* **2009**, *113*, 8710−8717.
(123) Haram, S. K.; Kshirsagar, A.; Gujarathi, Y. D.; Ingole, P. P.; Nene, O. A.; Markad, G. B.; Nanavati, S. P. Quantum Confinement in Cdte Quantum Dots: Investigation through Cyclic Voltarnmetry Supported by Density Functional Theory (DFT). *J. Phys. Chem. C* **2011**, *115*, 6243−6249.
(124) (a) Kilina, S.; Ivanov, S.; Tretiak, S. Effect of Surface Ligands on Optical and Electronic Spectra of Semiconductor Nanoclusters. *J. Am. Chem. Soc.* **2009**, *131*, 7717−7726. (b) Fischer, S. A.; Crotty, A. M.; Kilina, S. V.; Ivanov, S. A.; Tretiak, S. Passivating Ligand and Solvent Contributions to the Electronic Properties of Semiconductor Nanocrystals. *Nanoscale* **2012**, *4*, 904−914. (c) Koposov, A. Y.; Cardolaccia, T.; Albert, V.; Badaeva, E.; Kilina, S.; Meyer, T. J.; Tretiak, S.; Sykora, M. Formation of Assemblies Comprising Ru-Polypyridine Complexes and CdSe Nanocrystals Studied by ATR-FTIR Spectroscopy and DFT Modeling. *Langmuir* **2011**, *27*, 8377−8383.
(125) (a) Kuznetsov, A. E.; Beratan, D. N. Structural and Electronic Properties of Bare and Capped $Cd_{33}Se_{33}$ and $Cd_{33}Te_{33}$ Quantum Dots. *J. Phys. Chem. C* **2014**, *118*, 7094−7109. (b) Bhattacharya, S. K.; Kshirsagara, A. First Principle Study of Free and Surface Terminated CdTe Nanoparticles. *Eur. Phys. J. D* **2008**, *48*, 355−364.
(126) Azpiroz, J. M.; Lopez, X.; Ugalde, J. M.; Infante, I. Modeling Surface Passivation of ZnS Quantum Dots. *J. Phys. Chem. C* **2012**, *116*, 2740−2750.
(127) Puzder, A.; Williamson, A. J.; Zaitseva, N.; Galli, G.; Manna, L.; Alivisatos, A. P. The Effect of Organic Ligand Binding on the Growth of CdSe Nanoparticles Probed by Ab Initio Calculations. *Nano Lett.* **2004**, *4*, 2361−2365.
(128) Azpiroz, J. M.; Ugalde, J. M.; Infante, I. Benchmark Assessment of Density Functional Methods on Group II-Vi Mx (M = Zn, Cd; X = S, Se, Te) Quantum Dots. *J. Chem. Theory Comput.* **2014**, *10*, 76−89.
(129) Albert, V. V.; Ivanov, S. A.; Tretiak, S.; Kilina, S. V. Electronic Structure of Ligated CdSe Clusters: Dependence on DFT Methodology. *J. Phys. Chem. C* **2011**, *115*, 15793−15800.
(130) (a) Kilin, D. S.; Tsemekhman, K.; Prezhdo, O. V.; Zenkevich, E. I.; von Borczyskowski, C. Ab Initio Study of Exciton Transfer Dynamics from a Core-Shell Semiconductor Quantum Dot to a Porphyrin-Sensitizer. *J. Photochem. Photobiol., A* **2007**, *190*, 342−351. (b) Tamura, H.; Mallet, J.-M.; Oheim, M.; Burghardt, I. Ab Initio Study of Excitation Energy Transfer between Quantum Dots and Dye Molecules. *J. Phys. Chem. C* **2009**, *113*, 7548−7552.
(131) Abuelela, A. M.; Mohamed, T. A.; Prezhdo, O. V. Dft Simulation and Vibrational Analysis of the IR and Raman Spectra of a CdSe Quantum Dot Capped by Methylamine and Trimethylphosphine Oxide Ligands. *J. Phys. Chem. C* **2012**, *116*, 14674−14681.
(132) Kilina, S. V.; Kilin, D. S.; Prezhdo, V. V.; Prezhdo, O. V. Theoretical Study of Electron-Phonon Relaxation in PbSe and CdSe Quantum Dots: Evidence for Phonon Memory. *J. Phys. Chem. C* **2011**, *115*, 21641−21651.
(133) Ben, M. D.; Havenith, R. W. A.; Broer, R.; Stener, M. Density Functional Study on the Morphology and Photoabsorption of CdSe Nanoclusters. *J. Phys. Chem. C* **2011**, *115*, 16782−16796.
(134) Batista, E. R.; Martin, R. L. On the Excited States Involved in the Luminescent Probe Ru(Bpy)(2)Dppz (2+). *J. Phys. Chem. A* **2005**, *109*, 3128−3133.
(135) Kowalczyk, T.; Yost, S. R.; Van Voorhis, T. Assessment of the Delta Scf Density Functional Theory Approach for Electronic Excitations in Organic Dyes. *J. Chem. Phys.* **2011**, *134*, 054128.
(136) Wu, Q.; Van Voorhis, T. Constrained Density Functional Theory and Its Application in Long-Range Electron Transfer. *J. Chem. Theory Comput.* **2006**, *2*, 765−774.
(137) (a) Krylov, A. I. Equation-of-Motion Coupled-Cluster Methods for Open-Shell and Electronically Excited Species: The Hitchhiker's Guide to Fock Space. *Annu. Rev. Phys. Chem.* **2008**, *59*, 433−462. (b) Haettig, C.; Klopper, W.; Koehn, A.; Tew, D. P. Explicitly Correlated Electrons in Molecules. *Chem. Rev.* **2012**, *112*, 4−74.
(138) Gordon, M. S.; Smith, Q. A.; Xu, P.; Slipchenko, L. V. Accurate First Principles Model Potentials for Intermolecular Interactions. *Annu. Rev. Phys. Chem.* **2013**, *64*, 553−578.
(139) (a) Furche, F.; Ahlrichs, R. Adiabatic Time-Dependent Density Functional Methods for Excited State Properties. *J. Chem. Phys.* **2002**, *117*, 7433−7447. (b) Tretiak, S.; Isborn, C. M.; Niklasson, A. M. N.; Challacombe, M. Representation Independent Algorithms for Molecular Response Calculations in Time-Dependent Self-Consistent Field Theories. *J. Chem. Phys.* **2009**, *130*, 054111.
(140) (a) Marques, M. *Time-Dependent Density Functional Theory*; Springer: Berlin; New York, 2006. (b) Furche, F.; Burke, K. In *Time-Dependent Density Functional Theory in Quantum Chemistry: Annual Reports in Computational Chemistry*; Spellmeyer, D., Ed.; Elsevier: Amsterdam, 2005. (c) Dreuw, A.; Head-Gordon, M. Single-Reference Ab Initio Methods for the Calculation of Excited States of Large Molecules. *Chem. Rev.* **2005**, *105*, 4009−4037. (d) Onida, G.; Reining, L.; Rubio, A. Electronic Excitations: Density-Functional Versus Many-Body Green's-Function Approaches. *Rev. Mod. Phys.* **2002**, *74*, 601−659. (e) Jacquemin, D.; Perpte, E. A.; Scuseria, G. E.; Ciofini, I.; Adamo, C. TD-DFT Performance for the Visible Absorption Spectra of Organic Dyes: Conventional Versus Long-Range Hybrids. *J. Chem. Theory Comput.* **2008**, *4*, 123−135. (f) Antony, J.; Grimme, S. Density Functional Theory Including Dispersion Corrections for Intermolecular Interactions in a Large Benchmark Set of Biologically Relevant Molecules. *Phys. Chem. Chem. Phys.* **2006**, *8*, 5287−5293.
(141) Tretiak, S.; Chernyak, V. Resonant Nonlinear Polarizabilities in the Time-Dependent Density Functional Theory. *J. Chem. Phys.* **2003**, *119*, 8809−8823.
(142) (a) Stratmann, R. E.; Scuseria, G. E.; Frisch, M. J. An Efficient Implementation of Time-Dependent Density-Functional Theory for the Calculation of Excitation Energies of Large Molecules. *J. Chem. Phys.* **1998**, *109*, 8218−8224. (b) Saad, Y. *Numerical Methods for Large Eigenvalue Problems: Revised ed.*; Society for Industrial and Applied Mathematics: PA, 2011. (c) Chernyak, V.; Schulz, M. F.; Mukamel, S.; Tretiak, S.; Tsiper, E. V. Krylov-Space Algorithms for Time-Dependent Hartree−Fock and Density Functional Computations. *J. Chem. Phys.* **2000**, *113*, 36−43.
(143) Miranda, R. P.; Fisher, A. J.; Stella, L.; Horsfield, A. P. A Multiconfigurational Time-Dependent Hartree-Fock Method for Excited Electronic States. I. General Formalism and Application to Open-Shell States. *J. Chem. Phys.* **2011**, *134*, 244101.
(144) Kowalczyk, T.; Tsuchimochi, T.; Chen, P.-T.; Top, L.; Van Voorhis, T. Excitation Energies and Stokes Shifts from a Restricted Open-Shell Kohn-Sham Approach. *J. Chem. Phys.* **2013**, *138*, 164101.
(145) Huix-Rotllant, M.; Ipatov, A.; Rubio, A.; Casida, M. E. Assessment of Dressed Time-Dependent Density-Functional Theory for the Low-Lying Valence States of 28 Organic Chromophores. *Chem. Phys.* **2011**, *391*, 120−129.
(146) Sears, J. S.; Koerzdoerfer, T.; Zhang, C.-R.; Bredas, J.-L. Communication: Orbital Instabilities and Triplet States from Time-Dependent Density Functional Theory and Long-Range Corrected Functionals. *J. Chem. Phys.* **2011**, *135*, 151103.
(147) (a) Badaeva, E.; Albert, V. V.; Kilina, S.; Koposov, A.; Sykora, M.; Tretiak, S. Effect of Deprotonation on Absorption and Emission Spectra of Ru(II)-Bpy Complexes Functionalized with Carboxyl Groups. *Phys. Chem. Chem. Phys.* **2010**, *12*, 8902−8913. (b) Lundberg, M.; Siegbahn, P. E. M. Quantifying the Effects of the Self-Interaction

DOI: 10.1021/acs.chemrev.5b00012
Chem. Rev. 2015, 115, 5929−5978

Error in DFT: When Do the Delocalized States Appear? *J. Chem. Phys.* **2005**, *122*, 224103. (c) Magyar, R. J.; Tretiak, S. Dependence of Spurious Charge-Transfer Excited States on Orbital Exchange in TDDFT: Large Molecules and Clusters. *J. Chem. Theory Comput.* **2007**, *3*, 976−987.
(148) Bernardi, M.; Vigil-Fowler, D.; Lischner, J.; Neaton, J. B.; Louie, S. G. Ab Initio Study of Hot Carriers in the First Picosecond after Sunlight Absorption in Silicon. *Phys. Rev. Lett.* **2014**, *112*, 257402.
(149) Szabo, A.; Ostlund, N. S. *Modern Quantum Chemistry: Introduction to Advanced Electronic Structure Theory*; Dover Publications: NY, 2012.
(150) Schmidt, M. W.; Gordon, M. S. The Construction and Interpretation of MCSCF Wavefunctions. *Annu. Rev. Phys. Chem.* **1998**, *49*, 233−266.
(151) Mukamel, S. *Principles of Nonlinear Optical Spectroscopy*; Oxford University Press: New York, 1995.
(152) Perdew, J. P.; Levy, M. Physical Content of the Exact Kohn-Sham Orbital Energies: Band Gaps and Derivative Discontinuities. *Phys. Rev. Lett.* **1983**, *51*, 1884−1887.
(153) (a) Tretiak, S.; Chernyak, V.; Mukamel, S. Localized Electronic Excitations in Phenylacetylene Dendrimers. *J. Phys. Chem. B* **1998**, *102*, 3310. (b) Tretiak, S.; Saxena, A.; Martin, R. L.; Bishop, A. R. Interchain Electronic Excitations in Poly(Phenylenevinylene) (PPV) Aggregates. *J. Phys. Chem. B* **2000**, *104*, 7029−7037.
(154) (a) Reed, A. E.; Curtiss, L. A.; Weinhold, F. Intermolecular Interactions from a Natural Bond Orbital, Donor-Acceptor Viewpoint. *Chem. Rev.* **1988**, *88*, 899−926. (b) Glendening, E. D.; Landis, C. R.; Weinhold, F. Natural Bond Orbital Methods. *Wiley Interdiscip. Rev.: Comput. Mol. Sci.* **2012**, *2*, 1−42.
(155) Martin, R. L. Natural Transition Orbitals. *J. Chem. Phys.* **2003**, *118*, 4775−4777.
(156) Wise, F. W. Lead Salt Quantum Dots: The Limit of Strong Quantum Confinement. *Acc. Chem. Res.* **2000**, *33*, 773−780.
(157) Meulenberg, R. W.; Lee, J. R. I.; Wolcott, A.; Zhang, J. Z.; Terminello, L. J.; van Buuren, T. Determination of the Exciton Binding Energy in CdSe Quantum Dots. *ACS Nano* **2009**, *3*, 325−330.
(158) (a) Kamisaka, H.; Kilina, S. V.; Yamashita, K.; Prezhdo, O. V. Ultrafast Vibrationally-Induced Dephasing of Electronic Excitations in PbSe Quantum Dot. *Nano Lett.* **2006**, *6*, 2295−2300. (b) Kilina, S. V.; Neukirch, A. J.; Habenicht, B. F.; Kilin, D. S.; Prezhdo, O. V. Quantum Zeno Effect Rationalizes the Phonon Bottleneck in Semiconductor Quantum Dots. *Phys. Rev. Lett.* **2013**, *110*, 180404. (c) Kilina, S.; Velizhanin, K. A.; Ivanov, S.; Prezhdo, O. V.; Tretiak, S. Surface Ligands Increase Photoexcitation Relaxation Rates in CdSe Quantum Dots. *ACS Nano* **2012**, *6*, 6515−6524.
(159) Kilina, S.; Cui, P.; Fischer, S. A.; Tretiak, S. Conditions for Directional Charge Transfer in CdSe Quantum Dots Functionalized by Ru(II) Polypyridine Complexes. *J. Phys. Chem. Lett.* **2014**, *5*, 3565−3576.
(160) (a) Chandross, M.; Mazumdar, S.; Jeglinski, S.; Wei, X.; Vardeny, Z. V.; Kwock, E. W.; Miller, T. M. Excitons in Poly(Para-Phenylenevinylene). *Phys. Rev. B* **1994**, *50*, 14702−14705. (b) Kohler, A.; dos Santos, D. A.; Beljonne, D.; Shuai, Z.; Bredas, J. L.; Holmes, A. B.; Kraus, A.; Mullen, K.; Friend, R. H. Charge Separation in Localized and Delocalized Electronic States in Polymeric Semiconductors. *Nature* **1998**, *392*, 903−906.
(161) Tretiak, S.; Chernyak, V.; Mukamel, S. Two-Dimensional Real-Space Analysis of Optical Excitations in Acceptor-Substituted Carotenoids. *J. Am. Chem. Soc.* **1997**, *119*, 11408−11419.
(162) (a) Meng, K.; Ding, Q.; Wang, S.; Gong, Q. Ultrafast Energy Transfer in Blended Polyphenothiazine/Polyphenylene Vinylene Film. *Chem. Phys. Lett.* **2011**, *515*, 155−158. (b) Becker, K.; Da Como, E.; Feldmann, J.; Scheliga, F.; Csanyi, E. T.; Tretiak, S.; Lupton, J. M. How Chromophore Shape Determines the Spectroscopy of Phenylene-Vinylenes: Origin of Spectral Broadening in the Absence of Aggregation. *J. Phys. Chem. B* **2008**, *112*, 4859−4864.
(163) (a) Ghosh, H. Ground and Excited State Nonlinear Optical Properties of Poly(-Para Phenylene Vinylene). *Synth. Met.* **2008**, *158*, 320−329. (b) Sun, M.; Kjellberg, P.; Beenken, W. J. D.; Pullerits, T. Comparison of the Electronic Structure of PPV and Its Derivative Dioxa-Ppv. *Chem. Phys.* **2006**, *327*, 474−484. (c) Kilina, S.; Dandu, N.; Batista, E. R.; Saxena, A.; Martin, R. L.; Smith, D. L.; Tretiak, S. Effect of Packing on Formation of Deep Carrier Traps in Amorphous Conjugated Polymers. *J. Phys. Chem. Lett.* **2013**, *4*, 1453−1459. (d) Yang, P.; Batista, E. R.; Tretiak, S.; Saxena, A.; Martin, R. L.; Smith, D. L. Effect of Intramolecular Disorder and Intermolecular Electronic Interactions on the Electronic Structure of Poly-P-Phenylene Vinylene. *Phys. Rev. B* **2007**, *76*, 241201.
(164) Jiang, Y.; Xu, H.; Zhao, N.; Peng, Q.; Shuai, Z. Spectral Signature of Intrachain and Interchain Polarons in Donor-Acceptor Copolymers. *Acta Chim. Sin.* **2014**, *72*, 201−207.
(165) (a) Barford, W.; Boczarow, I.; Wharram, T. Ultrafast Dynamical Localization of Photoexcited States in Conformationally Disordered Poly(P-Phenylenevinylene). *J. Phys. Chem. A* **2011**, *115*, 9111−9119. (b) Tozer, O. R.; Barford, W. Exciton Dynamics in Disordered Poly(P-Phenylenevinylene): Ultrafast Interconversion and Dynamical Localization. *J. Phys. Chem. A* **2012**, *116*, 10310−10318.
(166) (a) Igumenshchev, K. I.; Tretiak, S.; Chernyak, V. Y. Excitonic Effects in a Time-Dependent Density Functional Theory. *J. Chem. Phys.* **2007**, *127*, 114902. (b) Tretiak, S.; Igumenshchev, K.; Chernyak, V. Exciton Sizes of Conducting Polymers Predicted by Time-Dependent Density Functional Theory. *Phys. Rev. B* **2005**, *71*, 033201.
(167) Arkhipov, V. I.; Bassler, H. Exciton Dissociation and Charge Photogeneration in Pristine and Doped Conjugated Polymers. *Phys. Status Solidi A* **2004**, *201*, 1152−1187.
(168) (a) Li, H.; Malinin, S. V.; Tretiak, S.; Chernyak, V. Y. Exciton Scattering Approach for Branched Conjugated Molecules and Complexes. Iv. Transition Dipoles and Optical Spectra. *J. Chem. Phys.* **2010**, *132*, 124103. (b) Li, H.; Malinin, S. V.; Tretiak, S.; Chernyak, V. Y. Effective Tight-Binding Models for Excitons in Branched Conjugated Molecules. *J. Chem. Phys.* **2013**, *139*, 064109.
(169) (a) Wu, C.; Malinin, S. V.; Tretiak, S.; Chernyak, V. Y. Exciton Scattering and Localization in Branched Dendrimeric Structures. *Nat. Phys.* **2006**, *2*, 631−635. (b) Chao, W.; Malinin, S. V.; Tretiak, S.; Chernyak, V. Y. Multiscale Modeling of Electronic Excitations in Branched Conjugated Molecules Using an Exciton Scattering Approach. *Phys. Rev. Lett.* **2008**, *100*, 057405. (c) Chao, W.; Malinin, S. V.; Tretiak, S.; Chernyak, V. Y. Exciton Scattering Approach for Branched Conjugated Molecules and Complexes. I. Formalism. *J. Chem. Phys.* **2008**, *129*, 174111.
(170) (a) Hendry, E.; Schins, J. M.; Candeias, L. P.; Siebbeles, L. D. A.; Bonn, M. Efficiency of Exciton and Charge Carrier Photogeneration in a Semiconducting Polymer. *Phys. Rev. Lett.* **2004**, *92*, 196601. (b) Cornil, J.; Beljonne, D.; Calbert, J. P.; Bredas, J. L. Interchain Interactions in Organic Pi-Conjugated Materials: Impact on Electronic Structure, Optical Response, and Charge Transport. *Adv. Mater.* **2001**, *13*, 1053−1067. (c) Spano, F. C. Excitons in Conjugated Oligomer Aggregates, Films, and Crystals. *Annu. Rev. Phys. Chem.* **2006**, *57*, 217−243. (d) Tretiak, S.; Saxena, A.; Martin, R. L.; Bishop, A. R. Photoexcited Breathers in Conjugated Polyenes: An Excited-State Molecular Dynamics Study. *Proc. Natl. Acad. Sci. U.S.A.* **2003**, *100*, 2185−2190.
(171) (a) Zhugayevych, A.; Postupna, O.; Bakus, R. C., II; Welch, G. C.; Bazan, G. C.; Tretiak, S. Ab Initio Study of a Molecular Crystal for Photovoltaics: Light Absorption, Exciton and Charge Carrier Transport. *J. Phys. Chem. C* **2013**, *117*, 4920−4930. (b) Coughlin, J. E.; Zhugayevych, A.; Bakus, R. C., II; van der Poll, T. S.; Welch, G. C.; Teat, S. J.; Bazan, G. C.; Tretiak, S. A Combined Experimental and Theoretical Study of Conformational Preferences of Molecular Semiconductors. *J. Phys. Chem. C* **2014**, *118*, 15610−15623. (c) Zhugayevych, A.; Tretiak, S. Theoretical Description of Structural and Electronic Properties of Organic Photovoltaic Materials. *Annu. Rev. Phys. Chem.* **2015**, *66*, 305−330.
(172) Kane, C. L.; Mele, E. J. Electron Interactions and Scaling Relations for Optical Excitations in Carbon Nanotubes. *Phys. Rev. Lett.* **2004**, *93*, 197402.

DOI: 10.1021/acs.chemrev.5b00012
Chem. Rev. 2015, 115, 5929−5978

(173) Korovyanko, O. J.; Sheng, C.-X.; Vardeny, Z. V.; Dalton, A. B.; Baughman, R. H. Ultrafast Spectroscopy of Excitons in Single-Walled Carbon Nanotubes. *Phys. Rev. Lett.* **2004**, *92*, 017403.
(174) Wang, F.; Dukovic, G.; Brus, L. E.; Heinz, T. F. The Optical Resonances in Carbon Nanotubes Arise from Excitons. *Science* **2005**, *308*, 838−841.
(175) Uryu, S.; Ando, T. Exciton Absorption of Perpendicularly Polarized Light in Carbon Nanotubes. *Phys. Rev. B* **2006**, *74*, 155411.
(176) Zhao, H. B.; Mazumdar, S. Electron-Electron Interaction Effects on the Optical Excitations of Semiconducting Single-Walled Carbon Nanotubes. *Phys. Rev. Lett.* **2004**, *93*, 57402.
(177) Spataru, C. D.; Ismail-Beigi, S.; Capaz, R. B.; Louie, S. G. Theory and Ab Initio Calculation of Radiative Lifetime of Excitons in Semiconducting Carbon Nanotubes. *Phys. Rev. Lett.* **2005**, *95*, 247402.
(178) Scholes, G. D.; Tretiak, S.; McDonald, T. J.; Metzger, W. K.; Engtrakul, C.; Rumbles, G.; Heben, M. J. Low-Lying Exciton States Determine the Photophysics of Semiconducting Single Wall Carbon Nanotubes. *J. Phys. Chem. C* **2007**, *111*, 11139−11149.
(179) Wang, F.; Dukovic, G.; Brus, L. E.; Heinz, T. F. Time-Resolved Fluorescence of Carbon Nanotubes and Its Implication for Radiative Lifetimes. *Phys. Rev. Lett.* **2004**, *92*, 177401.
(180) Srivastava, A.; Htoon, H.; Klimov, V. I.; Kono, J. Direct Observation of Dark Excitons in Individual Carbon Nanotubes: Inhomogeneity in the Exchange Splitting. *Phys. Rev. Lett.* **2008**, *101*, 087402.
(181) Capaz, R. B.; Spataru, C. D.; Ismail-Beigi, S.; Louie, S. G. Diameter and Chirality Dependence of Exciton Properties in Carbon Nanotubes. *Phys. Rev. B* **2006**, *74*, 121401.
(182) Khalil, M.; Demirdoven, N.; Tokmakoff, A. Coherent 2d Ir Spectroscopy: Molecular Structure and Dynamics in Solution. *J. Phys. Chem. A* **2003**, *107*, 5258−5279.
(183) Wei, H. H.-Y.; Evans, C. M.; Swartz, B. D.; Neukirch, A. J.; Young, J.; Prezhdo, O. V.; Krauss, T. D. Colloidal Semiconductor Quantum Dots with Tunable Surface Composition. *Nano Lett.* **2012**, *12*, 4465−4471.
(184) Karakoti, A. S.; Sanghavi, S.; Nachimuthu, P.; Yang, P.; Thevuthasan, S. Probing the Size- and Environment-Induced Phase Transformation in CdSe Quantum Dots. *J. Phys. Chem. Lett.* **2011**, *2*, 2925−2929.
(185) Omogo, B.; Aldana, J. F.; Heyes, C. D. Radiative and Nonradiative Lifetime Engineering of Quantum Dots in Multiple Solvents by Surface Atom Stoichiometry and Ligands. *J. Phys. Chem. C* **2013**, *117*, 2317−2327.
(186) Kim, D.; Kim, D.-H.; Lee, J.-H.; Grossman, J. C. Impact of Stoichiometry on the Electronic Structure of PbSe Quantum Dots. *Phys. Rev. Lett.* **2013**, *110*, 196802.
(187) Voznyy, O.; Zhitomirsky, D.; Stadler, P.; Ning, Z.; Hoogland, S.; Sargent, E. H. A Charge-Orbital Balance Picture of Doping in Colloidal Quantum Dot Solids. *ACS Nano* **2012**, *6*, 8448−8455.
(188) Voznyy, O.; Sargent, E. H. Atomistic Model of Fluorescence Intermittency of Colloidal Quantum Dots. *Phys. Rev. Lett.* **2014**, *112*, 157401.
(189) (a) Bloom, B. P.; Zhao, L.-B.; Wang, Y.; Waldeck, D. H.; Liu, R.; Zhang, P.; Beratan, D. N. Ligand-Induced Changes in the Characteristic Size-Dependent Electronic Energies of CdSe Nanocrystals. *J. Phys. Chem. C* **2013**, *117*, 22401−22411. (b) Carey, G. H.; Kramer, I. J.; Kanjanaboos, P.; Moreno-Bautista, G.; Voznyy, O.; Rollny, L.; Tang, J. A.; Hoogland, S.; Sargent, E. H. Electronically Active Impurities in Colloidal Quantum Dot Solids. *ACS Nano* **2014**, *8*, 11763−11769.
(190) (a) Sykora, M.; Petruska, M. A.; Alstrum-Acevedo, J.; Bezel, I.; Meyer, T. J.; Klimov, V. I. Photoinduced Charge Transfer between CdSe Nanocrystal Quantum Dots and Ru-Polypyridine Complexes. *J. Am. Chem. Soc.* **2006**, *128*, 9984−9985. (b) Gimenez, S.; Rogach, A. L.; Lutich, A. A.; Gross, D.; Poeschl, A.; Susha, A. S.; Mora-Sero, I.; Lana-Villarreal, T.; Bisquert, J. Energy Transfer Versus Charge Separation in Hybrid Systems of Semiconductor Quantum Dots and Ru-Dyes as Potential Co-Sensitizers of TiO_2-Based Solar Cells. *J. Appl. Phys.* **2011**, *110*, 014314.
(191) (a) van der Poll, T. S.; Zhugayevych, A.; Chertkov, E.; Bakus, R. C., II; Coughlin, J. E.; Teat, S. J.; Bazan, G. C.; Tretiak, S. Polymorphism of Crystalline Molecular Donors for Solution-Processed Organic Photovoltaics. *J. Phys. Chem. Lett.* **2014**, *5*, 2700−2704. (b) Jackson, N. E.; Savoie, B. M.; Kohlstedt, K. L.; de la Cruz, M. O.; Schatz, G. C.; Chen, L. X.; Ratner, M. A. Controlling Conformations of Conjugated Polymers and Small Molecules: The Role of Nonbonding Interactions. *J. Am. Chem. Soc.* **2013**, *135*, 10475−10483.
(192) Coropceanu, V.; Cornil, J.; da Silva, D. A.; Olivier, Y.; Silbey, R.; Bredas, J. L. Charge Transport in Organic Semiconductors. *Chem. Rev.* **2007**, *107*, 926−952.
(193) Albu, N. M.; Yaron, D. J. Brownian Dynamics Simulations of Charge Mobility on Conjugated Polymers in Solution. *J. Chem. Phys.* **2013**, *138*, 224902.
(194) Hu, Z.; Liu, J.; Simón-Bower, L.; Zhai, L.; Gesquiere, A. J. Influence of Backbone Rigidness on Single Chain Conformation of Thiophene-Based Conjugated Polymers. *J. Phys. Chem. B* **2012**, *117*, 4461−4467.
(195) (a) Granadino-Roldan, J. M.; Vukmirovic, N.; Fernandez-Gomez, M.; Wang, L.-W. The Role of Disorder on the Electronic Structure of Conjugated Polymers. The Case of Poly-2,5-Bis-(Phenylethynyl)-1,3,4-Thiadiazole. *Phys. Chem. Chem. Phys.* **2011**, *13*, 14500−14509. (b) Vukmirovic, N.; Wang, L.-W. Charge Carrier Motion in Disordered Conjugated Polymers: A Multiscale Ab Initio Study. *Nano Lett.* **2009**, *9*, 3996−4000.
(196) Liu, L. A.; Yaron, D. J. Modeling Outer-Sphere Disorder in the Symmetry Breaking of PPV. *J. Chem. Phys.* **2009**, *130*, 154701-1−10.
(197) (a) Vukmirovic, N. A Comparative Study of Electronic Properties of Disordered Conjugated Polymers. *Phys. Chem. Chem. Phys.* **2013**, *15*, 3543−3551. (b) Ruehle, V.; Kirkpatrick, J.; Andrienko, D. A Multiscale Description of Charge Transport in Conjugated Oligomers. *J. Chem. Phys.* **2010**, *132*, 134103.
(198) Ono, Y.; Ohtsuki, T.; Kramer, B. Inverse Participation Number and Fractal Dimensionality of Electronic States in Strong Perpendicular Magnetic Field. *J. Phys. Soc. Jpn.* **1989**, *58*, 1705−1716.
(199) Abtew, T. A.; Drabold, D. A. Hydrogen Dynamics and Light-Induced Structural Changes in Hydrogenated Amorphous Silicon. *Phys. Rev. B* **2006**, *74*, 085201.
(200) Melzer, C.; Koop, E. J.; Mihailetchi, V. D.; Blom, P. W. M. Hole Transport in Poly(Phenylene Vinylene)/Methanofullerene Bulk-Heterojunction Solar Cells. *Adv. Funct. Mater.* **2004**, *14*, 865−870.
(201) Mihailetchi, V. D.; Koster, L. J. A.; Blom, P. W. M.; Melzer, C.; de Boer, B.; van Duren, J. K. J.; Janssen, R. A. J. Compositional Dependence of the Performance of Poly(P-Phenylene Vinylene): Methanofullerene Bulk-Heterojunction Solar Cells. *Adv. Funct. Mater.* **2005**, *15*, 795−801.
(202) O'Connell, M. J.; Bachilo, S. M.; Huffman, C. B.; Moore, V. C.; Strano, M. S.; Haroz, E. H.; Rialon, K. L.; Boul, P. J.; Noon, W. H.; Kittrell, C.; Ma, J. P.; Hauge, R. H.; Weisman, R. B.; Smalley, R. E. Band Gap Fluorescence from Individual Single-Walled Carbon Nanotubes. *Science* **2002**, *297*, 593−596.
(203) Ju, S. Y.; Kopcha, W. P.; Papadimitrakopoulos, F. Brightly Fluorescent Single-Walled Carbon Nanotubes Via an Oxygen-Excluding Surfactant Organization. *Science* **2009**, *323*, 1319−1323.
(204) Ando, T. Excitons in Carbon Nanotubes. *J. Phys. Soc. Jpn.* **1997**, *66*, 1066−1073.
(205) (a) Hartschuh, A.; Pedrosa, H. N.; Novotny, L.; Krauss, T. D. Simultaneous Fluorescence and Raman Scattering from Single Carbon Nanotubes. *Science* **2003**, *301*, 1354−1356. (b) Htoon, H.; O'Connell, M. J.; Cox, P. J.; Doorn, S. K.; Klimov, V. I. Low Temperature Emission Spectra of Individual Single-Walled Carbon Nanotubes: Multiplicity of Subspecies within Single-Species Nanotube Ensembles. *Phys. Rev. Lett.* **2004**, *93*, 027401.
(206) Piao, Y.; Meany, B.; Powell, L. R.; Valley, N.; Kwon, H.; Schatz, G. C.; Wang, Y. Brightening of Carbon Nanotube Photoluminescence through the Incorporation of sp(3) Defects. *Nat. Chem.* **2013**, *5*, 840−845.

DOI: 10.1021/acs.chemrev.5b00012
Chem. Rev. 2015, 115, 5929−5978

(207) Matsunaga, R.; Matsuda, K.; Kanemitsu, Y. Origin of Low-Energy Photoluminescence Peaks in Single Carbon Nanotubes: K-Momentum Dark Excitons and Triplet Dark Excitons. *Phys. Rev. B* **2010**, *81*, 033401.
(208) Blackburn, J. L.; McDonald, T. J.; Metzger, W. K.; Engtrakul, C.; Rumbles, G.; Heben, M. J. Protonation Effects on the Branching Ratio in Photoexcited Single-Walled Carbon Nanotube Dispersions. *Nano Lett.* **2008**, *8*, 1047−1054.
(209) (a) Zhou, W.; Vavro, J.; Nemes, N. M.; Fischer, J. E. Charge Transfer and Fermi Level Shift in p-Doped Single-Walled Carbon Nanotubes. *Phys. Rev. B* **2005**, *71*, 205423. (b) Strano, M. S.; Huffman, C. B.; Moore, V. C.; O'Connell, M. J.; Haroz, E. H.; Hubbard, J.; Miller, M.; Rialon, K.; Kittrell, C.; Ramesh, S.; Hauge, R. H.; Smalley, R. E. Reversible, Band-Gap-Selective Protonation of Single-Walled Carbon Nanotubes in Solution. *J. Phys. Chem. B* **2003**, *107*, 6979−6985.
(210) (a) Wang, H.-M.; Wang, H.-X.; Chen, Y.; Liu, Y.-J.; Zhao, J.-X.; Cai, Q.-H.; Wang, X.-Z. Phosphorus-Doped Graphene and (8,0) Carbon Nanotube: Structural, Electronic, Magnetic Properties, and Chemical Reactivity. *Appl. Surf. Sci.* **2013**, *273*, 302−309. (b) Ma, X.; Adamska, L.; Yamaguchi, H.; Yalcin, S. E.; Tretiak, S.; Doorn, S. K.; Htoon, H. Electronic Structure and Chemical Nature of Oxygen Dopant States in Carbon Nanotubes. *ACS Nano* **2014**, *8*, 10782−10789.
(211) Mayo, M. L.; Hogle, D.; Yilmaz, B.; Ḱose, M. E.; Kilina, S. Morphology and Dispersion of Polycarbazole Wrapped Carbon Nanotubes. *RSC Adv.* **2013**, *3*, 20492−20502.
(212) Mayo, M. L.; Chen, Z. Q.; Kilina, S. V. Computational Studies of Nucleotide Selectivity in DNA-Carbon Nanotube Hybrids. *J. Phys. Chem. Lett.* **2012**, *3*, 2790−2797.
(213) (a) Tallury, S. S.; Pasquinelli, M. A. Molecular Dynamics Simulations of Polymers with Stiff Backbones Interacting with Single-Walled Carbon Nanotubes. *J. Phys. Chem. B* **2010**, *114*, 9349−9355. (b) Nish, A.; Hwang, J. Y.; Doig, J.; Nicholas, R. J. Highly Selective Dispersion of Singlewalled Carbon Nanotubes Using Aromatic Polymers. *Nat. Nanotechnol.* **2007**, *2*, 640−646.
(214) Gurevitch, I.; Srebnik, S. Monte Carlo Simulation of Polymer Wrapping of Nanotubes. *Chem. Phys. Lett.* **2007**, *444*, 96−100.
(215) (a) Lacerda, L.; Ali-Boucettal, H.; Herrero, M. A.; Pastorin, G.; Bianco, A.; Prato, M.; Kostarelos, K. Tissue Histology and Physiology Following Intravenous Administration of Different Types of Functionalized Multiwalled Carbon Nanotubes. *Nanomedicine* **2008**, *3*, 149−161. (b) Lacerda, L.; Herrero, M. A.; Venner, K.; Bianco, A.; Prato, M.; Kostarelos, K. Carbon-Nanotube Shape and Individualization Critical for Renal Excretion. *Small* **2008**, *4*, 1130−1132.
(216) (a) Ozawa, H.; Fujigaya, T.; Niidome, Y.; Hotta, N.; Fujiki, M.; Nakashima, N. Rational Concept to Recognize/Extract Single-Walled Carbon Nanotubes with a Specific Chirality. *J. Am. Chem. Soc.* **2011**, *133*, 2651−2657. (b) Liu, Y. Z.; Chipot, C.; Shao, X. G.; Cai, W. S. Free-Energy Landscape of the Helical Wrapping of a Carbon Nanotube by a Polysaccharide. *J. Phys. Chem. C* **2011**, *115*, 1851−1856.
(217) Yang, M. J.; Koutsos, V.; Zaiser, M. Interactions between Polymers and Carbon Nanotubes: A Molecular Dynamics Study. *J. Phys. Chem. B* **2005**, *109*, 10009−10014.
(218) Kang, Y. K.; Lee, O. S.; Deria, P.; Kim, S. H.; Park, T. H.; Bonnell, D. A.; Saven, J. G.; Therien, M. J. Helical Wrapping of Single-Walled Carbon Nanotubes by Water Soluble Poly(P-Phenyleneethynylene). *Nano Lett.* **2009**, *9*, 1414−1418.
(219) Luer, L.; Hoseinkhani, S.; Meneghetti, M.; Lanzani, G. Dynamical Screening of the Exciton Resonance in Conjugated Polymers/Carbon Nanotubes Composites. *Phys. Rev. B* **2010**, *81*, 155411.
(220) Prezhdo, O. V.; Rossky, P. J. Evaluation of Quantum Transition Rates from Quantum-Classical Molecular Dynamics Simulations. *J. Chem. Phys.* **1997**, *107*, 5863−5878.
(221) Heeger, A. J.; Kivelson, S.; Schrieffer, J. R.; Su, W. P. Soliton in Conducting Polymers. *Rev. Mod. Phys.* **1988**, *60*, 781−850.
(222) Batista, E. R.; Martin, R. L. Exciton Localization in a Pt-Acetylide Complex. *J. Phys. Chem. A* **2005**, *109*, 9856−9859.
(223) Dexheimer, S. L.; Van Pelt, A. D.; Brozik, J. A.; Swanson, B. I. Femtosecond Vibrational Dynamics of Self-Trapping in a Quasi-One-Dimensional System. *Phys. Rev. Lett.* **2000**, *84*, 4425−4428.
(224) (a) Klessinger, M.; Michl, J. *Excited States and Photochemistry of Organic Molecules*; VCH: New York, 1995. (b) Balzani, V. *Supramolecular Photochemistry*; Springer: Netherlands, 2011.
(225) Spano, F. C. The Spectral Signatures of Frenkel Polarons in H- and J-Aggregates. *Acc. Chem. Res.* **2010**, *43*, 429−439.
(226) Tretiak, S.; Piryatinski, A.; Saxena, A.; Martin, R. L.; Bishop, A. R. On the Existence of Photoexcited Breathers in Conducting Polymers. *Phys. Rev. B* **2004**, *70*, 233203.
(227) Haber, T.; Seefeld, K.; Engler, G.; Grimme, S.; Kleinermanns, K. Ir/Uv Spectra and Quantum Chemical Calculations of Trp-Ser: Stacking Interactions between Backbone and Indole Side-Chain. *Phys. Chem. Chem. Phys.* **2008**, *10*, 2844−2851.
(228) Condon, E. A Theory of Intensity Distribution in Band Systems. *Phys. Rev.* **1926**, *28*, 1182−1201.
(229) Krauss, T. D.; Wise, F. W. Raman-Scattering Study of Exciton-Phonon Coupling in PbS Nanocrystals. *Phys. Rev. B* **1997**, *55*, 9860−9865.
(230) Krauss, T. D.; Wise, F. W. Coherent Acoustic Phonons in a Semiconductor Quantum Dot. *Phys. Rev. Lett.* **1997**, *79*, 5102−5105.
(231) Karabunarliev, S.; Bittner, E. R.; Baumgarten, M. Franck-Condon Spectra and Electron-Libration Coupling in Para-Polyphenyls. *J. Chem. Phys.* **2001**, *114*, 5863−5870.
(232) (a) Franco, I.; Tretiak, S. Electron-Vibrational Dynamics of Photoexcited Polyfluorenes. *J. Am. Chem. Soc.* **2004**, *126*, 12130−12140. (b) Furche, F. On the Density Matrix Based Approach to Time-Dependent Density Functional Response Theory. *J. Chem. Phys.* **2001**, *114*, 5982−5992.
(233) Chen, D.; Liu, J.; Ma, H.; Zeng, Q.; Liang, W. Analytical Derivative Techniques for Tddft Excited-State Properties: Theory and Application. *Sci. China: Chem.* **2014**, *57*, 48−57.
(234) (a) Franceschetti, A. Structural and Electronic Properties of PbSe Nanocrystals from First Principles. *Phys. Rev. B* **2008**, *78*, 075418. (b) Franceschetti, A.; Pantelides, S. T. Excited-State Relaxations and Franck-Condon Shift in Si Quantum Dots. *Phys. Rev. B* **2003**, *68*, 033313.
(235) Leitsmann, R.; Bechstedt, F. Characteristic Energies and Shifts in Optical Spectra of Colloidal IV-VI Semiconductor Nanocrystals. *ACS Nano* **2009**, *3*, 3505−3512.
(236) Spano, F. C.; Silva, C. H- and J-Aggregate Behavior in Polymeric Semiconductors. *Annu. Rev. Phys. Chem.* **2014**, *65*, 477−500.
(237) Barbara, P. F.; Meyer, T. J.; Ratner, M. A. Contemporary Issues in Electron Transfer Research. *J. Phys. Chem.* **1996**, *100*, 13148−13168.
(238) Skinner, J. L. Theory of Pure Dephasing in Crystals. *Annu. Rev. Phys. Chem.* **1988**, *39*, 463−478.
(239) Zhuravlev, K. K.; Pietryga, J. M.; Sander, R. K.; Schaller, R. D. Optical Properties of PbSe Nanocrystal Quantum Dots under Pressure. *Appl. Phys. Lett.* **2007**, *90*, 043110.
(240) Murphy, J. E.; Beard, M. C.; Norman, A. G.; Ahrenkiel, S. P.; Johnson, J. C.; Yu, P. R.; Micic, O. I.; Ellingson, R. J.; Nozik, A. J. Pbte Colloidal Nanocrystals: Synthesis, Characterization, and Multiple Exciton Generation. *J. Am. Chem. Soc.* **2006**, *128*, 3241−3247.
(241) Lifshitz, E.; Brumer, M.; Kigel, A.; Sashchiuk, A.; Bashouti, M.; Sirota, M.; Galun, E.; Burshtein, Z.; Le Quang, A. Q.; Ledoux-Rak, I.; Zyss, J. Stable PbSe/PbS and PbSe/$PbSe_xS_{1-X}$ Core-Shell Nanocrystal Quantum Dots and Their Applications. *J. Phys. Chem. B* **2006**, *110*, 25356−25365.
(242) Rogach, A. L.; Franzl, T.; Klar, T. A.; Feldmann, J.; Gaponik, N.; Lesnyak, V.; Shavel, A.; Eychmueller, A.; Rakovich, Y. P.; Donegan, J. F. Aqueous Synthesis of Thiol-Capped Cdte Nanocrystals: State-of-the-Art. *J. Phys. Chem. C* **2007**, *111*, 14628−14637.

DOI: 10.1021/acs.chemrev.5b00012
Chem. Rev. 2015, 115, 5929−5978

(243) An, J. M.; Franceschetti, A.; Zunger, A. The Excitonic Exchange Splitting and Radiative Lifetime in PbSe Quantum Dots. *Nano Lett.* **2007**, *7*, 2129−2135.
(244) Liu, W.; Zhang, Y.; Zhai, W.; Wang, Y.; Zhang, T.; Gu, P.; Chu, H.; Zhang, H.; Cui, T.; Wang, Y.; Zhao, J.; Yu, W. W. Temperature-Dependent Photoluminescence of ZnCuInS/ZnSe/ZnS Quantum Dots. *J. Phys. Chem. C* **2013**, *117*, 19288−19294.
(245) Kang, I.; Wise, F. W. Electronic Structure and Optical Properties of PbS and PbSe Quantum Dots. *J. Opt. Soc. Am. B* **1997**, *14*, 1632−1646.
(246) Takagahara, T. Electron-Phonon Interactions in Semiconductor Nanocrystals. *J. Lumin.* **1996**, *70*, 129−143.
(247) Baker, J. A.; Kelley, D. F.; Kelley, A. M. Resonance Raman and Photoluminescence Excitation Profiles and Excited-State Dynamics in CdSe Nanocrystals. *J. Chem. Phys.* **2013**, *139*, 024702.
(248) Alivisatos, A. P.; Harris, T. D.; Carroll, P. J.; Steigerwald, M. L.; Brus, L. E. Electron-Vibration Coupling in Semiconductor Clusters Studied by Resonance Raman Spectroscopy. *J. Chem. Phys.* **1989**, *90*, 3463−3468.
(249) Sagar, D. M.; Cooney, R. R.; Sewall, S. L.; Dias, E. A.; Barsan, M. M.; Butler, I. S.; Kambhampati, P. Size Dependent, State-Resolved Studies of Exciton-Phonon Couplings in Strongly Confined Semiconductor Quantum Dots. *Phys. Rev. B* **2008**, *77*, 235321.
(250) Salvador, M. R.; Graham, M. W.; Scholes, G. D. Exciton-Phonon Coupling and Disorder in the Excited States of CdSe Colloidal Quantum Dots. *J. Chem. Phys.* **2006**, *125*, 184709.
(251) Oron, D.; Aharoni, A.; Donega, C. d. M.; van Rijssel, J.; Meijerink, A.; Banin, U. Universal Role of Discrete Acoustic Phonons in the Low-Temperature Optical Emission of Colloidal Quantum Dots. *Phys. Rev. Lett.* **2009**, *102*, 177402.
(252) Sewall, S. L.; Cooney, R. R.; Anderson, K. E. H.; Dias, E. A.; Sagar, D. M.; Kambhampati, P. State-Resolved Studies of Biexcitons and Surface Trapping Dynamics in Semiconductor Quantum Dots. *J. Chem. Phys.* **2008**, *129*, 084701.
(253) Klein, M. C.; Hache, F.; Ricard, D.; Flytzanis, C. Size Dependence of Electron-Phonon Coupling in Semiconductor Nanospheres - the Case of CdSe. *Phys. Rev. B* **1990**, *42*, 11123−11132.
(254) Kelley, A. M. Electron-Phonon Coupling in CdSe Nanocrystals from an Atomistic Phonon Model. *ACS Nano* **2011**, *5*, 5254−5262.
(255) Prabhu, S. S.; Vengurlekar, A. S.; Roy, S. K.; Shah, J. Nonequilibrium Dynamics of Hot Carriers and Hot Phonons in CdSe and GaAs. *Phys. Rev. B* **1995**, *51*, 14233−14246.
(256) Mittleman, D. M.; Schoenlein, R. W.; Shiang, J. J.; Colvin, V. L.; Alivisatos, A. P.; Shank, C. V. Quantum-Size Dependence of Femtosecond Electronic Dephasing and Vibrational Dynamics in CdSe Nanocrystals. *Phys. Rev. B* **1994**, *49*, 14435−14447.
(257) Fernee, M. J.; Jensen, P.; Rubinsztein-Dunlop, H. Origin of the Large Homogeneous Line Widths Obtained from Strongly Quantum Confined PbS Nanocrystals at Room Temperature. *J. Phys. Chem. C* **2007**, *111*, 4984−4989.
(258) Morello, G.; De Giorgi, M.; Kudera, S.; Manna, L.; Cingolani, R.; Anni, M. Temperature and Size Dependence of Nonradiative Relaxation and Exciton-Phonon Coupling in Colloidal CdTe Quantum Dots. *J. Phys. Chem. C* **2007**, *111*, 5846−5849.
(259) (a) Peterson, J. J.; Krauss, T. D. Fluorescence Spectroscopy of Single Lead Sulfide Quantum Dots. *Nano Lett.* **2006**, *6*, 510−514. (b) Mathew, R.; Dilcher, E.; Gamouras, A.; Ramachandran, A.; Yang, H. Y. S.; Freisem, S.; Deppe, D.; Hall, K. C. Subpicosecond Adiabatic Rapid Passage on a Single Semiconductor Quantum Dot: Phonon-Mediated Dephasing in the Strong-Driving Regime. *Phys. Rev. B* **2014**, *90*, 035316.
(260) Liu, J.; Neukirch, A. J.; Prezhdo, O. V. Phonon-Induced Pure-Dephasing of Luminescence, Multiple Exciton Generation, and Fission in Silicon Clusters. *J. Chem. Phys.* **2013**, *139*, 164303.
(261) (a) Dobson, K. D.; McQuillan, A. J. An Infrared Spectroscopic Study of Carbonate Adsorption to Zirconium Dioxide Sol-Gel Films from Aqueous Solutions. *Langmuir* **1997**, *13*, 3392−3396. (b) Dobson, K. D.; McQuillan, A. J. In Situ Infrared Spectroscopic Analysis of the Adsorption of Aromatic Carboxylic Acids to TiO_2, ZrO_2, Al_2O_3, and Ta_2O_5 from Aqueous Solutions. *Spectrochim. Acta, Part A* **2000**, *56*, 557−565.
(262) Deacon, G. B.; Phillips, R. J. Relationship between the Carbon-Oxygen Stretching Frequencies of Carboxylato Complexes and the Type of Carboxylate Coordination. *Coord. Chem. Rev.* **1980**, *33*, 227−250.
(263) Herzberg, G.; Spinks, J. W. T. *Molecular Spectra and Molecular Structure: Diatomic Molecules*; Prentice-Hall: New York, 1939.
(264) Peierls, R. E. *Quantum Theory of Solids*; Clarendon Press: New York, 1996.
(265) Terenziani, F.; Katan, C.; Badaeva, E.; Tretiak, S.; Blanchard-Desce, M. Enhanced Two-Photon Absorption of Organic Chromophores: Theoretical and Experimental Assessments. *Adv. Mater.* **2008**, *20*, 4641−4678.
(266) White, A. J.; Gorshkov, V. N.; Wang, R. X.; Tretiak, S.; Mozyrsky, D. Semiclassical Monte Carlo: A First Principles Approach to Non-Adiabatic Molecular Dynamics. *J. Chem. Phys.* **2014**, *141*, 84101−84101.
(267) Tempelaar, R.; Stradomska, A.; Knoester, J.; Spano, F. C. Antomy of an Exciton: Vibrational Distortion and Exciton Coherence in H- and J-Aggregates. *J. Phys. Chem. B* **2012**, *117*, 457−466.
(268) (a) Plentz, F.; Ribeiro, H. B.; Jorio, A.; Strano, M. S.; Pimenta, M. A. Direct Experimental Evidence of Exciton-Phonon Bound States in Carbon Nanotubes. *Phys. Rev. Lett.* **2005**, *95*, 247401. (b) Qiu, X. H.; Freitag, M.; Perebeinos, V.; Avouris, P. Photoconductivity Spectra of Single-Carbon Nanotubes: Implications on the Nature of Their Excited States. *Nano Lett.* **2005**, *5*, 749−752.
(269) (a) Satishkumar, B. C.; Goupalov, S. V.; Haroz, E. H.; Doorn, S. K. Transition Level Dependence of Raman Intensities in Carbon Nanotubes: Role of Exciton Decay. *Phys. Rev. B* **2006**, *74*, 155409. (b) Moura, L. G.; Moutinho, M. V. O.; Venezuela, P.; Fantini, C.; Righi, A.; Strano, M. S.; Pimenta, M. A. Raman Excitation Profile of the G Band in Single-Chirality Carbon Nanotubes. *Phys. Rev. B* **2014**, *89*, 035402.
(270) Heller, I.; Kong, J.; Heering, H. A.; Williams, K. A.; Lemay, S. G.; Dekker, C. Individual Single-Walled Carbon Nanotubes as Nanoelectrodes for Electrochemistry. *Nano Lett.* **2005**, *5*, 137−142.
(271) (a) Lueer, L.; Gadermaier, C.; Crochet, J.; Hertel, T.; Brida, D.; Lanzani, G. Coherent Phonon Dynamics in Semiconducting Carbon Nanotubes: A Quantitative Study of Electron-Phonon Coupling. *Phys. Rev. Lett.* **2009**, *102*, 127401. (b) Yin, Y.; Vamivakas, A. N.; Walsh, A. G.; Cronin, S. B.; Unlu, M. S.; Goldberg, B. B.; Swan, A. K. Optical Determination of Electron-Phonon Coupling in Carbon Nanotubes. *Phys. Rev. Lett.* **2007**, *98*, 037404.
(272) (a) Machon, M.; Reich, S.; Telg, H.; Maultzsch, J.; Ordejon, P.; Thomsen, C. Strength of Radial Breathing Mode in Single-Walled Carbon Nanotubes. *Phys. Rev. B* **2005**, *71*, 205423. (b) Machon, M.; Reich, S.; Thomsen, C. Strong Electron-Phonon Coupling of the High-Energy Modes of Carbon Nanotubes. *Phys. Rev. B* **2006**, *74*, 205423.
(273) Nanot, S.; Haroz, E. H.; Kim, J.-H.; Hauge, R. H.; Kono, J. Optoelectronic Properties of Single-Wall Carbon Nanotubes. *Adv. Mater.* **2012**, *24*, 4977−4994.
(274) Styers-Barnett, D. J.; Ellison, S. P.; Mehl, B. P.; Westlake, B. C.; House, R. L.; Park, C.; Wise, K. E.; Papanikolas, J. M. Exciton Dynamics and Biexciton Formation in Single-Walled Carbon Nanotubes Studied with Femtosecond Transient Absorption Spectroscopy. *J. Phys. Chem. C* **2008**, *112*, 4507−4516.
(275) (a) Piscanec, S.; Lazzeri, M.; Robertson, J.; Ferrari, A. C.; Mauri, F. Optical Phonons in Carbon Nanotubes: Kohn Anomalies, Peierls Distortions, and Dynamic Effects. *Phys. Rev. B* **2007**, *75*, 035427. (b) Rafailov, P. M.; Maultzsch, J.; Thomsen, C.; Kataura, H. Electrochemical Switching of the Peierls-Like Transition in Metallic Single-Walled Carbon Nanotubes. *Phys. Rev. B* **2005**, *72*, 045411. (c) Figge, M. T.; Mostovoy, M.; Knoester, J. Peierls Transition with Acoustic Phonons and Solitwistons in Carbon Nanotubes. *Phys. Rev. Lett.* **2001**, *86*, 4572−4575.
(276) Condon, E. U. Nuclear Motions Associated with Electron Transitions in Diatomic Molecules. *Phys. Rev.* **1928**, *32*, 0858−0872.

DOI: 10.1021/acs.chemrev.5b00012
Chem. Rev. 2015, 115, 5929−5978

(277) Myers Kelley, A. Resonance Raman and Resonance Hyper-Raman Intensities: Structure and Dynamics of Molecular Excited States in Solution. *J. Phys. Chem. A* **2008**, *112*, 11975−11991.
(278) (a) Hirst, E. S.; Jasti, R. Bending Benzene: Syntheses of N Cycloparaphenylenes. *J. Org. Chem.* **2012**, *77*, 10473−10478. (b) Xia, J.; Jasti, R. Synthesis, Characterization, and Crystal Structure of 6 Cycloparaphenylene. *Angew. Chem., Int. Ed.* **2012**, *51*, 2474−2476.
(279) Adamska, L.; Nayyar, I.; Chen, H.; Swan, A. K.; Oldani, N.; Fernandez-Alberti, S.; Golder, M. R.; Jasti, R.; Doorn, S. K.; Tretiak, S. Self-Trapping of Excitons, Violation of Condon Approximation, and Efficient Fluorescence in Conjugated Cycloparaphenylenes. *Nano Lett.* **2014**, *14*, 6539−6546.
(280) Duque, J. G.; Chen, H.; Swan, A. K.; Haroz, E. H.; Kono, J.; Tu, X.; Zheng, M.; Doorn, S. K. Revealing New Electronic Behaviours in the Raman Spectra of Chirality-Enriched Carbon Nanotube Ensembles. *Phys. Status Solidi B* **2010**, *247*, 2768−2773.
(281) Duque, J. G.; Telg, H.; Chen, H.; Swan, A. K.; Shreve, A. P.; Tu, X.; Zheng, M.; Doorn, S. K. Quantum Interference between the Third and Fourth Exciton States in Semiconducting Carbon Nanotubes Using Resonance Raman Spectroscopy. *Phys. Rev. Lett.* **2012**, *108*, 117404.
(282) Sun, Z.; Liu, D. S.; Stafstrom, S.; An, Z. Scattering Process between Polaron and Exciton in Conjugated Polymers. *J. Chem. Phys.* **2011**, *134*, 044906.
(283) van Reenen, S.; Vitorino, M. V.; Meskers, S. C. J.; Janssen, R. A. J.; Kemerink, M. Photoluminescence Quenching in Films of Conjugated Polymers by Electrochemical Doping. *Phys. Rev. B* **2014**, *89*, 205206.
(284) (a) Moliton, A.; Hiorns, R. C. Review of Electronic and Optical Properties of Semiconducting Pi-Conjugated Polymers: Applications in Optoelectronics. *Polym. Int.* **2004**, *53*, 1397−1412. (b) Bredas, J. L.; Street, G. B. Polarons, Bipolarons, and Solitons in Conducting Polymers. *Acc. Chem. Res.* **1985**, *18*, 309−315.
(285) (a) Geskin, V. M.; Cornil, J.; Bredas, J. L. Comment on 'Polaron Formation and Symmetry Breaking' by L Zuppiroli, et al. *Chem. Phys. Lett.* **2005**, *403*, 228−231. (b) Geskin, V. M.; Grozema, F. C.; Siebbeles, L. D. A.; Beljonne, D.; Bredas, J. L.; Cornil, J. Impact of the Computational Method on the Geometric and Electronic Properties of Oligo(Phenylene Vinylene) Radical Cations. *J. Phys. Chem. B* **2005**, *109*, 20237−20243.
(286) Lee, M. H.; Dunietz, B. D.; Geva, E. Donor-to-Donor vs Donor-to-Acceptor Interfacial Charge Transfer States in the Phthalocyanine−Fullerene Organic Photovoltaic System. *J. Phys. Chem. Lett.* **2014**, *5*, 3810−3816.
(287) (a) Nayyar, I. H.; Batista, E. R.; Tretiak, S.; Saxena, A.; Smith, D. L.; Martin, R. L. Effect of Trans- and Cis-Isomeric Defects on the Localization of the Charged Excitations in π-Conjugated Organic Polymers. *J. Polym. Sci., Part B: Polym. Phys.* **2013**, *51*, 935−942. (b) Nayyar, I. H.; Batista, E. R.; Tretiak, S.; Saxena, A.; Smith, D. L.; Martin, R. L. Localization of Electronic Excitations in Conjugated Polymers Studied by DFT. *J. Phys. Chem. Lett.* **2011**, *2*, 566−571.
(288) Moro, G.; Scalmani, G.; Cosentino, U.; Pitea, D. On the Structure of Polaronic Defects in Thiophene Oligomers: A Combined Hartree-Fock and Density Functional Theory Study. *Synth. Met.* **2000**, *108*, 165−172.
(289) Zuppiroli, L.; Bieber, A.; Michoud, D.; Galli, G.; Gygi, F.; Bussac, M. N.; Andre, J. J. Polaron Formation and Symmetry Breaking. *Chem. Phys. Lett.* **2003**, *374*, 7−12.
(290) Geskin, V. M.; Dkhissi, A.; Bredas, J. L. Oligothiophene Radical Cations: Polaron Structure in Hybrid DFT and MP2 Calculations. *Int. J. Quantum Chem.* **2003**, *91*, 350−354.
(291) Nguyen, T. D.; Hukic-Markosian, G.; Wang, F.; Wojcik, L.; Li, X.-G.; Ehrenfreund, E.; Vardeny, Z. V. Isotope Effect in Spin Response of Pi-Conjugated Polymer Films and Devices. *Nat. Mater.* **2010**, *9*, 345−352.
(292) Kuroda, S. Esr and Endor Studies of Solitons and Polarons in Conjugated Polymers. *Appl. Magn. Reson.* **2003**, *23*, 455−468.
(293) Norton, J. E.; Bredas, J.-L. Polarization Energies in Oligoacene Semiconductor Crystals. *J. Am. Chem. Soc.* **2008**, *130*, 12377−12384.
(294) McCamey, D. R.; van Schooten, K. J.; Baker, W. J.; Lee, S. Y.; Paik, S. Y.; Lupton, J. M.; Boehme, C. Hyperfine-Field-Mediated Spin Beating in Electrostatically Bound Charge Carrier Pairs. *Phys. Rev. Lett.* **2010**, *104*, 017601.
(295) Li, Y.; Xu, H.; Wu, L.; He, F.; Shen, F.; Liu, L.; Yang, B.; Ma, Y. NMR Signal Assignment of Segments in MEH-CN-PPV Cis/Trans-Conformational Segments in MEH-CN-PPV. *J. Polym. Sci., Part B: Polym. Phys.* **2008**, *46*, 1105−1113.
(296) Harbron, E. J.; Hadley, D. H.; Imm, M. R. Solvent Effects on Phototriggered Conformational Changes in an Azobenzene-Functionalized Poly(P-Phenylene Vinylene). *J. Photochem. Photobiol., A* **2007**, *186*, 151−157.
(297) Grimes, A. F.; Call, S. E.; Harbron, E. J.; English, D. S. Wavelength-Resolved Studies of Forster Energy Transfer in Azobenzene-Modified Conjugated Polymers: The Competing Roles of Exciton Migration and Spectral Resonance. *J. Phys. Chem. C* **2007**, *111*, 14257−14265.
(298) Lewis, S. M.; Harbron, E. J. Photomodulated Ppv Emission in a Photochromic Polymer Film. *J. Phys. Chem. C* **2007**, *111*, 4425−4430.
(299) Son, S.; Dodabalapur, A.; Lovinger, A. J.; Galvin, M. E. Luminescence Enhancement by the Introduction of Disorder Ino Poly(P-Phenylene Vinylene). *Science* **1995**, *269*, 376−378.
(300) Liu, D.; Yin, S.; Xu, H.; Liu, X.; Sun, G.; Xie, Z.; Yang, B.; Ma, Y. Cis- and Trans-Isomerization-Induced Transition of Charge Transport Property in Ppv Oligomers. *J. Chem. Phys.* **2011**, *388*, 69−77.
(301) Marcus, R. A. Electron-transfer Reactions in Chemistry - Theory and Experiment. *Rev. Mod. Phys.* **1993**, *65*, 599−610.
(302) Ochsenbein, S. T.; Feng, Y.; Whitaker, K. M.; Badaeva, E.; Liu, W. K.; Li, X.; Gamelin, D. R. Charge-Controlled Magnetism in Colloidal Doped Semiconductor Nanocrystals. *Nat. Nanotech.* **2009**, *4*, 681−687.
(303) Kislitsyn, D. A.; Gervasi, C. F.; Allen, T.; Palomaki, P. K. B.; Hackley, J. D.; Maruyama, R.; Nazin, G. V. Spatial Mapping of Sub-Bandgap States Induced by Local Nonstoichiometry in Individual Lead Sulfide Nanocrystals. *J. Phys. Chem. Lett.* **2014**, *5*, 3701−3707.
(304) Forster, T. Zwischenmolekulare Energiewanderung Und Fluoreszenz. *Ann. Phys. (Berlin, Ger.)* **1948**, *2*, 55−75.
(305) Beljonne, D.; Cornil, J.; Muccioli, L.; Zannoni, C.; Bredas, J.-L.; Castet, F. Electronic Processes at Organic-Organic Interfaces: Insight from Modeling and Implications for Opto-Electronic Devices. *Chem. Mater.* **2011**, *23*, 591−609.
(306) Jean, J. M.; Friesner, R. A.; Fleming, G. R. Application of a Multilevel Redfield Theory to Electron-Transfer in Condensed Phases. *J. Chem. Phys.* **1992**, *96*, 5827−5842.
(307) Lee, M. H.; Dunietz, B. D.; Geva, E. Calculation from First Principles of Intramolecular Golden-Rule Rate Constants for Photo-Induced Electron Transfer in Molecular Donor−Acceptor Systems. *J. Phys. Chem. C* **2013**, *117*, 23391−23401.
(308) Huynh, T. D.; Sun, K.-W.; Gelin, M.; Zhao, Y. Polaron Dynamics in Two-Dimensional Photon-Echo Spectroscopy of Molecular Rings. *J. Chem. Phys.* **2013**, *139*, 104103.
(309) (a) Niklasson, A. M. N.; Steneteg, P.; Odell, A.; Bock, N.; Challacombe, M.; Tymczak, C. J.; Holmstrom, E.; Guishan, Z.; Weber, V. Extended Lagrangian Born-Oppenheimer Molecular Dynamics with Dissipation. *J. Chem. Phys.* **2009**, *130*, 214109. (b) Niklasson, A. M. N.; Tymczak, C. J.; Challacombe, M. Time-Reversible Ab Initio Molecular Dynamics. *J. Chem. Phys.* **2007**, *126*, 144103.
(310) May, V.; Kühn, O. *Charge and Energy Transfer Dynamics in Molecular Systems*; Wiley-VCH: New York, 2004.
(311) Rebentrost, P.; Mohseni, M.; Kassal, I.; Lloyd, S.; Aspuru-Guzik, A. Environment-Assisted Quantum Transport. *New J. Phys.* **2009**, *11*, 033003.
(312) Tempel, D. G.; Aspuru-Guzik, A. Relaxation and Dephasing in Open Quantum Systems Time-Dependent Density Functional Theory: Properties of Exact Functionals from an Exactly-Solvable Model System. *Chem. Phys.* **2011**, *391*, 130−142.
(313) (a) Domcke, W.; Yarkony, D.; Köppel, H. *Conical Intersections: Electronic Structure, Dynamics & Spectroscopy*; World Scientific Pub.

DOI: 10.1021/acs.chemrev.5b00012
Chem. Rev. 2015, 115, 5929−5978

Co. Inc.: NJ, 2004. (b) Martinez, T. J. Insights for Light-Driven Molecular Devices from Ab Initio Multiple Spawning Excited-State Dynamics of Organic and Biological Chromophores. *Acc. Chem. Res.* **2006**, *39*, 119−126. (c) Virshup, A. M.; Punwong, C.; Pogorelov, T. V.; Lindquist, B. A.; Ko, C.; Martinez, T. J. Photodynamics in Complex Environments: Ab Initio Multiple Spawning Quantum Mechanical/Molecular Mechanical Dynamics. *J. Phys. Chem. B* **2009**, *113*, 3280−3291. (d) Piryatinski, A.; Stepanov, M.; Tretiak, S.; Chernyak, V. Semiclassical Scattering on Conical Intersections. *Phys. Rev. Lett.* **2005**, *95*, 223001.

(314) (a) Gao, J. L.; Truhlar, D. G. Quantum Mechanical Methods for Enzyme Kinetics. *Annu. Rev. Phys. Chem.* **2002**, *53*, 467−505. (b) Makri, N. Time-Dependent Quantum Methods for Large Systems. *Annu. Rev. Phys. Chem.* **1999**, *50*, 167−191.

(315) (a) Santer, M.; Manthe, U.; Stock, G. Quantum-Classical Liouville Description of Multidimensional Nonadiabatic Molecular Dynamics. *J. Chem. Phys.* **2001**, *114*, 2001−2012. (b) Worth, G. A. Accurate Wave Packet Propagation for Large Molecular Systems: The Multiconfiguration Time-Dependent Hartree (MCTDH) Method with Selected Configurations. *J. Chem. Phys.* **2000**, *112*, 8322−8329.

(316) Levine, B. G.; Martinez, T. J. Isomerization through Conical Intersections. *Annu. Rev. Phys. Chem.* **2007**, *58*, 613−634.

(317) Tully, J. C. Perspective: Nonadiabatic Dynamics Theory. *J. Chem. Phys.* **2012**, *137*, 22A301.

(318) (a) Craig, C. F.; Duncan, W. R.; Prezhdo, O. V. Trajectory Surface Hopping in the Time-Dependent Kohn-Sham Approach for Electron-Nuclear Dynamics. *Phys. Rev. Lett.* **2005**, *95*, 163001. (b) Nelson, T.; Fernandez-Alberti, S.; Roitberg, A. E.; Tretiak, S. Nonadiabatic Excited-State Molecular Dynamics: Modeling Photophysics in Organic Conjugated Materials. *Acc. Chem. Res.* **2014**, *47*, 1155−1164. (c) Leathers, A. S.; Micha, D. A.; Kilin, D. S. Density Matrix Treatment of Combined Instantaneous and Delayed Dissipation for an Electronically Excited Adsorbate on a Solid Surface. *J. Chem. Phys.* **2009**, *131*, 144106. (d) Kilin, D. S.; Micha, D. A. Relaxation of Photoexcited Electrons at a Nanostructured Si(111) Surface. *J. Phys. Chem. Lett.* **2010**, *1*, 1073−1077. (e) Neukirch, A. J.; Shamberger, L. C.; Abad, E.; Haycock, B. J.; Wang, H.; Ortega, J.; Prezhdo, O. V.; Lewis, J. P. Nonadiabatic Ensemble Simulations of cis-Stilbene and cis-Azobenzene Photoisomerization. *J. Chem. Theory Comput.* **2014**, *10*, 14−23.

(319) Li, X. S.; Tully, J. C.; Schlegel, H. B.; Frisch, M. J. Ab Initio Ehrenfest Dynamics. *J. Chem. Phys.* **2005**, *123*, 084106.

(320) Chen, J.; Meng, Q.; Stanley May, P.; Berry, M. T.; Kilin, D. S. Time-Dependent Excited-State Molecular Dynamics of Photodissociation of Lanthanide Complexes for Laser-Assisted Metal-Organic Chemical Vapour Deposition. *Mol. Phys.* **2013**, *112*, 508−517.

(321) Tully, J. C.; Preston, R. K. Trajectory Surface Hopping Approach to Nonadiabatic Molecular Collisions - Reaction of H^+ with H_2. *J. Chem. Phys.* **1971**, *55*, 562−572.

(322) Tully, J. C. Molecular Dynamics with Electronic Transitions. *J. Chem. Phys.* **1990**, *93*, 1061−1071.

(323) Drukker, K. Basics of Surface Hopping in Mixed Quantum/Classical Simulations. *J. Comput. Phys.* **1999**, *153*, 225−272.

(324) Parandekar, P. V.; Tully, J. C. Mixed Quantum-Classical Equilibrium. *J. Chem. Phys.* **2005**, *122*, 094102.

(325) Shu, Y.; Levine, B. G. Do Excited Silicon−Oxygen Double Bonds Emit Light? *J. Phys. Chem. C* **2014**, *118*, 7669−7677.

(326) Barbatti, M.; Granucci, G.; Persico, M.; Ruckenbauer, M.; Vazdar, M.; Eckert-Maksic, M.; Lischka, H. The on-the-Fly Surface-Hopping Program System Newton-X: Application to Ab Initio Simulation of the Nonadiabatic Photodynamics of Benchmark Systems. *J. Photochem. Photobiol., A* **2007**, *190*, 228−240.

(327) Nelson, T.; Fernandez-Alberti, S.; Roitberg, A. E.; Tretiak, S. Conformational Disorder in Energy Transfer: Beyond Forster Theory. *Phys. Chem. Chem. Phys.* **2013**, *15*, 9245−9256.

(328) Subotnik, J. E.; Shenvi, N. A New Approach to Decoherence and Momentum Rescaling in the Surface Hopping Algorithm. *J. Chem. Phys.* **2011**, *134*, 024105.

(329) Petit, A. S.; Subotnik, J. E. Calculating Time-Resolved Differential Absorbance Spectra for Ultrafast Pump-Probe Experiments with Surface Hopping Trajectories. *J. Chem. Phys.* **2014**, *141*, 154108.

(330) Prezhdo, O. V.; Duncan, W. R.; Prezhdo, V. V. Photoinduced Electron Dynamics at the Chromophore-Semiconductor Interface: A Time-Domain Ab Initio Perspective. *Prog. Surf. Sci.* **2009**, *84*, 30−68.

(331) Hammes-Schiffer, S.; Tully, J. C. Proton Transfer in Solution - Molecular Dynamics with Quantum Transitions. *J. Chem. Phys.* **1994**, *101*, 4657−4667.

(332) Craig, C. F.; Duncan, W. R.; Prezhdo, O. V. Trajectory Surface Hopping in the Time-Dependent Kohn-Sham Approach for Electron-Nuclear Dynamics. *Phys. Rev. Lett.* **2005**, *95*, 163001.

(333) Fischer, S. A.; Habenicht, B. F.; Madrid, A. B.; Duncan, W. R.; Prezhdo, O. V. Regarding the Validity of the Time-Dependent Kohn-Sham Approach for Electron-Nuclear Dynamics via Trajectory Surface Hopping. *J. Chem. Phys.* **2011**, *134*, 024102.

(334) (a) Duncan, W. R.; Prezhdo, O. V. Theoretical Studies of Photoinduced Electron Transfer in Dye-Sensitized Tio_2. *Annu. Rev. Phys. Chem.* **2007**, *58*, 143−184. (b) Prezhdo, O. V. Quantized Hamilton Dynamics. *Theor. Chem. Acc.* **2006**, *116*, 206−218.

(335) (a) Fischer, S. A.; Lingerfelt, D. B.; May, J. W.; Li, X. Non-Adiabatic Molecular Dynamics Investigation of Photoionization State Formation and Lifetime in Mn^{2+}-Doped ZnO Quantum Dots. *Phys. Chem. Chem. Phys.* **2014**, *16*, 17507−17514. (b) Lingerfelt, D. B.; Fischer, S. A.; May, J. W.; Li, X. Dynamical Investigations of Inhomogeneous Vibrational Broadening in Diluted Magnetic Semiconductor Nanocrystals. *J. Phys. Chem. C* **2014**, *118*, 3266−3273. (c) Yao, G.; Meng, Q.; Berry, M. T.; May, P. S.; Kilin, S. D. Molecular Dynamics in Finding Nonadiabatic Coupling for beta-NaYF4: Ce3+ Nanocrystals. *Mol. Phys.* **2015**, *113*, 385−391.

(336) Plasser, F.; Crespo-Otero, R.; Pederzoli, M.; Pittner, J.; Lischka, H.; Barbatti, M. Surface Hopping Dynamics with Correlated Single-Reference Methods: 9h-Adenine as a Case Study. *J. Chem. Theory Comput.* **2014**, *10*, 1395−1405.

(337) Barbatti, M.; Ruckenbauer, M.; Plasser, F.; Pittner, J.; Granucci, G.; Persico, M.; Lischka, H. Newton-X: A Surface-Hopping Program for Nonadiabatic Molecular Dynamics. *Wiley Interdiscip. Rev.: Comput. Mol. Sci.* **2014**, *4*, 26−33.

(338) Nelson, T.; Fernandez-Alberti, S.; Chernyak, V.; Roitberg, A. E.; Tretiak, S. Nonadiabatic Excited-State Molecular Dynamics Modeling of Photoinduced Dynamics in Conjugated Molecules. *J. Phys. Chem. B* **2011**, *115*, 5402−5414.

(339) Send, R.; Furche, F. First-Order Nonadiabatic Couplings from Time-Dependent Hybrid Density Functional Response Theory: Consistent Formalism, Implementation, and Performance. *J. Chem. Phys.* **2010**, *132*, 044107.

(340) Tavernelli, I.; Curchod, B. F. E.; Laktionov, A.; Rothlisberger, U. Nonadiabatic Coupling Vectors for Excited States within Time-Dependent Density Functional Theory in the Tamm−Dancoff Approximation and Beyond. *J. Chem. Phys.* **2010**, *133*, 194104.

(341) Ou, Q.; Fatehi, S.; Alguire, E.; Shao, Y.; Subotnik, J. E. Derivative Couplings between TDDFT Excited States Obtained by Direct Differentiation in the Tamm-Dancoff Approximation. *J. Chem. Phys.* **2014**, *141*, 069903.

(342) Zhu, C. Y.; Nangia, S.; Jasper, A. W.; Truhlar, D. G. Coherent Switching with Decay of Mixing: An Improved Treatment of Electronic Coherence for Non-Born-Oppenheimer Trajectories. *J. Chem. Phys.* **2004**, *121*, 7658−7670.

(343) Granucci, G.; Persico, M.; Zoccante, A. Including Quantum Decoherence in Surface Hopping. *J. Chem. Phys.* **2010**, *133*, 134111.

(344) Ouyang, W.; Subotnik, J. E. Estimating the Entropy and Quantifying the Impurity of a Swarm of Surface-Hopping Trajectories: A New Perspective on Decoherence. *J. Chem. Phys.* **2014**, *140*, 204102.

(345) Shenvi, N.; Yang, W. Achieving Partial Decoherence in Surface Hopping through Phase Correction. *J. Chem. Phys.* **2012**, *137*, 22A528.

(346) Subotnik, J. E. Fewest-Switches Surface Hopping and Decoherence in Multiple Dimensions. *J. Phys. Chem. A* **2011**, *115*, 12083−12096.

DOI: 10.1021/acs.chemrev.5b00012
Chem. Rev. 2015, 115, 5929−5978

(347) Yao, Y.; Zhao, Y. A Variational Surface Hopping Algorithm for the Sub-Ohmic Spin-Boson Model. *J. Chem. Phys.* **2013**, *139*, 014102.
(348) Jaeger, H. M.; Fischer, S.; Prezhdo, O. V. Decoherence-Induced Surface Hopping. *J. Chem. Phys.* **2012**, *137*, 22A545.
(349) Gorshkov, V. N.; Tretiak, S.; Mozyrsky, D. Semiclassical Monte-Carlo Approach for Modelling Non-Adiabatic Dynamics in Extended Molecules. *Nat. Commun.* **2013**, *4*, 2144.
(350) Redfield, A. G. On the Theory of Relaxation Processes. *IBM J. Res. Dev.* **1957**, *1*, 19−31.
(351) Sundstrom, V.; Pullerits, T.; van Grondelle, R. Photosynthetic Light-Harvesting: Reconciling Dynamics and Structure of Purple Bacterial Lh2 Reveals Function of Photosynthetic Unit. *J. Phys. Chem. B* **1999**, *103*, 2327−2346.
(352) (a) Kuhn, O.; May, V.; Schreiber, M. Dissipative Vibrational Dynamics in a Curve-Crossing System. *J. Chem. Phys.* **1994**, *101*, 10404−10415. (b) Schreiber, M.; Kilin, D.; Kleinekathofer, U. Comparison of Two Models for Bridge-Assisted Charge Transfer. *J. Lumin.* **1999**, *83*−*84*, 235−240.
(353) Egorova, D.; Thoss, M.; Domcke, W.; Wang, H. B. Modeling of Ultrafast Electron-Transfer Processes: Validity of Multilevel Redfield Theory. *J. Chem. Phys.* **2003**, *119*, 2761−2773.
(354) Huang, S. P.; Kilin, D. S. Charge Transfer, Luminescence, and Phonon Bottleneck in TiO_2 Nanowires Computed by Eigenvectors of Liouville Superoperator. *J. Chem. Theory Comput.* **2014**, *10*, 3996−4005.
(355) Worth, G. A.; Hunt, P.; Robb, M. A. Nonadiabatic Dynamics: A Comparison of Surface Hopping Direct Dynamics with Quantum Wavepacket Calculations. *J. Phys. Chem. A* **2003**, *107*, 621−631.
(356) (a) Kilin, D. S.; Micha, D. A. Modeling the Photovoltage of Doped Si Surfaces. *J. Phys. Chem. C* **2011**, *115*, 770−775. (b) Vazhappilly, T.; Kilin, D. S.; Micha, D. Modeling the Surface Photovoltage of Silicon Slabs with Varying Thickness. *J. Phys.: Condens. Matter* **2015**, *27*, 134204.
(357) (a) Inerbaev, T. M.; Hoefelmeyer, J. D.; Kilin, D. S. Photoinduced Charge Transfer from Titania to Surface Doping Site. *J. Phys. Chem. C* **2013**, *117*, 9673−9692. (b) Jensen, S.; Kilin, D. Electronic Properties of Nickel Doped TiO2 Anatase. *J. Phys.: Condens. Matter* **2015**, *27*, 134207.
(358) Huang, S.; Inerbaev, T. M.; Kilin, D. Excited State Dynamics of Ru10 Cluster Interfacing Anatase TiO_2(101) Surface and Liquid Water. *J. Phys. Chem. Lett.* **2014**, *5*, 2823−2829.
(359) (a) Schaller, R. D.; Pietryga, J. M.; Goupalov, S. V.; Petruska, M. A.; Ivanov, S. A.; Klimov, V. I. Breaking the Phonon Bottleneck in Semiconductor Nanocrystals Via Multiphonon Emission Induced by Intrinsic Nonadiabatic Interactions. *Phys. Rev. Lett.* **2005**, *95*, 196401. (b) García-Santamaría, F.; Chen, Y.; Vela, J.; Schaller, R. D.; Hollingsworth, J. A.; Klimov, V. I. Suppressed Auger Recombination in Giant Nanocrystals Boosts Optical Gain Performance. *Nano Lett.* **2009**, 3482−3488.
(360) (a) Alivisatos, A. P. Semiconductor Clusters, Nanocrystals, and Quantum Dots. *Science* **1996**, *271*, 933−937. (b) Nozik, A. J. Spectroscopy and Hot Electron Relaxation Dynamics in Semiconductor Quantum Wells and Quantum Dots. *Annu. Rev. Phys. Chem.* **2001**, *52*, 193−231.
(361) Pandey, A.; Guyot-Sionnest, P. Slow Electron Cooling in Colloidal Quantum Dots. *Science* **2008**, *322*, 929−932.
(362) Hendry, E.; Koeberg, M.; Wang, F.; Zhang, H.; Donega, C. D.; Vanmaekelbergh, D.; Bonn, M. Direct Observation of Electron-to-Hole Energy Transfer in CdSe Quantum Dots. *Phys. Rev. Lett.* **2006**, *96*, 057408.
(363) Cooney, R. R.; Sewall, S. L.; Dias, E. A.; Sagar, D. M.; Anderson, K. E. H.; Kambhampati, P. Unified Picture of Electron and Hole Relaxation Pathways in Semiconductor Quantum Dots. *Phys. Rev. B* **2007**, *75*, 245311.
(364) Hyeon-Deuk, K.; Prezhdo, O. V. Time-Domain Ab Initio Study of Auger and Phonon-Assisted Auger Processes in a Semiconductor Quantum Dot. *Nano Lett.* **2011**, *11*, 1845−1850.
(365) Harbold, J. M.; Du, H.; Krauss, T. D.; Cho, K. S.; Murray, C. B.; Wise, F. W. Time-Resolved Intraband Relaxation of Strongly Confined Electrons and Holes in Colloidal PbSe Nanocrystals. *Phys. Rev. B* **2005**, *72*, 195312.
(366) Ridley, B. K. *Quantum Processes in Semiconductors*; OUP: Oxford, 2013.
(367) Ledebo, L. A.; Ridley, B. K. On the Position of Energy-Levels Related to Transition Metal Impurities in III-V Semiconductors. *J. Phys. C: Solid State Phys.* **1982**, *15*, L961−L964.
(368) Chen, J.; Schmitz, A.; Inerbaev, T.; Meng, Q.; Kilina, S.; Tretiak, S.; Kilin, D. S. First-Principles Study of P-N-Doped Silicon Quantum Dots: Charge Transfer, Energy Dissipation, and Time-Resolved Emission. *J. Phys. Chem. Lett.* **2013**, *4*, 2906−2913.
(369) Han, Y.; Tretiak, S.; Kilin, D. Dynamics of Charge Transfer at Au/Si Metal-Semiconductor Nano-Interface. *Mol. Phys.* **2014**, *112*, 474−484.
(370) Fujii, M.; Yamaguchi, Y.; Takase, Y.; Ninomiya, K.; Hayashi, S. Control of Photoluminescence Properties of Si Nanocrystals by Simultaneously Doping N- and P-Type Impurities. *Appl. Phys. Lett.* **2004**, *85*, 1158−1160.
(371) Chu, I.-H.; Kilin, D. S.; Cheng, H.-P. First-Principles Studies of Photoinduced Charge Transfer in Noncovalently Functionalized Carbon Nanotubes. *J. Phys. Chem. C* **2013**, *117*, 17909−17918.
(372) Postupna, O.; Jaeger, H. M.; Prezhdo, O. V. Photoinduced Dynamics in Carbon Nanotube Aggregates Steered by Dark Excitons. *J. Phys. Chem. Lett.* **2014**, *5*, 3872−3877.
(373) Fernandez-Alberti, S.; Roitberg, A. E.; Kleiman, V. D.; Nelson, T.; Tretiak, S. Shishiodoshi Unidirectional Energy Transfer Mechanism in Phenylene Ethynylene Dendrimers. *J. Chem. Phys.* **2012**, *137*, 22A526.
(374) Fernandez-Alberti, S.; Kleiman, V. D.; Tretiak, S.; Roitberg, A. E. Nonadiabatic Molecular Dynamics Simulations of the Energy Transfer between Building Blocks in a Phenylene Ethynylene Dendrimer. *J. Phys. Chem. A* **2009**, *113*, 7535−7542.
(375) Nelson, T.; Fernandez-Alberti, S.; Chernyak, V.; Roitberg, A. E.; Tretiak, S. Nonadiabatic Excited-State Molecular Dynamics: Numerical Tests of Convergence and Parameters. *J. Chem. Phys.* **2012**, *136*, 054108.
(376) Soler, M. A.; Nelson, T.; Roitberg, A. E.; Tretiak, S.; Fernandez-Alberti, S. Signature of Nonadiabatic Coupling in Excited-State Vibrational Modes. *J. Phys. Chem. A* **2014**, *118*, 10372−10379.
(377) Ondarse-Alvarez, D.; Oldani, N.; Tretiak, S.; Fernandez-Alberti, S. Computational Study of Photoexcited Dynamics in Bichromophoric Cross-Shaped Oligofluorene. *J. Phys. Chem. A* **2014**, *118*, 10742−10753.
(378) Oldani, N.; Tretiak, S.; Bazan, G.; Fernandez-Alberti, S. Modeling of Internal Conversion in Photoexcited Conjugated Molecular Donors Used in Organic Photovoltaics. *Energy Environ. Sci.* **2014**, *7*, 1175−1184.
(379) Klaumunzer, B.; Kroner, D.; Lischka, H.; Saalfrank, P. Non-Adiabatic Excited State Dynamics of Riboflavin after Photoexcitation. *Phys. Chem. Chem. Phys.* **2012**, *14*, 8693−8702.
(380) Bolinger, J. C.; Traub, M. C.; Brazard, J.; Adachi, T.; Barbara, P. F.; Vanden Bout, D. A. Conformation and Energy Transfer in Single Conjugated Polymers. *Acc. Chem. Res.* **2012**, *45*, 1992−2001.

DOI: 10.1021/acs.chemrev.5b00012
Chem. Rev. 2015, 115, 5929−5978